Nano Research

ISSN 1998-0124 CN 11-5974/O4
https://doi.org/10.26599/NR.2026.94908786

Review Article

Electrochromic technology for flexible self-powered multifunctional systems from materials, devices to applications

Hao Zhang[1,2,3], Shouyi Tang[1], Hongjian Wang[1,2,3], Xin Huang[4,5], Henggao Xiang[6], Weibin Zhu[4,5](✉)

[1] College of Mechanical Engineering, Chongqing Technology and Business University, Chongqing 400067, China

[2] Chongqing Key Laboratory of Green Design and Manufacturing of Intelligent Equipment, Chongqing Technology and Business University, Chongqing 400067, China

[3] Key Laboratory of Green Remanufacturing of Advanced Equipment of Chongqing Education Commission of China, Chongqing Technology and Business University, Chongqing 400067, China

[4] Department of Biomedical Engineering, City University of Hong Kong, Hong Kong, China

[5] Hong Kong Center for Cerebro-Cardiovascular Health Engineering, Hong Kong Science Park, New Territories, Hong Kong, China

[6] School of Materials Science and Engineering, Nanjing University of Science and Technology, Nanjing 210094, China

Nano Res., **Just Accepted Manuscript** • https://doi.org/10.26599/NR.2026.94908786

https://www.sciopen.com/journal/1998-0124 on Apr. 29, 2026

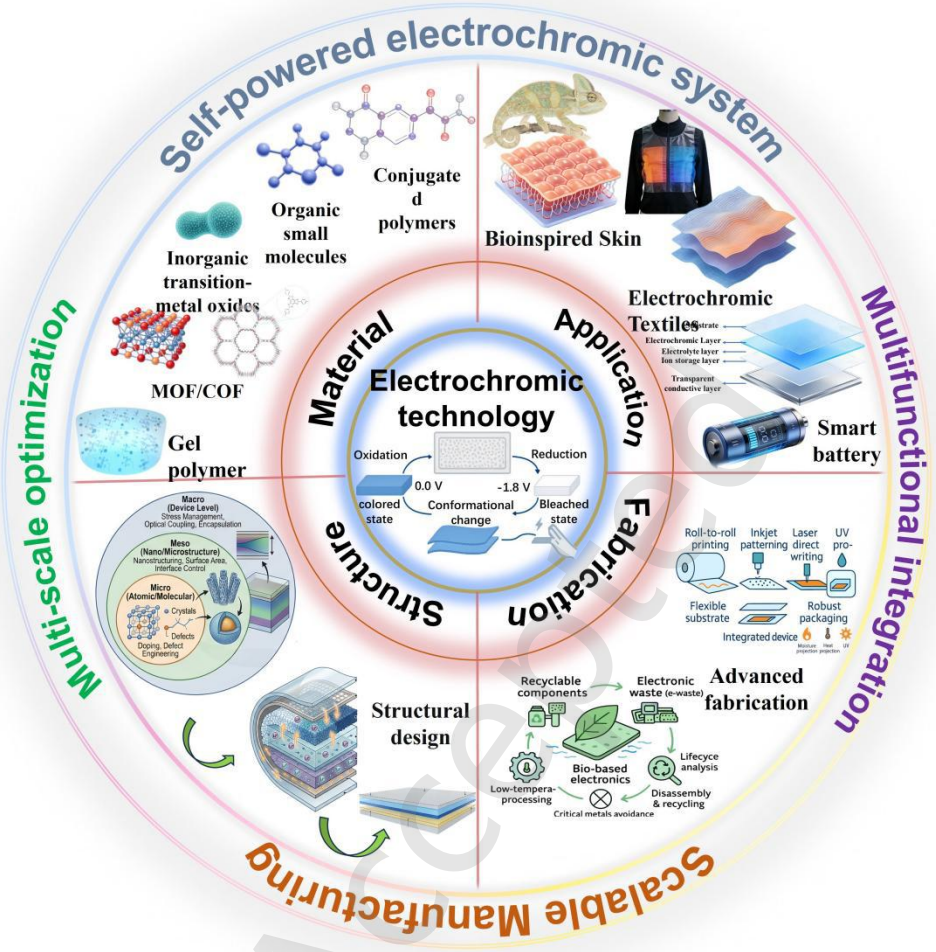

This paper reviews four categories of advanced electrochromic technologies for flexible, self- powered multifunctional systems and highlights their cutting- edge applications, with a focus on clarifying the relationships among materials, structures, fabrication methods, and performances.

Review Article

Electrochromic technology for flexible self- powered multifunctional systems from materials, devices to applications

Hao Zhang[1,2,3], Shouyi Tang[1], Hongjian Wang[1,2,3], Xin Huang[4,5], Henggao Xiang[6], and Weibin Zhu[4,5]* (ORCID:0000-0003-2310-0058)

1.College of Mechanical Engineering, Chongqing Technology and Business University, Chongqing 400067, China

2.Chongqing Key Laboratory of Green Design and Manufacturing of Intelligent Equipment, Chongqing Technology and Business University, Chongqing 400067, China

3.Key Laboratory of Green Remanufacturing of Advanced Equipment of Chongqing Education Commission of China, Chongqing Technology and Business University, Chongqing 400067, China

4.Department of Biomedical Engineering, City University of Hong Kong, Hong Kong, China

5.Hong Kong Center for Cerebro-Cardiovascular Health Engineering, Hong Kong Science Park, New Territories, Hong Kong, China

6. School of Materials Science and Engineering, Nanjing University of Science and Technology, Nanjing 210094, China

Received: 4 March 2026; Revised: 21 April 2026; Accepted: 24 April 2026

*Address correspondence to wbzhu0628@126.com

Weibin Zhu (ORCID: 0000-0003-2310-0058)

Cite this article: Nano Research, 2026, 19, 94908786

https://doi.org/10.26599/NR.2026.94908786

ABSTRACT

Electrochromic (EC) technology has progressed rapidly from simple inorganic thin films to a broad library of organic molecules, conjugated polymers, and porous framework materials, thereby enabling higher coloration efficiency, wider spectral

tunability, and improved mechanical flexibility. Contemporary flexible EC devices leverage hybrid material systems, engineered micro/nanostructures, and scalable manufacturing routes to realize faster switching and enhanced optical contrast. Nevertheless, the field continues to confront critical challenges including sluggish ion transport, complex system-level integration, and the difficulty of decoupling piezoelectric and triboelectric signals, which call for coordinated advances in materials design, device engineering, and intelligent control strategies. Against this backdrop, the present review first clarifies the importance of EC technology and elucidates the fundamental mechanisms of redox-driven optical modulation and ion insertion/extraction. It then systematically categorizes EC material systems, spanning inorganic transition-metal oxides, organic small molecules, conjugated polymers, and emerging hybrid platforms such as metal–supramolecular polymers, porous MOF/COF frameworks, and flexible polymer-based electrolytes. Subsequently, the review examines the structural design and performance optimization of flexible EC devices, including multiscale optimization strategies and scalable fabrication techniques. Finally, it highlights advanced application scenarios from bioinspired electronic skin and smart textiles to self-powered EC energy-storage devices and smart batteries with self-diagnostic functionalities, which also concludes with a discussion of future research directions and outstanding challenges.

KEYWORDS: electrochromic materials, self-powered systems, flexible devices, energy-storage visualization

1. Introduction

Escalating global energy demand and the mounting threat of climate change have pushed building energy conservation to the forefront of national sustainability agendas. Buildings now account for roughly 40% of worldwide final energy use, and windows, long the thermal weak point of building envelopes, directly determine daylighting quality, solar heat gain, and cooling loads through their optical and thermal characteristics, thus exerting a decisive influence on both energy consumption and associated carbon emissions[1-3]. As a result, smart window technologies capable of actively and intelligently modulating solar radiation have become pivotal to achieving near-zero-energy buildings and carbon neutrality[4, 5].

Electrochromic (EC) technology offers dynamic control of visible and near-infrared transmittance by harnessing reversible redox processes under comparatively low biases[6, 7]. Unlike static or passive dimming solutions, EC devices can actively tune optical throughput, making them promising for

energy-efficient smart windows, low-power displays, adaptive camouflage, and spacecraft thermal management[8-10]. Since the concept's inception in the 1960s, EC materials have diversified from inorganic transition-metal oxides and organic small molecules to conjugated polymers, metal-supramolecular polymers, and porous frameworks[11, 12]. Prototypical examples, including tungsten trioxide [13, 14], viologen derivatives[15, 16], and poly(3,4-ethylenedioxythiophene) [17, 18], each deliver distinct advantages in coloration efficiency, chromatic range, mechanical flexibility, and processability. Nevertheless, several critical bottlenecks persist: sluggish ionic kinetics that cap modulation speed; structural degradation triggered by repeated ion insertion/extraction cycles, eroding long-term stability; and the difficulty of rapidly and independently coordinating broadband (visible to near-IR-II) optical control [19-21]. Moreover, integrating EC functionality with energy storage, sensing, and energy harvesting to build self-powered, multimodal intelligent systems remains an emerging frontier in **Fig. 1**, with outstanding challenges in integration density, reliability, and scalable manufacturing [22].

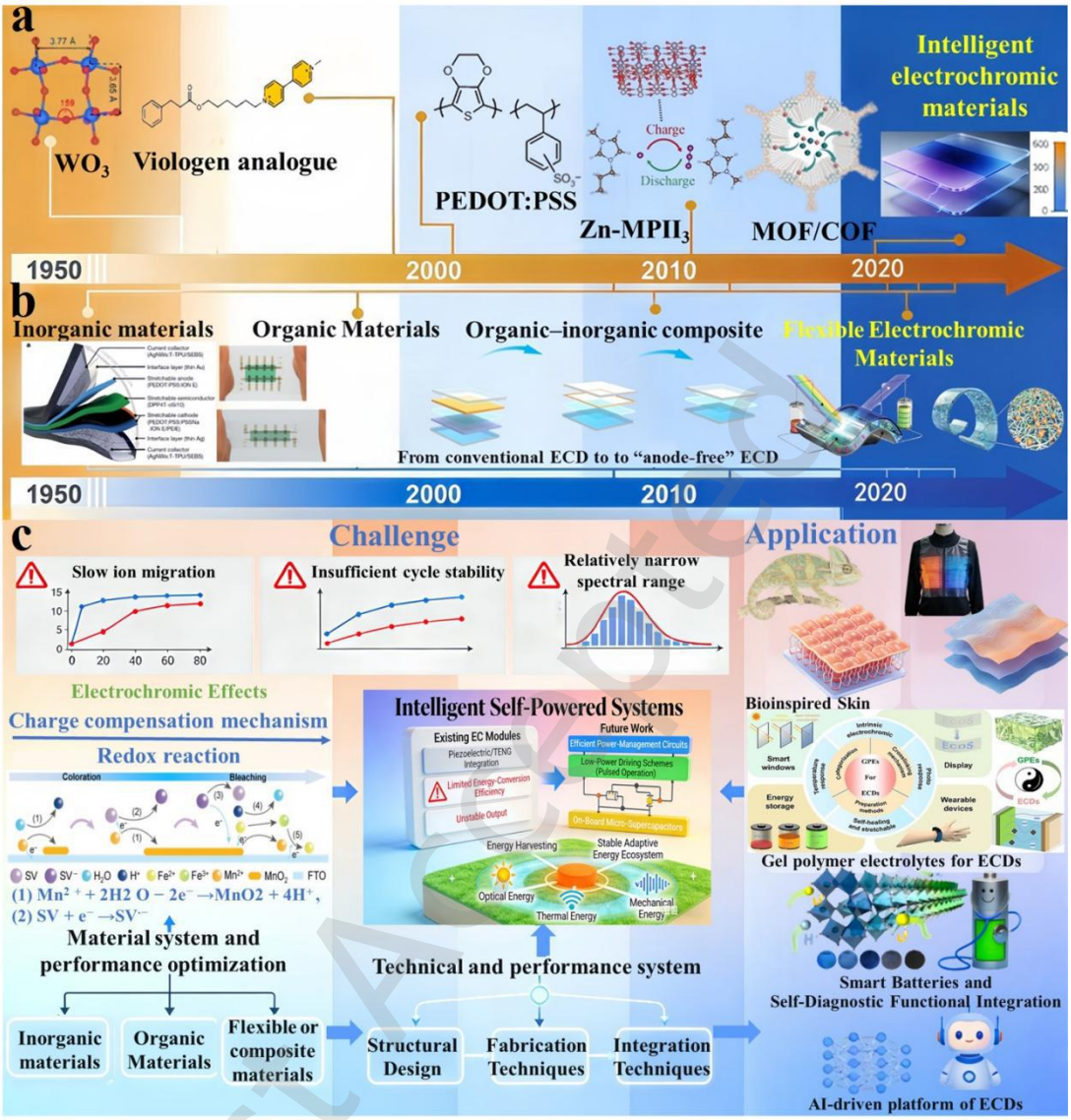

Fig. 1 Roadmap for electrochromic devices (ECDs). (a) The material evolution of ECDs, (b) the structural design of ECDs, (c) roadmap for mechanism, materials, structure, integration techniques, typical applications and their integrated platform of ECDs[23-32]. Reproduced with permission.[24] Copyright 2021, Springer Nature. Reproduced with permission.[25] Copyright 2021, Springer Nature. Reproduced with permission.[26] Copyright 2025, Wiley-VCH GmbH. Reproduced with permission.[28] Copyright 2016, The Royal Society of Chemistry. Reproduced with permission.[29] Copyright 2026, Wiley-VCH GmbH.

To systematically map the progress and challenges in this field, this review first elucidates the fundamental physico-chemical mechanisms of electrochromism, then comprehensively surveys the strategies of diverse electrochromic material systems. It

subsequently concentrates on performance-optimization pathways encompassing flexible device architecture design, material composites and microstructural engineering, and advanced fabrication processes. Finally, the review surveys cutting-edge applications including health-monitoring interfaces, smart textiles, EC energy-storage components, and intelligent batteries equipped with built-in diagnostics, and projects future trajectories for the field. Taken together, as shown in **Fig.2**, this systematic appraisal provides actionable guidance for designing next-generation, high-performance, multifunctional EC materials and for accelerating AI and robotics-enabled device innovation.

Fig. 2 Summary of electrochromic technologies from materials, microstructures, fabrication to advanced applications.

2. Mechanism of Electrochromic Effects

Electrochromic effect describes the reversible change in a material's optical properties

under an applied electric field, mediated by redox reactions that involve the concerted transport of electrons and ions. This dual charge-carrier participation alters the band structure or molecular orbital energies, thereby modulating light absorption—for example, toggling between transparent and colored states [33]. Owing to this electrically tunable optical response, electrochromic materials hold promise in **Fig. 3** for smart windows[34-36], low-power [37, 38] and multicolor displays[39-41], adaptive military camouflage[42], and thermal management in space applications [43, 44].

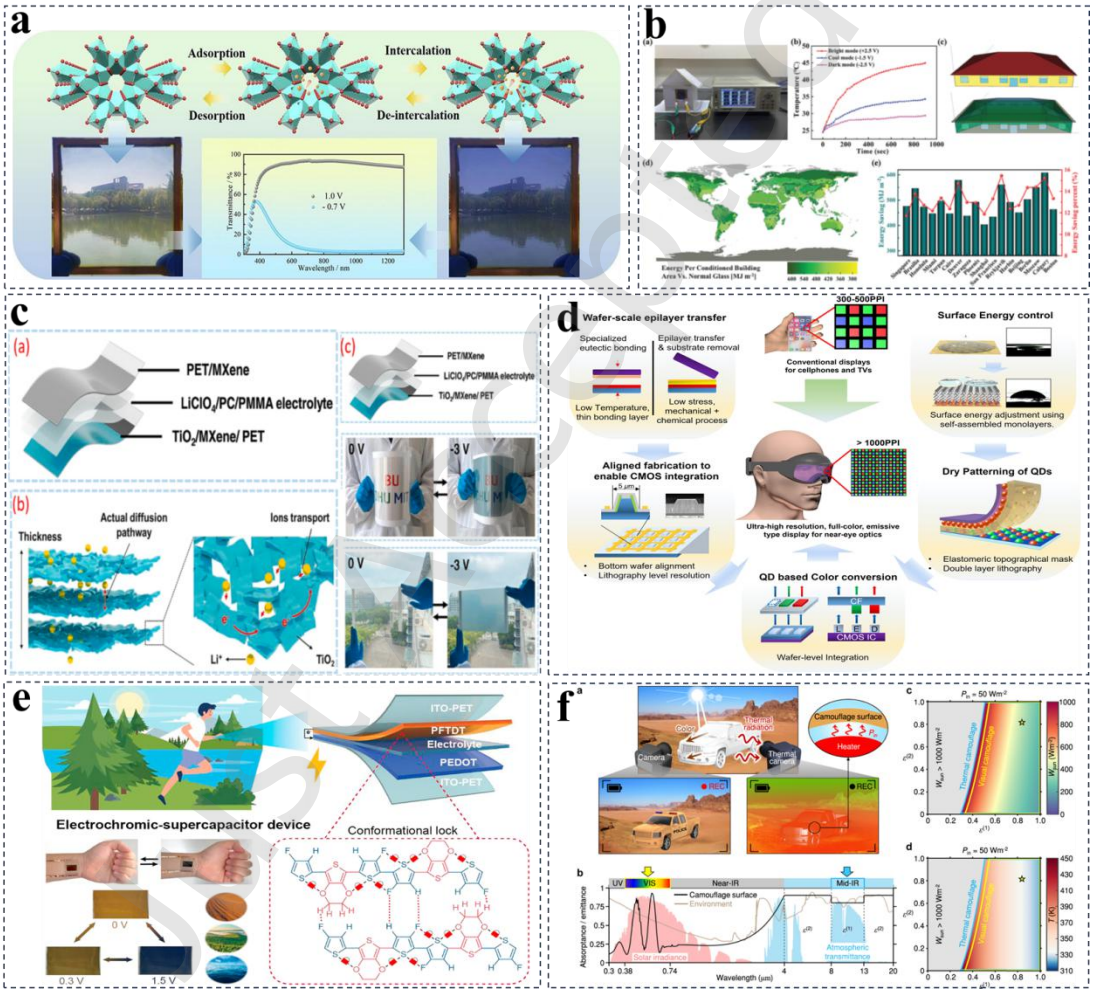

Fig.3 (a) Electrochromic performance of the small/large-area electrochromic devices[36]. Reproduced with permission.[36] Copyright 2023, Elsevier. (b) Thermal regulation and energy-saving performance of inorganic electrochromic devices [35]. Reproduced with permission.[35] Copyright 2024, Wiley-VCH GmbH. (c) Schematic representation of Mxene based flexible EESD [38]. (d) An emissive-type RGB micro-LED array with over 1000-PPI resolution[41]. (e) Wearable camouflage scene diagram of the device[45]. Reproduced with permission.[45] Copyright 2025, Elsevier. (f) Dual-band camouflage in a single environment [43].

2.1 Redox-Driven Optical Modulation

Regulation of electrochromic optical properties is primarily achieved through redox reactions. Under an applied voltage to electrochromic devices, electrons are injected from the external circuit into the electrochromic layer, while counterions in the electrolyte (e.g., H^+ , Li^+) migrate into the material under the electric field to maintain charge neutrality. This coupled insertion/extraction of electrons and ions modifies the band structure or molecular orbital energies, thereby altering visible-light absorption and enabling reversible switching of color or transmittance in **Fig.4a** [46, 47]. Tungsten trioxide (WO_3), one of the most extensively investigated inorganic electrochromic materials, provides a representative example. Upon reduction, WO_3 reacts with inserted metal cations (M^+) and electrons (e^-) to form the colored phase M_xWO_3 through the reaction: WO_3 (colorless) + xM^+ + xe^- → M_xWO_3 (blue). Within the WO_3 lattice, the concurrent incorporation of electrons and ions generates polarons or color centers, significantly enhancing absorption across the visible and near‑ infrared spectrum and imparting a deep-blue appearance. This redox-driven color modulation affords rapid response, high optical contrast, low energy consumption, and bistability—i.e., the ability to retain the attained optical state even after the external bias is removed—thereby positioning WO_3 -based systems as highly promising candidates for smart windows, anti-glare rearview mirrors, and flexible displays in **Fig.4b** [37, 48].

2.2 Ion Insertion/Extraction and Charge Compensation

The charge-compensation mechanism associated with ion insertion and extraction is fundamental to achieving reversible optical modulation in electrochromic devices. A complete electrochromic cell typically consists of two functional electrodes (at least one of which is electrochromic), an electrolyte layer, and transparent conductive substrates. Under a forward bias, the anode is oxidized and releases electrons, whereas the cathode is reduced by accepting electrons[49]. Concurrently, cations in the electrolyte (e.g., Li^+) migrate toward the cathode and intercalate into the lattice of the electrochromic material (such as WO_3) to preserve charge neutrality, reversing the bias drives deintercalation of these ions back into the electrolyte, thereby restoring

the material to its original optical state. This ion migration not only dictates the kinetics of the color change (e.g., response time) but also critically influences cycling durability [50]. When ion transport is sluggish or the host lattice undergoes irreversible structural damage during repeated insertion/extraction, coloration efficiency deteriorates and device lifetime is reduced[51]. Accordingly, improving the ionic conductivity of electrolytes, designing electrochromic materials with open ion-diffusion pathways, and constructing robust, stable interfaces have emerged as key strategies for enhancing overall device performance.

Substituting conventional liquid electrolytes with gel formulations suppresses leakage and enhances mechanical flexibility, while nanoporous electrode architectures shorten ion-diffusion paths and accelerate electrochromic response. Santosa et al.[52], for example, realized high-resolution e-paper comprising 560 nm superpixels (>25,000 ppi) made from WO_3 nanodisks that switch reversibly between insulating and metallic states in the course of electrochemical reduction, thereby enabling nanoscale control of refractive index, absorption, reflectivity, and contrast (**Fig. 4c**). Deng et al.[53] reported a water-in-eutectic gel (WIEG) electrolyte featuring a dual-network structure in which water molecules are confined within a eutectic solvent and a UV-cured hydrogen-bonded polymer matrix, and the WIEG electrolyte demonstrates a relatively wide electrochemical stability window of 3.6 V along with a high ionic conductivity of 1.1×10^{-4} S cm^{-1}. The hydrogen-bond-rich scaffold yields a broad electrochemical stability window, strong mechanical robustness, and excellent adhesion (**Fig. 4d**). The anion-selective ion conductor (ASIC) is developed by the interaction difference between ions and electronegative functional groups in the fabric substrate. Benefiting from cation immobilization and free anion transport, the anion transference number and ionic conductivity of ASIC reached 0.75 and 2.41×10^{-3} S cm^{-1} at room temperature, respectively (**Fig. 4e**)[54]. Lan et al.[55] fabricated quasi-solid-state electrolytes by electrospinning high-polarity nanofiber membranes comprising ionic liquids within a polyvinylidene fluoride (PVDF)-HFP host; the resulting PVDF-HFP/IL gel polymer electrolyte delivers >95% visible transmittance, a ionic conductivity (5.67 mS cm^{-1} at 25 °C) and a 4.40 V electrochemical window, enabling Prussian blue/WO_3 -based devices to switch reversibly from transparent to deep blue (**Fig. 4f**). Electrochromic reactions hinge on the concurrent transport of both ions and electrons to facilitate redox processes. However, electron transfer within conductive materials occurs relatively swiftly, ion migration through solid or gel electrolytes encounters a significantly higher energy barrier. Consequently, the overall reaction rate is constrained by the comparatively sluggish ion transport mechanism.

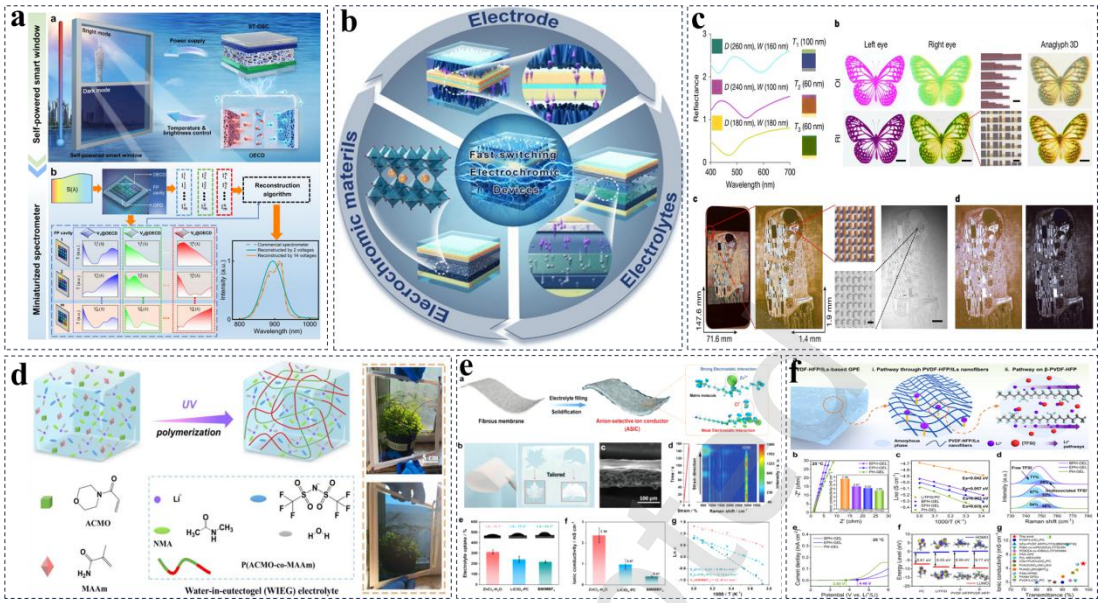

Fig.4 (a) Design and working principles of the multifunctional electrochromic platform[47].(b) Electrochromic devices based on electrodes, electrochromic materials, and electrolytes[48]. Reproduced with permission.[48] Copyright 2023, Wiley-VCH GmbH. (c) Characterization of retina E-paper display performance[52]. Reproduced with permission.[52] Copyright 2025, Springer Nature. (d) Preparation, structure, and internal interactions of the WIEG electrolyte [53]. Reproduced with permission.[53] Copyright 2025, Elsevier. (e) Characterizations and ionic conductivity of the anion-selective ion conductor (ASIC)[54]. Reproduced with permission.[54] Copyright 2025, Wiley-VCH GmbH. (f) The ionic transport pathways and electrochemical characterization of the PVDF-HFP/ILs-based GPEs[55]. Reproduced with permission.[55] Copyright 2025, Wiley-VCH GmbH.

3. Electrochromic Materials

3.1 Inorganic Materials: Transition-Metal Oxides

Transition-metal oxides were the first electrochromic materials to be explored and commercialized, with tungsten trioxide (WO_3) serving as the canonical case. Although WO_3's color change under hydrogenation was noted in the nineteenth century, systematic electrochromic investigations began in the 1970s. Thanks to its chemical stability, high coloration efficiency, and strong cycling durability, WO_3 has

become a mainstay in smart windows and anti-glare rearview mirrors[56-58], as illustrated in **Fig. 5a–c**. Nickel oxide (NiO), a prototypical anodic electrochromic material, is often paired with WO_3 in complementary configurations to lower operating voltages and boost optical modulation depth [59, 60]. Prussian blue and related analogues behave similarly, providing fast blue-to-colorless switching at low voltages with high color saturation (**Fig. 5e–f**) [61, 62]. That said, these inorganic platforms generally demand high processing temperatures, exhibit intrinsic mechanical rigidity, and pose challenges for large-area integration on flexible substrates; furthermore, their color gamut typically remains confined to blue, gray, or violet, which limits their broader deployment in flexible electronic architectures.

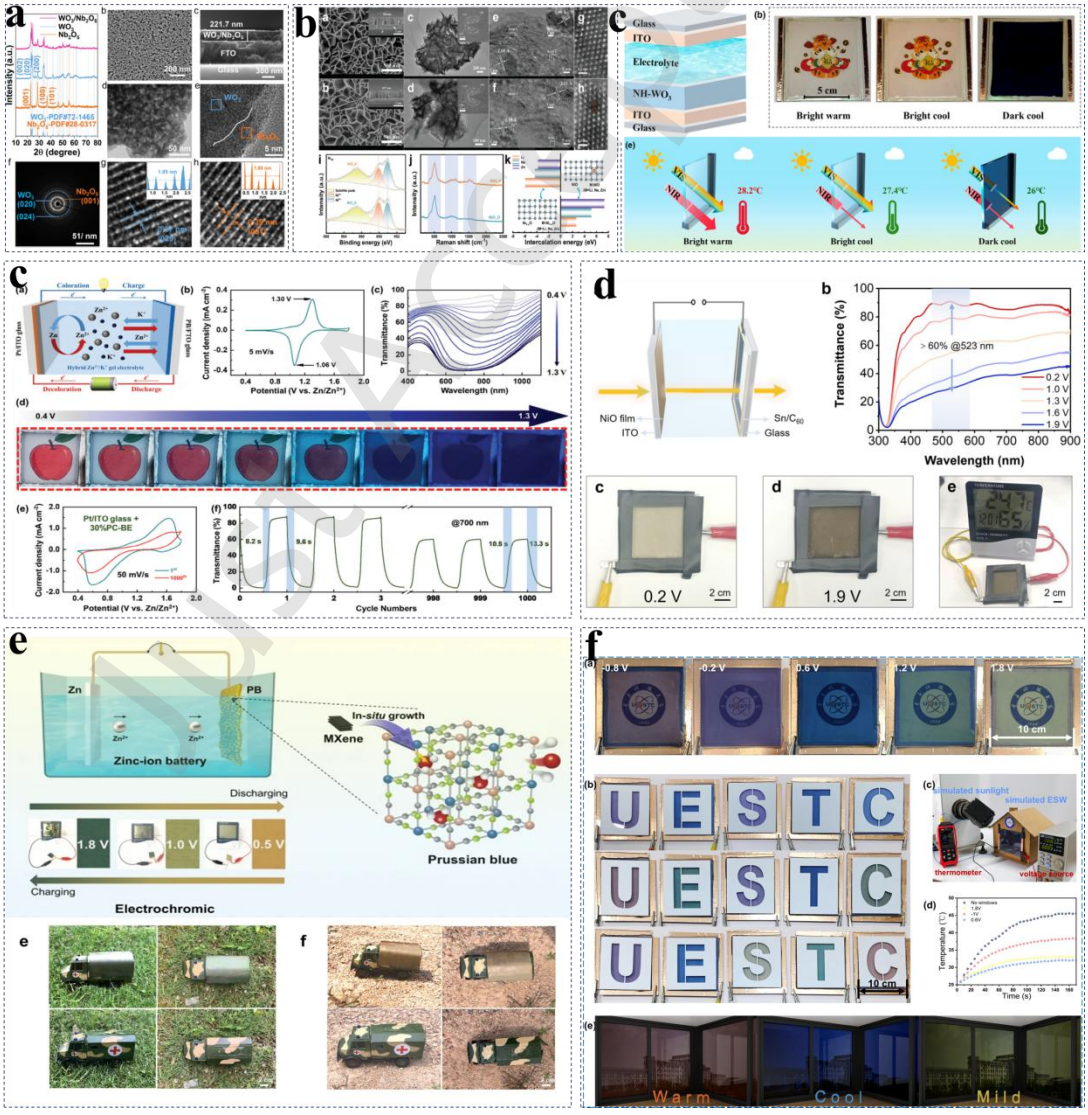

Fig.5 (a) Crystal structure and morphology of electrochromic films[56]. Reproduced

with permission.[56] Copyright 2025, Wiley-VCH GmbH. (b) Characterization of NiO_A and NiO_O electrodes[57]. Reproduced with permission.[57] Copyright 2025, Wiley-VCH GmbH. (c) Schematic diagram of the device structure [58].(d) A NiO//Sn/C_{60} electrochromic battery with its optical modulation and colored/bleached states [60].(e) Schematic diagram of the flexible electrochromic zinc ion battery based on Prussian blue, which is applied to military camouflage in grassy areas and deserts[61].(f) The AM@PB-AM@CoHCF device (10 × 10 cm^2) [62]. Reproduced with permission.[62] Copyright 2025, Elsevier.

3.2 Organic Materials

3.2.1 Small Molecule Electrochromics

To overcome the intrinsic limitations of inorganic electrochromic systems, extensive effort has been invested in creating organic small-molecule platforms, among which viologens (1,1′-disubstituted-4,4′-bipyridinium salts) are particularly prominent. Under an applied negative bias, viologens undergo two sequential one-electron reductions to form first a colored radical cation (typically purple) and then a fully reduced, nearly colorless species, thereby generating pronounced color contrast via a stepwise redox process. Their molecular framework is highly amenable to structural modification, enabling fine-tuning of side chains to precisely regulate solubility, redox potential, and chromatic response [63]. This design flexibility supports a broad range of application scenarios and has steered current research toward the systematic control of solubility, electrochemical behavior, and color through targeted molecular engineering, alongside the development of solution‑derived processing methods like spin coating and inkjet printing, while also addressing parasitic side reactions and encapsulation strategies for extended operational lifetimes[64]. As a representative example, Zhang et al. [65] developed an interfacial-chemistry strategy that decouples and simultaneously optimizes electrochromic and energy-storage functionalities in aqueous systems. By constructing TiO_2 /viologen-derivative hybrids with chemically bonded interfaces, they effectively alleviated the conventional trade-off between these two properties, thereby establishing a new materials paradigm for multifunctional electrochromic energy devices.

(1) Molecular structure modification and performance tuning

Viologen-based materials have become leading electrochromic candidates because of their excellent electrochemical stability, outstanding optical performance, and high molecular tunability. Their two-step, reversible single-electron redox

behavior underpins superior cycling durability and reliable switching between distinct optical states. Nevertheless, conventional viologen-based devices predominantly display blue-violet coloration and realizing highly stable black electrochromism requires strengthening the light-absorption capabilities of viologens. The viologen scaffold is highly amenable to structural modification, allowing precise adjustment of physicochemical properties through substitution at the 1,1'-positions. Current molecular-engineering strategies include: (i) alkyl-chain substitution, where variation of chain length and the use of symmetric or asymmetric patterns enables color tuning from blue to magenta or reddish violet; (ii) aryl substitution, in which the introduction of aromatic moieties extends or perturbs the conjugated system; (iii) asymmetric molecular design, which can support switching between colorless and black states; and (iv) incorporation of strong electron-withdrawing groups, which narrows the molecular orbital energy gap, thereby enhancing optical contrast and prolonging device lifetime.

(2) Solubility control:

Introducing alkyl chains of different lengths and polarities, polyether segments, or other functional moieties allows precise tuning of viologen solubility to match specific solution-processing routes. Viologen derivatives with long alkyl chains, for example, tend to dissolve readily in common organic solvents[66]. Hwang et al.[67] incorporated sulfonate and ester groups into a viologen-based anodic electrolyte, which boosted solubility and consequently improved both energy density and operating stability (**Fig. 6a**). Nandi et al.[68] explored B–N-fused dipyridylanthracene (BDPA) as a novel linker within viologen architectures, clarifying how this fragment influences electronic structure, optical behavior, and overall electrochromic response (**Fig. 6b**). Zong et al.[69] proposed a universal strategy for fabricating flexible, multicolor hydrogel devices from different viologen derivatives; these viologen "artificial synapses" use optical transmittance as a postsynaptic signal and exhibit coloration plasticity governed by stimulus amplitude, duration, pulse count, and frequency. Under a 1.0 V, 2.0 Hz drive, the devices displayed an 84% transmittance drop after 100 pulses and preserved short-term memory for more than 300 s (**Fig. 6c**). Bian et al.[70] synthesized one symmetrically substituted viologen (Bu_2 V) and two asymmetric analogues (BuMprV and BuEbuV), then assembled electrochromic devices employing deep eutectic solvent (DES) electrolytes. The quaternary ammonium groups yielded distinct color evolutions—yellow/green to black and red to brown. Using asymmetric viologens in BuMprV-ECD2 and BuEbuV-ECD3, together with steric and electrostatic effects from the DES media, broadened the visible/near-infrared absorption bandwidth and stabilized redox intermediates,

achieving high solar-regulation efficiencies of 35.7% and 35.3% and enhanced photothermal modulation (**Fig. 6d**).

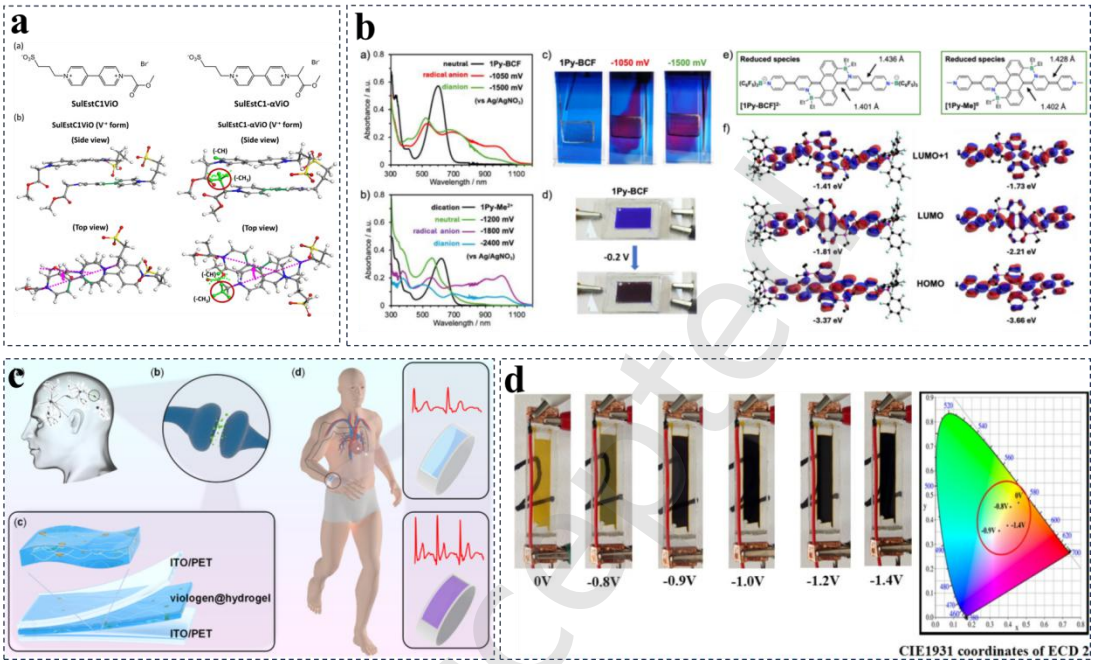

Fig.6 (a) Structural formula of two viologen derivatives[67]. Reproduced with permission.[67] Copyright 2024, American Chemical Society. (b) Spectro-electrochemical, visual, device-level, and density functional theory calculations to analyze the redox-induced electron and structural changes [68]. Reproduced with permission.[68] Copyright 2025, Wiley-VCH GmbH. (c) Schematic illustration of the human brain, biological synapse, electrochromic viologen hydrogel–based visualized synaptic device[69]. Reproduced with permission.[69] Copyright 2025, Elsevier. (d) Physical appearance and CIE1931 chromaticity coordinates of ECD1[70]. Reproduced with permission.[70] Copyright 2025, Elsevier.

(3) Redox-potential tuning.

The electronegativity and donor/acceptor character of substituents modulate the electron density on the bipyridinium core, thereby enabling fine control over the redox potentials of viologen materials—a key lever for optimizing device operating voltage and energy consumption. To clarify the origin of electrolyte alkalization in viologen systems, Jiang et al. [71] established a multimodal in situ platform combining pH monitoring, gas chromatography, and a flow cell, enabling the identification of a two- stage dynamic alkalization mechanism. Guided by this understanding, they effectively suppressed parasitic hydrogen evolution simply by

increasing the KCl concentration to 3 M, ultimately realizing a viologen-based flow battery with high energy density and excellent cycling stability (**Fig. 7a**). Gao et al.[72] synthesized a family of sulfur-bridged 2,2′-viologens, termed 2,2′-thienoviologens (2,2-SV^{2+}). Compared with conventional 2,2′-viologens and previously reported sulfur-containing 4,4′-viologens, 2,2-SV^{2+} exhibits stronger visible-light absorption, narrower band gaps, more negative reduction potentials (by 160 mV relative to sulfur-containing 4,4′ analogues), and more stable radical states (**Fig. 7b**). Zhang et al. [63] extended the conjugation of viologens by introducing phenyl substituents on the pyridyl side chains and appending strong terminal electron-withdrawing groups such as $–CF_3$, $–OCF_3$, and $–SCF_3$, thereby lowering band gaps and enhancing electronic transition efficiency. Using these viologen derivatives as cathodic materials paired with 2-chloro-6-(diethylamino)fluorescein (F-Cl) counter electrodes, they assembled complementary bipolar electrochromic devices, as illustrated in **Fig.7c**.

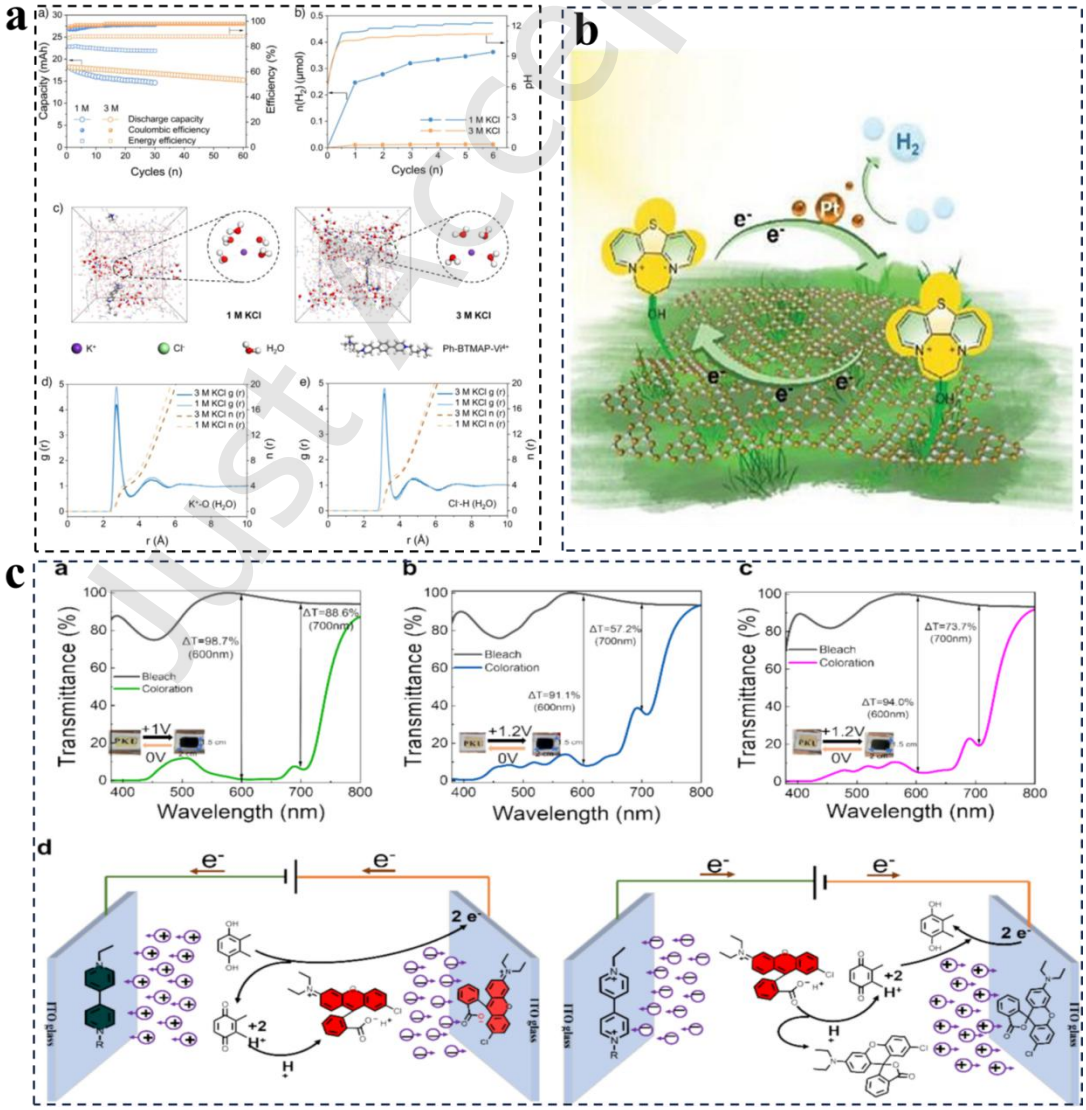

Fig.7 (a) Influence of ion concentration on hydrogen evolution and solvation structure in viologen‐ based anolytes [71]. Reproduced with permission.[71] Copyright 2025, Wiley-VCH GmbH. (b) Schematic diagram of 2,2′-thienoviologens for electrochromism coupled with visible‐ light‐ driven hydrogen production [72]. Reproduced with permission.[72] Copyright 2024, Wiley-VCH GmbH. (c) Spectroelectrochemistry of ECDs under different voltages and maximum optical contrast, and electrochromic schematic of devices[63]. Reproduced with permission.[63] Copyright 2025, Elsevier.

(4) Side-chain modification and color tuning.

Beyond shifting redox potentials, strategic tailoring of side chains can alter the absorption spectra of both radical cations and fully reduced species, enabling fine-grained control over electrochromic color. Although classical viologens typically display blue–violet hues, judicious molecular design broadens the chromatic palette [73, 74]. For example, introducing methyl-β-cyclodextrin into a benzacetyl viologen derivative markedly enhances solid/liquid-state fluorescence, yields photo-/thermo-/chemo-responsive tristimulus coloration with excellent reversibility and cycling durability, and allows dynamic fluorescence modulation synchronized with color transitions, offering new avenues for information security and smart-window applications (**Fig. 8a**) [40]. Coupling upconversion nanoparticles with electrochemically responsive molecules permits time modulation of anti-Stokes emission by electrically tuning the orbital energy levels of ligands; this demonstration of reversible molecular absorption control enables real‐ time color modulation of anti‐ Stokes emission from individual particles (**Fig. 8b**) [75]. In addition, an electrochromic system based on heteroaromatic tripyridine (H-TriPy) leverages π-stacking engineering to substantially enhance near-infrared absorption and achieve dual-band modulation across the visible and NIR regions. Incorporating fluorinated ionic liquids suppresses irreversible aggregation at high H-TriPy concentrations, producing near-zero transmittance (<1.6% average) across both bands and retaining 89.1% performance after 100,000 cycles, while large-area devices deliver uniform coloration and robust durability, underscoring their promise for green-building deployment (**Fig. 8c**) [76]. Moreover, employing bipolar (triethylene glycol and ester) side chains in conjugated-polymer electrochromic devices generates a pronounced synergistic effect: substituting bipolar for alkyl side chains boosts cycling stability by more than 1,600%, shortens coloration time by 58%, raises coloration efficiency by 57%, and lowers driving voltage by 25%. This synergy arises because bipolar side chains facilitate charge transport and accelerate ion diffusion, thereby creating more favorable pathways for ionic motion (**Fig. 8d**) [77].

Viologens remain compelling because their readily adjustable molecular frameworks support targeted side-chain engineering, enabling simultaneous control over solubility, redox potential, and optical output while preserving compatibility with solution‐ phase fabrication routes such as spin coating or inkjet printing [16, 66]. Nonetheless, their deployment is hampered by irreversible side reactions that accumulate during extended cycling—leading to gradual degradation and diminished performance—and by the prevalence of liquid-state configurations that demand careful encapsulation to avert electrolyte leakage, collectively complicating large-scale integration and long-term reliability.

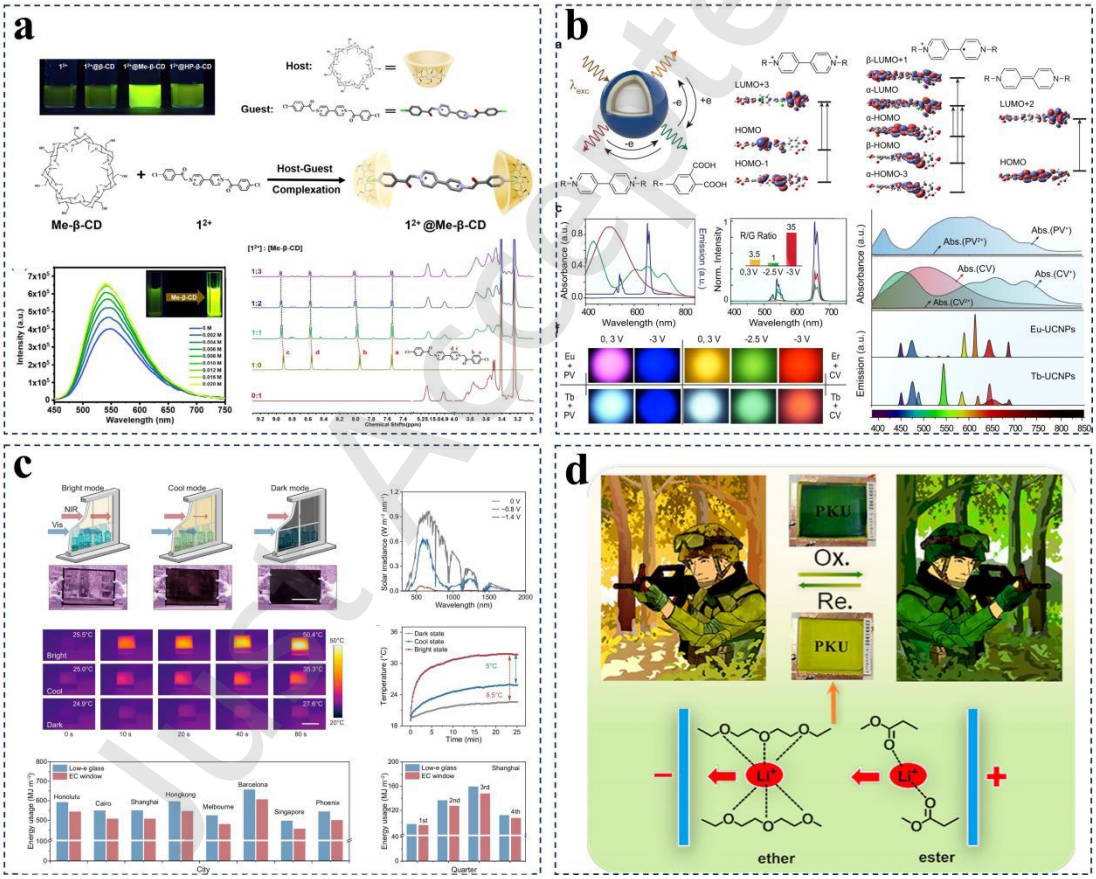

Fig.8 (a) Fluorescence titration, emission spectroscopy [40]. (b) Multicolour luminescence switching of UCNPs through opto-electrochemical modulation[75]. (c) Energy‐ efficient dual‐ band electrochromic window enabled by H‐ TriPy [76].(d) photo of PFS-2 device in coloring state and neutral state [77]. Reproduced with permission.[77] Copyright 2024, Wiley-VCH GmbH.

3.2.2 Conjugated Polymers

Conjugated polymers integrate intrinsic electrochemical activity, broad and tunable color ranges, solution-processable film formation, and mechanical flexibility, positioning them at the forefront of electrochromic research since Garnier's seminal 1983 work on pyrrole- and thiophene-based systems. Prototypical examples such as PANI, PPy, and PEDOT can access multiple distinct optical states (e.g., PANI cycling among colorless/green/blue), and PEDOT:PSS dispersions have become ubiquitous in flexible electronic platforms. Recent progress includes: (i) Ga-nanoparticle-doped PEDOT:PSS composites in which rapidly generated/reduced Ga_2O_3 shells fracture under an applied field to create additional ion/electron transport channels and thereby accelerate charge transfer (**Fig. 9a**) [78]; (ii) lactone-functionalized oxa-anthracene copolymers whose acid- and electrochemically responsive backbones modulate π–π overlap to yield programmable optical responses (**Fig. 9b**) [79]; (iii) dual-cathode electrochromic energy-storage devices using polyviologen/$WO_3 \cdot 2H_2O$ cathodes, PEDOT:PSS as a protective/proton-conducting layer, and Zn-mesh anodes, achieving four distinct optical modes, sub-2 s switching, a coloration efficiency of 389.44 C cm^{-2}, an areal energy density of 141.9 mAh m^{-2}, 6,600-cycle stability, self-coloring/bleaching behavior, and up to 44.4% energy recovery (**Fig. 9c**) [80]; and (iv) PEDOT:PSS-based optical artificial synapses that leverage optimized gel electrolytes to realize millisecond-scale responses, 82.9% modulation at 700 nm, multilevel states, and biologically inspired paired-pulse facilitation (**Fig. 9d**) [81]. Despite these advances, persistent challenges arise from the electrically insulating PSS component: while it imparts water dispersibility and mechanical robustness, it simultaneously limits charge transport, thereby reducing coloration efficiency and slowing switching kinetics—key obstacles to deploying PEDOT:PSS in next-generation high-performance smart devices.

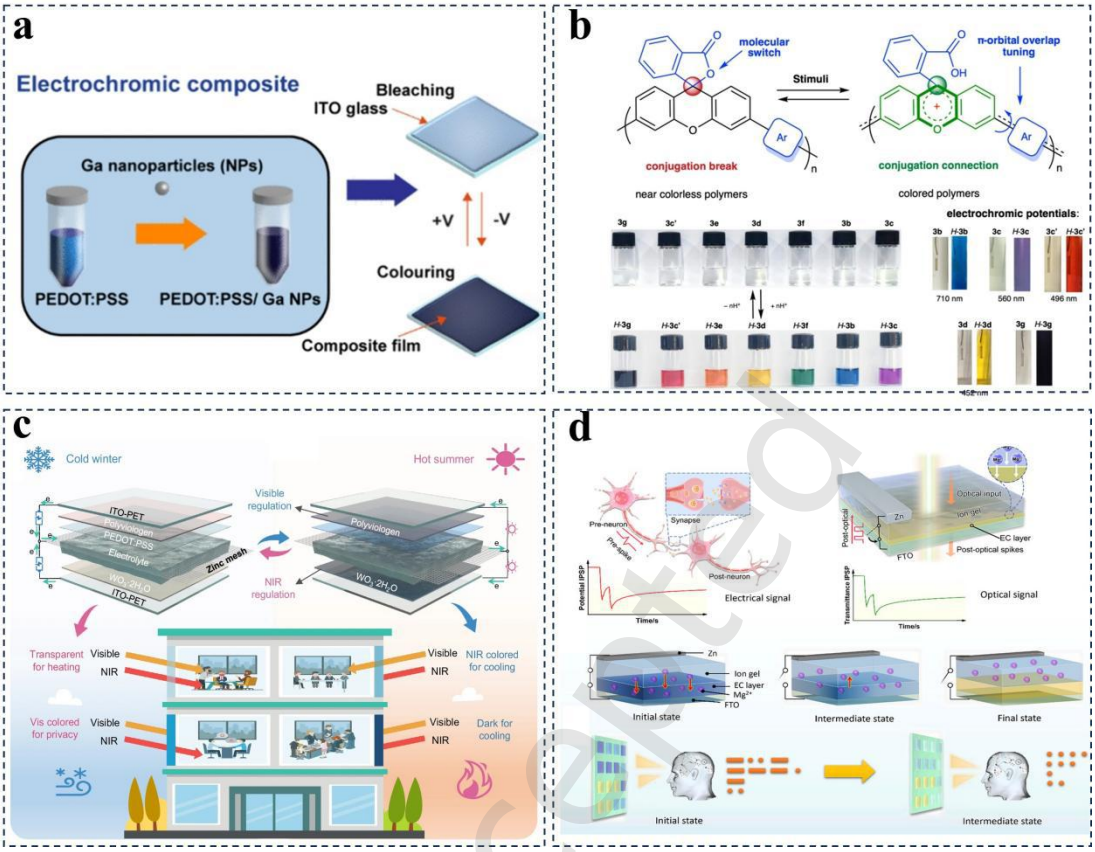

Fig.9 (a) Schematic representation of the step-by-step fabrication process of the PEDOT:PSS/Ga NP composite films[78]. Reproduced with permission.[78] Copyright 2025, American Chemical Society. (b) Design, synthesis and reversible control of the conjugation-tunable polymer [79]. Reproduced with permission.[79] Copyright 2025, Springer Nature. (c) Diagram depicting the structural design and operation principle of the devices[80].(d) A bioinspired electrochromic artificial synapse mimics neuronal signal transduction via optically modulated ionic/electronic coupling[81]. Reproduced with permission.[81] Copyright 2025, Wiley-VCH GmbH.

3.2.3 Aromatic Polymers

Aromatic polymer–based electrochromic materials are typically anodic, undergoing oxidation-induced color changes (from colorless to green/blue/purple) that broaden the attainable device color palette. Among them, triphenylamine (TPA)-containing systems—including polyimides, polyamides, and related architectures—address earlier solubility and processability challenges by incorporating TPA units into the polymer backbone. This design strategy enhances solubility in organic solvents while retaining excellent thermal and electrochemical stability. Representative developments in **Fig.10a** include TPA-functionalized MR- TADF emitters

(BNCz- pTPA/mTPA) that leverage aggregation-induced emission enhancement (AIEE) to balance charge-transfer and locally excited states for spectrally narrow emission[82]; TPA/thiophene dual-redox polymer electrodes that enable flexible electrochromic supercapacitors with a specific capacitance of 37 F g^{-1} at 1 A g^{-1} and 54% transmittance modulation at 550 nm in **Fig. 10b** [83]; TPA–Mn polymer films exhibiting voltage-dependent three-state color switching (colorless→brown-yellow→blue) in solid-state devices in **Fig. 10c** [84]; and TPA–imidazolium ionic-liquid hybrids (EFIL- TPA) that realize dual-mode (reflective/emissive) displays driven at <1.0 V, with 0.57–1.8 s switching times and 91% retention after 10,000 cycles, even when powered by body-motion–harvesting piezoelectric nanogenerators in **Fig. 10d** [85]. Collectively, these studies highlight how careful molecular engineering around TPA motifs can deliver high-performance anodic materials tailored for low-power, long-lifetime complementary electrochromic devices[86].

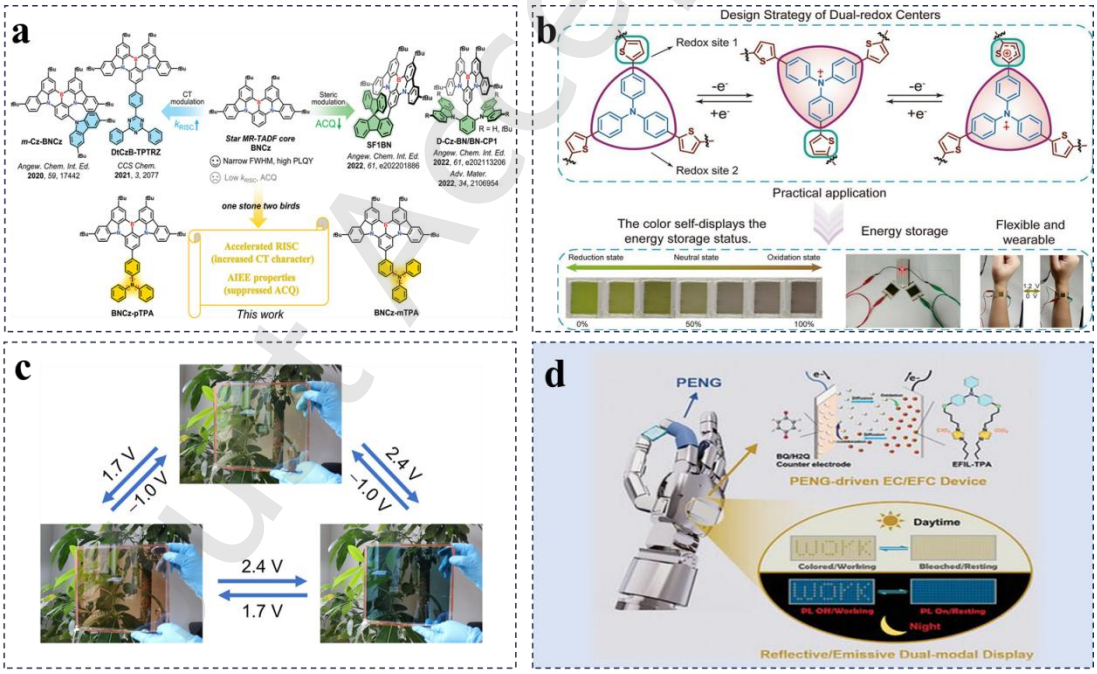

Fig.10 (a) Molecular structure and design strategy of BNCz-pTPA and BNCz-mTPA[82]. Reproduced with permission.[82] Copyright 2023, Wiley-VCH GmbH. (b) Expected double redox mechanism of PTTPA, and implementation of a patterned PTTPA- based flexible EC–SC device in real- world scenarios[83]. Reproduced with permission.[83] Copyright 2025, Elsevier. (c) Images of the large- area (20 × 20 cm^2) electrochromic device under different bias voltages [84]. Reproduced with permission.[84] Copyright 2025, Wiley-VCH GmbH. (d) Structure

illustration and electrochemical properties of EC/EFC device[85]. Reproduced with permission.[85] Copyright 2023, Wiley-VCH GmbH.

3.3 Hybrid and advanced materials

3.3.1 Metal-Supramolecular Polymers

Metal–supramolecular polymers (MSPs) couple solution-processable organic backbones with metal-centered d–d or metal-to-ligand charge-transfer transitions, producing strong—often near-infrared—electrochromic responses well suited for IR camouflage and thermal-management applications[87, 88]. Early work was constrained by poor solubility and sparse structural insight, but recent coordination-chemistry advances now permit well-defined, reversibly redox-active architectures. For instance, Wang et al.[89] used supramolecular interactions to realize bistable color states, achieving deep-purple↔transparent switching with 1.3 s/3.8 s response times, a coloration efficiency of 1052.5 $cm^2 C^{-1}$ at 576 nm, and only 14.1% performance loss after 1000 cycles (**Fig. 11a**). Incorporating molecularly engineered conjugated spacers into PolyFe-PF_6 strengthened optical memory while preserving comparable metrics (**Fig. 11b**) [90]. Electrostatic spray deposition of tris(bipyridyl)benzene–Fe(II) coordination networks yielded uniform MSP-Fe films that combine electrochromism with charge storage, delivering ~1104 $cm^2 C^{-1}$ coloration efficiency, 71.7% optical contrast, and 12.01 $mAh\ g^{-1}$ capacity (**Fig. 11c**)[46]. Hybrid architectures that integrate poly-ProDOT with rhodamine-based switchable chromophores exploit ProDOT's film quality and optical memory together with the rhodamine's tunable, high-contrast bistability to realize dual-responsive devices (**Fig. 11d**)[91].

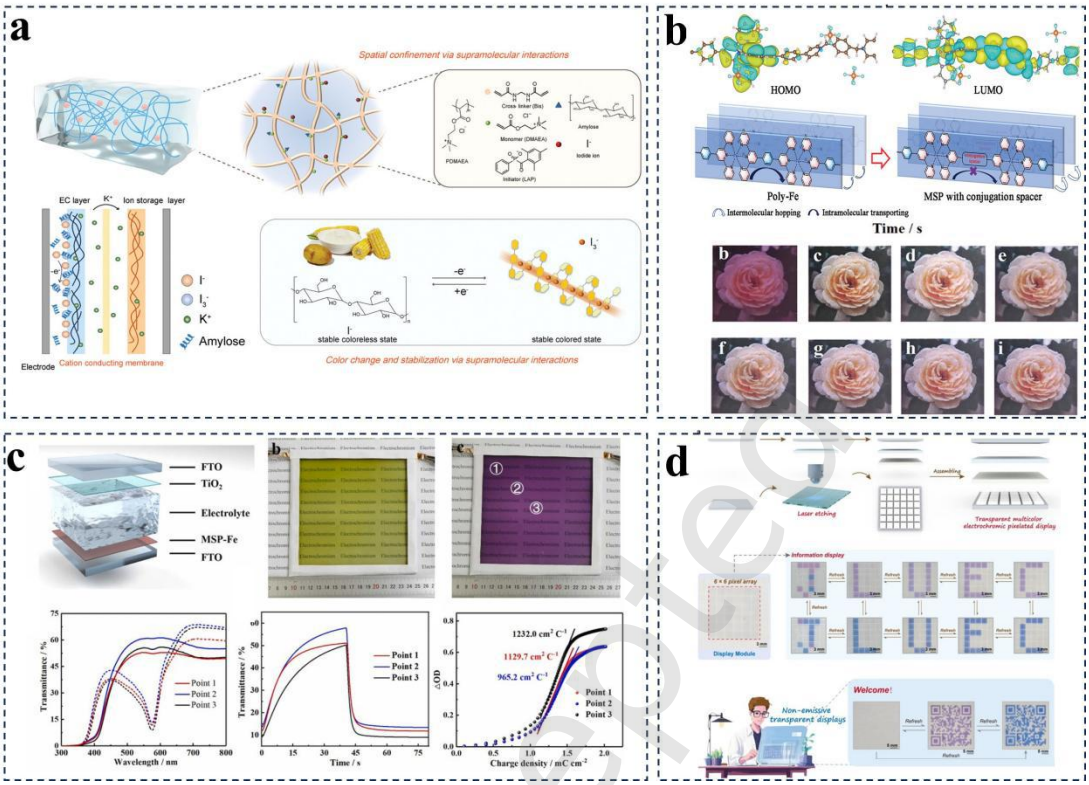

Fig.11 (a) Design of bistable eletrochromic systems based on supramolecular interactions[89]. Reproduced with permission.[89] Copyright 2024, Wiley-VCH GmbH. (b) The theoretical analysis and the optical photographs of PolyFe-PF6 [90]. Reproduced with permission.[90] Copyright 2025, Wiley-VCH GmbH. (c) A large-area semi-solid-state electrochromic device—comprising an MSP-Fe electrochromic layer[46]. Reproduced with permission.[46] Copyright 2023, Elsevier. (d) Digital-controlled information and potential application[91].

3.3.2 Porous Frameworks (MOFs/COFs)

Metal–organic frameworks (MOFs) and covalent organic frameworks (COFs) provide ultrahigh surface areas, ordered porosity, and programmable active sites that collectively promote rapid ion transport and maximize exposure of electroactive centers—attributes that suit them particularly well for high-efficiency electrochromism [92-95]. MOF-based electrochromic research began with Dincă 2013 Zn–bis(pyrazolyl) naphthalene diimide films, which formed robust, adherent coatings capable of multicolor, solid-state reversible switching, as confirmed by cyclic voltammetry and in situ UV/Vis spectroscopy (**Fig. 12a**) [96]. A more recent exemplar is conductive Cu-truxone, whose electrochromism originates solely from linker-localized, oxygen-reducible carbonyl units rather than metal nodes; the material operates below 1 V and achieves a coloration efficiency of 193.6 $cm^2 C^{-1}$, underscoring its low-power promise (**Fig. 12b**) [97].

COFs, first demonstrated for electrochromism in 2019 with triphenylamine–dithienyl conjugated frameworks, leverage crystalline order and tunable building blocks to deliver efficient charge transport and color control across optoelectronic platforms[98]. Although several electrochromic COFs (ecCOFs) have been reported, multicolor assemblies (≥3 redox states) remain scarce; Silori et al. [99] advanced the field by constructing a metal-free Schiff-base COF from tris(4-aminophenyl)amine and terephthalaldehyde that exhibits four distinct electrochromic states—orange, pear-green, green, and cyan—expanding the achievable palette (**Fig. 12c**).

MOF/COF hybrids aim to unite the chemical versatility of metal nodes with the structural robustness of covalent frameworks, simultaneously addressing MOFs' stability issues in polar media and the catalytic or electronic limitations of all-organic COFs[100]. Representative advances include NKM-908, a zirconium MOF built from a tetradentate NDI ligand that reversibly cycles through colorless→pale yellow→green states (Li et al. [101], **Fig. 12d**); Shupletsov's conformationally constrained MOFs that lock Picard-type linkers into fixed geometries, achieving 12.5 s coloration, 90 % transmittance modulation, and transparent/red/black tristability comparable to inorganic electrochromics (**Fig. 12e**) [102]; and multivariate UiO-67 frameworks co-doped with Ru-bipyridyl centers and sulfonated linkers to enhance charge transport and electrochromic efficiency (Thomas et al.[103], **Fig. 12f**). Extending the hybrid concept to 3D metalized COFs, Hao et al. [104] fabricated Ti-DHTA-Py, which exhibits narrowed band gaps, 2.5 s/0.5 s coloration/bleaching times, a coloration efficiency of 423 $cm^2 C^{-1}$, and 93.6 % retention after 500 cycles (**Fig. 12g**).

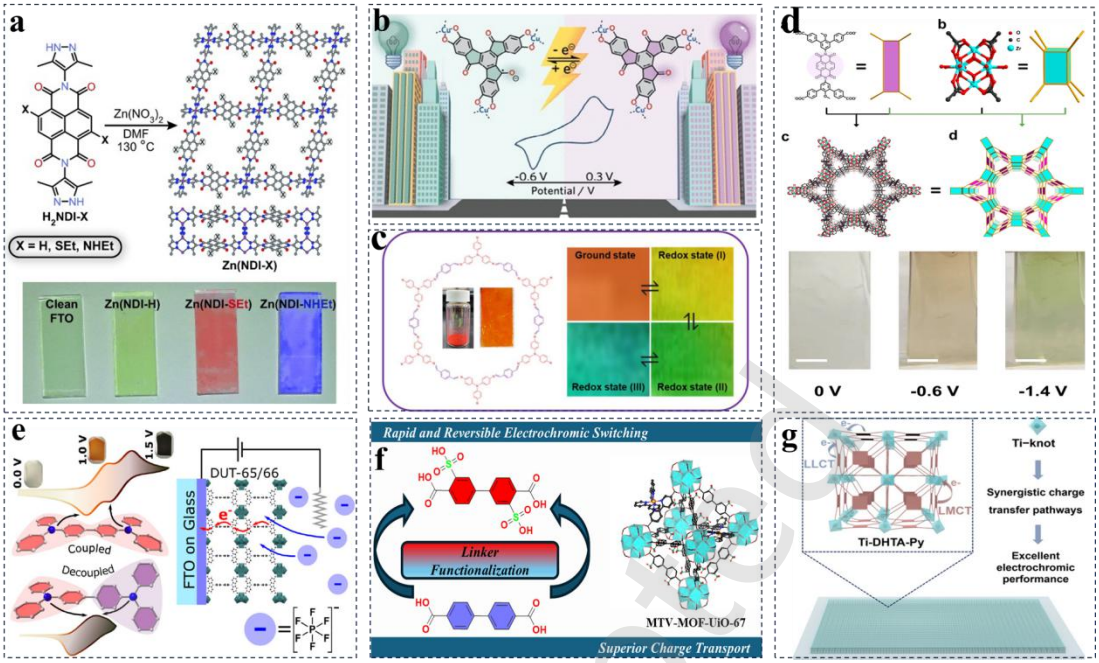

Fig.12 (a) Synthetic route and DFT- simulated structures of Zn(NDI- X) [96]. Reproduced with permission.[96] Copyright 2013, Wiley-VCH GmbH. (b) Proposed electrochromic mechanism of Cu-truxone[97]. Reproduced with permission.[97] Copyright 2025, American Chemical Society. (c) As-synthesized TAPA-PDA ecCOF film and visuals of four-state multielectrochromism [99]. Reproduced with permission.[99] Copyright 2025, Wiley-VCH GmbH. (d) Construction of NKM-908 and optical images of NKM-908 thin film[101].(e) Integration of the Piccard- type ligand N,N,N′,N′- benzidinetetrabenzoate into Zr- MOF frameworks [102]. Reproduced with permission.[102] Copyright 2024, American Chemical Society. (f) Linker structures of single cage of RuBPY-UiO-67-SO3H[103]. Reproduced with permission.[103] Copyright 2025, American Chemical Society. (g) Charge transfer pathways in 3D Ti-DHTA-Py and 2D DHTA-Py framework structures[104]. Reproduced with permission.[104] Copyright 2024, American Chemical Society.

MOF/COF have attracted much attention due to their unique ultra-high specific surface area, adjustable pore size and abundant active sites. These materials have their own advantages in specific surface area and pore size (for example, COF usually has a larger pore size to facilitate ion diffusion). However, most MOFs/COFs exhibit relatively low conductivity/ion conductivity, resulting in higher drive voltages (>1 V) to translate MOF/COF architectures into fast-switching electrochromic devices. Conductive MOFs (c-MOFs) can address the issue of conductivity, but they are often restricted to the redox activity of metal nodes[97, 105]. Approaches such as infiltrating conductive polymers into COF pores can improve charge mobility[106], yet device-grade conductivity levels that are both high and reproducible have not been realized. Manufacturing constraints add further impediments: solvothermal syntheses

and complex interface or microfluidic assembly routes limit throughput, and even nascent 3D-printing methods must preserve the frameworks' surface area, porosity, and morphology to avoid performance losses[107]. Consequently, commercial deployment of MOF/COF electrochromics will require coordinated advances in conductivity enhancement, process simplification, and adaptive form-factor engineering.

3.3.3 Flexible Polymer Electrochromic Materials

Electrochromic technology has progressed dramatically since Platt's 1961 concept, driven in recent years by the rise of flexible, multifunctional wearables[108]. Notable milestones include high-lithium solid electrolytes (LiRSEs) that integrate excess $LiBF_4$, deep-eutectic liquid phases, and polyurethane matrices to form 88.7% transparent, well-adhered films. These support flexible electrochromic devices with 2.5 s/4.5 s coloration/bleaching times, 7,500-cycle endurance with 94.1% retention, and robust temperature tolerance (**Fig. 13a**)[109]. Oxygen-deficient $W_{18}O_{49}$ nanowire-based dual-band EC/energy-storage modules deliver large optical modulation, long operating lifetimes, and high energy-recovery efficiencies while relying on a single tungsten-oxide component to ensure spectral selectivity (**Fig. 13b**) [110]. Localized-dissociation solid polymer electrolytes plasticized with succinonitrile achieve rapid Li^+ transport without sacrificing solid-state integrity, yielding dual-band smart windows that switch quickly, remain highly stable, modulate 85% at 673 nm, 70% at 1200 nm, and 43% at 1600 nm, and operate in three distinct modes (bright/cool/dark) to enhance building energy efficiency (**Fig. 13c**) [111]. Finally, n-doped capacitive transparent conductors (n-PBDF) function simultaneously as ion reservoirs, streamlining all-polymer EC displays that are solution-processable, flexible, low-power, bistable, and capable of full-color output—traits that broaden their suitability for wearable electronics (**Fig. 13d**) [112]. As a result, In **Table 1**, it compares the overall performance envelope of organic/hybrid systems with inorganic EC materials and identifies specific improvement strategies for long-term stability and high coloration efficiency that remain to be addressed.

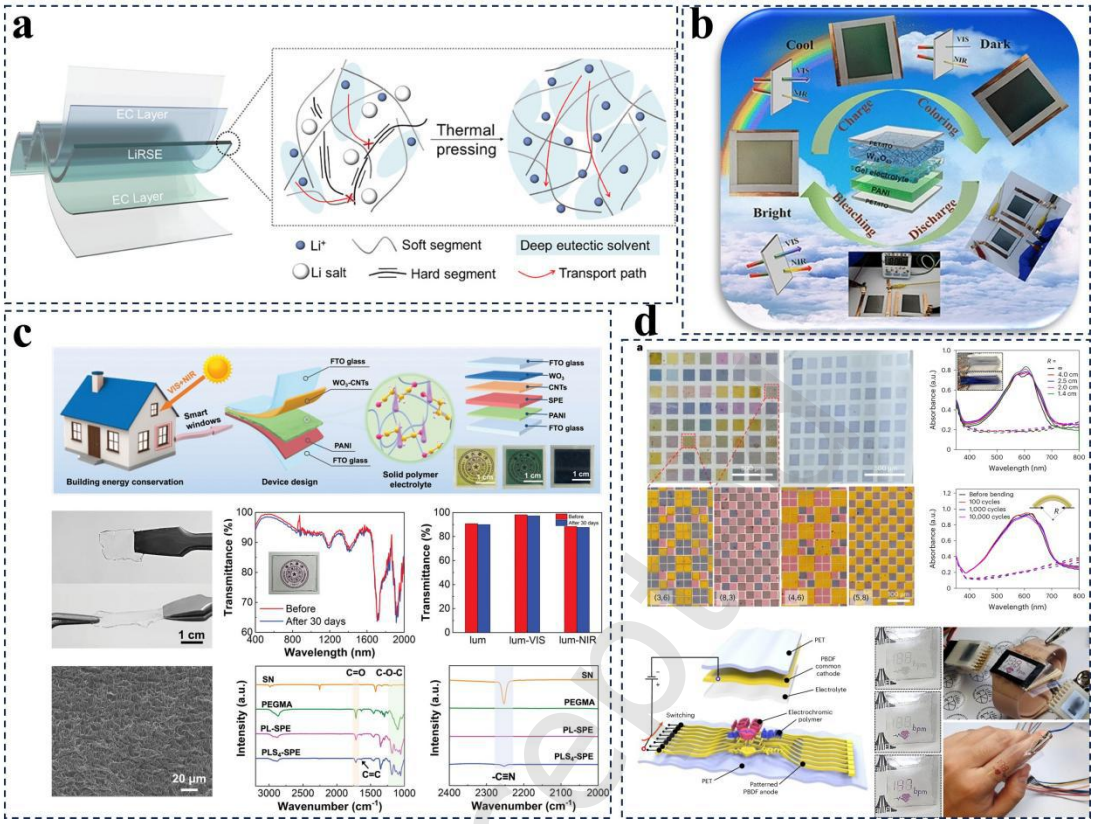

Fig.13 (a) Flexible EC devices with the LiRSE [109]. Reproduced with permission.[109] Copyright 2025, Wiley-VCH GmbH. (b) Dual- band electrochromic devices for spectrally selective modulation of VIS and NIR light [110].(c) Schematic illustration of the SPE-based EC smart windows and the characterization of PLS4-SPE films[111]. Reproduced with permission.[111] Copyright 2024, Wiley-VCH GmbH. (d) Photographs and optical images of a full-colour, all-polymer electrochromic display[112]. Reproduced with permission.[112] Copyright 2024, Springer Nature.

Table 1. Comparison with different electrochromic materials

Materials	Merits	Drawbacks	Improvement strategies	Ref.
Cu	Cost-effectiveness; mirror state	Poor stability; red color change	Electrolyte optimization	[113, 114]
TiO_2	Robust photothermal and environmental stability; cost-effectiveness	Imperceptible color change; slow color switching	Composite with other conductive materials	[115]
WO_3	VIS-NIR regulation; large optical modulation	Eye unfriendly blue; low conductivity	Doping; oxygen vacancy	[116, 117]
Organic molecules	Quick response; rich color variation	Poor photothermal	Composite with counter ions and redox agents	[79, 118,

		stability		119]
Conducting polymers	Rich color variation;rapid switching speed; high coloration efficiency	Poor cycling and photothermal stability	Morphology regulation	[120, 121]
Organic metal complexes	Rich color variation; high coloration efficiency	Narrow band regulation	Adjustment of the ligand structure	[80]

4. Electrochromic integrated devices

4.1 Macroscopic Structural Design

Conventional flexible electrochromic devices (FECDs) typically adopt a five-layer configuration—flexible substrate, transparent conductor (e.g., ITO, Ag nanowires), electrochromic layer, ion-conducting electrolyte, and counter/ion-storage electrode—in which an applied bias drives ion migration and associated redox reactions, producing color changes [122]. Although this stacked architecture has been widely demonstrated in smart windows and displays, it suffers from several drawbacks: (i) interfacial fragility arising from the integration of dissimilar layers, which can lead to delamination, void formation, or mechanical failure under bending or prolonged cycling; (ii) complex fabrication workflows (photolithography, masked deposition, sequential spin coating under cleanroom conditions) that increase cost and hinder scalable or customized production; and (iii) impedance mismatches between individual layers, which become particularly problematic under large-strain deformation, thereby limiting charge transport and degrading switching speed as well as sensing accuracy [123-125].

To address these challenges, next-generation FECDs prioritize simplified architectures with multifunctional layers to reduce interfacial defects and processing complexity. Xue et al. [126] developed a self-charging/discharging flexible trilayer "sandwich" (NiHCF electrochromic cathode / PAM ion gel / PB electrochromic cathode) that autonomously drives multicolor switching without auxiliary electrodes. Zhang et al. [47] designed a five-layer complementary stack (ITO/PEDOT:PSS/gel/PBFDO/ITO) in which PEDOT:PSS functions concurrently as anodic electrochromic material and ion-storage layer, enhancing energy utilization while removing redundant components. Wang et al. [127] realized a trilayer nanogel coating via microemulsion polymerization: a hydrophobic PDMS top layer suppresses moisture ingress and hydrogen evolution, a fluorinated middle layer accelerates Zn^{2+} desolvation and transport, and a viscoelastic adhesive bottom layer preserves intimate electrode contact during repeated cycling. In a complementary approach, n-PBDF operates as both transparent conductor and ion reservoir in all-polymer EC displays,

eliminating a discrete counter electrode and enabling single-sheet, fully solution-processable integration with high mechanical flexibility [112].

4.2 Microscopic Collaborative Optimization Path

Maintaining low elastic moduli while sustaining fast electrochromic switching is central to FECD performance under high strain[128]. Conventional PET substrates[129] paired with brittle TCOs (e.g., ITO or IZTO) preserve optical transparency yet fracture when flexed [130, 131], motivating the adoption of tougher transparent conductors such as Ag-nanowire/PEDOT:PSS hybrids and other adaptive architectures[132]. Electrolyte advances are likewise crucial: ionic-conductive films that simultaneously offer >90% transparency, room-temperature ion conductivity of 0.11 mS cm^{-1}, broad electrochemical windows (3.55 V), and ultrathin flexibility—exemplified by Gong et al.'s PVDF-based composites for multicolor devices—highlight the potential of tailored polymer blends [133]. In parallel, integrated platforms that combine stretchable organic/nanomaterial electrodes, semiconductors, current collectors, and co-fabricated diodes, sensors, EC displays, and antennas (as demonstrated by Matsuhisa et al. [25]) address the challenges of high-frequency operation under deformation, collectively charting a path toward robust, strain-tolerant electrochromic systems.

4.2.1 Nanocomposite Reinforcement Strategies

Electrochromic performance improvements rely on two complementary approaches: (i) introducing dopants or forming composites that enhance mechanical robustness without compromising redox kinetics, and (ii) engineering hierarchical architectures that facilitate efficient charge and ion transport [134-136]. Among available co-components, carbon nanotubes[137-139], rGO[22, 140, 141], and MXenes[142-144] are particularly effective. For example, MXene/WO_{3-x} hybrid films exhibit higher Li^+ diffusion coefficients and improved stability over 200 cycles compared with pristine WO_{3-x} in micro-supercapacitors (**Fig. 14a**) [135], while MXene/WO_3 Fabry–Pérot microcavity actuators integrate large, reversible bending deformations (up to 95°) with electrochromic modulation under low bias through ion-insertion-induced stress and concomitant absorption shifts (**Fig. 14b**) [145]. MXene–rGO aerogel scaffolds mitigate nanosheet restacking and enhance mechanical

durability (**Fig. 14c**) [146], and covalently crosslinked blue-phase liquid crystals combined with low-emissivity MXenes form 3D soft photonic crystals capable of simultaneously tuning visible coloration and mid-IR emissivity for stealth applications (**Fig. 14d)** [147]. Taken together, these bilayer and multilayer configurations improve electronic percolation and structural resilience, emphasizing composite design as a key strategy for next-generation electrochromic systems.

4.2.2 Micro/Nanostructure Regulation and Reaction Kinetics

Micro/nanostructuring electrochromic layers expands electrochemically active surface area, enhances optical throughput, and enables auxiliary sensing functions. Hu et al. [148] stacked patterned chromatic layers on metal-mesh transparent electrodes to realize EC/transparent supercapacitor/Zn-battery hybrids with 88% visible transmittance (**Fig. 14e**). Chen et al. [149] introduced a hemispherical ECPVD architecture—Ag-nanowire conductor/H_3PO_4–PVA microstructured electrolyte/$W_{18}O_{49}$ electrochromic layer—that offers spacing-defined tunability over 0–250 kPa, reflective coloration for high outdoor visibility, and repeatable erasure (+1 V bleaching retaining 75% modulation after 200 cycles) to deliver "sense-and-display" functionality under intense lighting (**Fig. 14f**). Zhu et al. [150] directly ink-printed convex parallel-line microarrays serving as pressure-sensing layers (20.25 kPa^{-1} sensitivity, 35 kPa linear range, ~5000-cycle endurance) integrated with patterned electrochromic displays that switch in <0.4 s and sustain >6000 s continuous operation (**Fig. 14g**). Wrinkled polyaniline films formed via in situ self-wrinkling were theoretically and experimentally validated to bolster strain tolerance (**Fig. 14h**) [151], whereas Zhao et al. [152] engineered three-dimensional "nanoknot" interphases in $W_{17}O_{47}$/($NaWO_3$-knots)@PEDOT:PSS hybrids to strengthen interfacial electron pathways, producing flexible bifunctional electrodes with superior electrochromic response (**Fig. 14i**). Collectively, such hierarchical motifs accelerate reaction kinetics, preserve optical clarity, and impart multimodal capabilities to next-generation electrochromic composites. However, the micro and macro structure design is only the basis to promote the development of multifunctional electrochromic technology, and it is also necessary to develop various materials, structures and fabrication methods to improve the performance of devices（**Table 2**）.

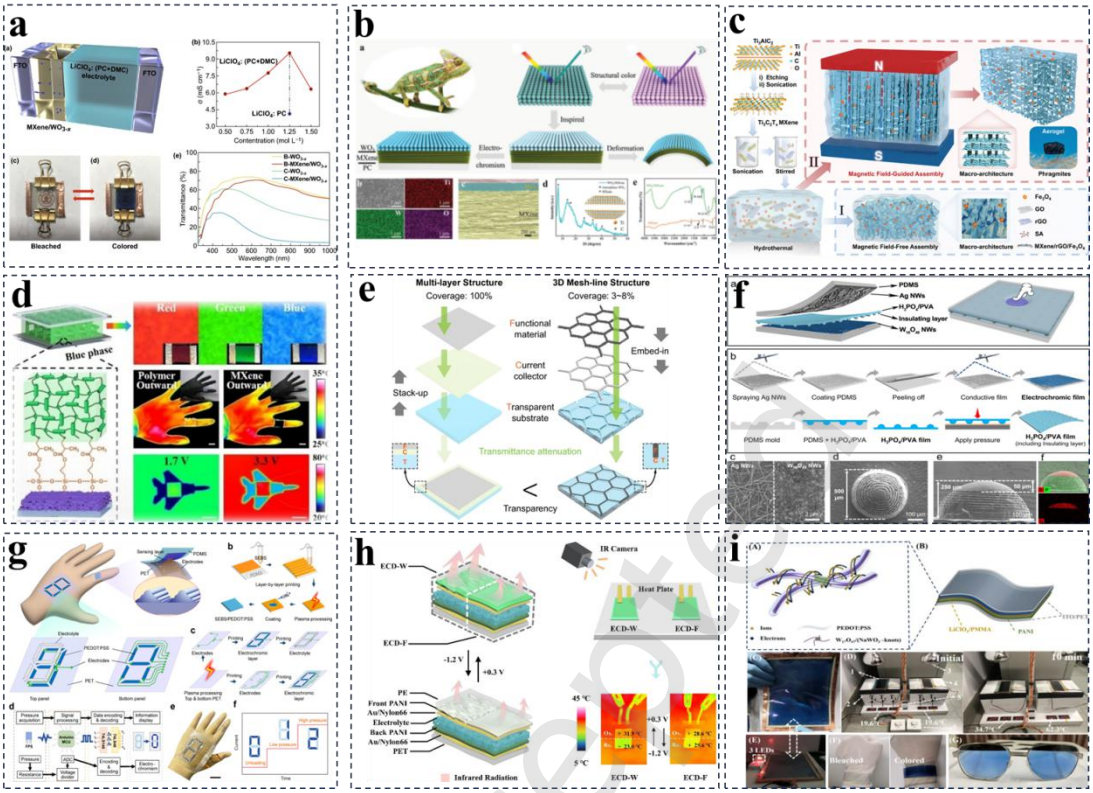

Fig.14 (a) Schematic diagram of the MXene/WO_3 - $_x$-based electrochromic device architecture[135]. (b)The MXene/WO_3 bilayer film [145]. Reproduced with permission.[145] Copyright 2024, Wiley-VCH GmbH. (c) Synthesis process of MXene/rGO-based aerogels [146]. Reproduced with permission.[146] Copyright 2024, Wiley-VCH GmbH. (d) Bioinspired visible–infrared camouflage materials through the controlled in situ formation of electrochromic soft photonic crystals on MXene films [147]. Reproduced with permission.[147] Copyright 2022, Wiley-VCH GmbH. (e) Schematic diagrams of the electrodes in different structures[148]. (f) Schematic diagram of the ECPVD structure, fabrication process, and comprehensive microstructural characterization [149]. Reproduced with permission.[149] Copyright 2025, American Chemical Society. (g) A fully DIW-printed flexible pressure sensing system integrating a piezoresistive sensor and electrochromic display [150]. Reproduced with permission.[150] Copyright 2025, American Chemical Society. (h) Electrochromic devices based on polyaniline [151]. Reproduced with permission.[151] Copyright 2024, Elsevier. (i) A 3D architecture made by knotting $W_{17}O_{47}$@PEDOT:PSS nanowires [152].

Table 2. Comparison with advanced flexible electrochromic sensing devices

Material	Structure	Sensitivity/Detection Range	Response/ Recovery Time	Cycle/Pressure	Stretchability/ Capacitive property	Ref.

Amorphous WO_3 / ITO/PET	Films	N/A	N/A	Performance degrades after 1000 cycles but is recoverable.	N/A	[153]
Monoclinic γ-WO_3	Single-crystal nanosheets	Up to 96% reflectance modulation	N/A	N/A	Thinner nanosheets (15 nm) accumulate charge (1.2 C, 60 s).	[23]
Hexagonal-phase WO_3	Nanoparticle	N/A	~6.8 s (coloring), ~3.2 s (bleaching)	N/A	N/A	[154]
ITO / PEDOT	Films	N/A	N/A	N/A	Lowest charge transfer resistance (11.03 Ω), and highest specific capacitance (21.15 $F \cdot g^{-1}$).	[155]
Multiple Crosslinked Network Hydrogel	Porous structure with an average pore size of 30 μm	GF= 0.83, R2 = 0.997 0–100% strain	Recovery from 100% strain with 3 seconds.	Performance deviation is less than 4% after 10 cycles	A maximum fracture elongation of ~2143% (over 2000% strain).	[156]
PVA-borax-$IL_{0.3}$ Hydrogel	Porous network with pore diameter of 5–20 μm,	Bending (0–90°)	N/A	After 3000 cycles (90000 s) with 6.9% decay	The self-healed hydrogel stretched to 700%	[157]
$W_{18}O_{49}$ / $Ti_3C_2T_x$ MXene composite	Microflower-like $W_{18}O_{49}$ composed of nanofibers	N/A	~6.5 s (coloring), ~5.6 s (bleaching).	The device achieved 61% optical modulation at 850 nm, and excellent cyclic stability over 1000 cycles.	Areal capacitance of 25 mF cm^{-2} at 0.5 mA cm^{-2}.	[158]
PET/ITO / $W_{18}O_{49}$ Nanowires (NWs) / Ion-Selective Membrane	$W_{18}O_{49}$ nanowires	A linear transmittance modulation sensitivity of ≈0.6%	coloration time: 15 s.	Standalone electrode retains 96% optical modulation after switching cycles (10000 s);	N/A	[158]
Amorphous WO_3 /CDs/ carbomer	Composite structure	Photochromic: ΔT = 80.1%	Coloring time: 2.6 s, bleaching	N/A	N/A	[159]

		Electrochromic: ΔT = 76.8%	time: 1.9 s			
SEBS/PEDOT:PSS	Multilayer step-like structure	Sensitivity: 20.25 kPa^{-1}; Linear Range: Up to 35 kPa.	Sensor Response Time: < 0.4 s. ECD Switching Time: Coloring < 0.3 s, Bleaching < 0.3 s.	Cycling Stability: ~5000 cycles at 150 kPa; ECD Stability: >3000 cycles, 0.5 Hz. Bending Durability: >1200 cycles.	N/A	[150]
D-A Conjugated Polymers	PDPPCz36 Film: Porous, rough surface. PDPPCz27 Film:	N/A	Polymer Film: PDPPCz27: coloring time = 2.1 s, 1.6 s; bleaching time = 0.6 s, 0.5 s.	100 cycles	N/A	[160]
Triphenylamine and m-phenylenediamine cross-linked polyaniline derivative	porous structure (~20% porosity).	N/A	Response times: 6.5 s (coloring) and 5.7 s (bleaching)	70% average emissivity modulation range after 10000 cycling.	Bendability: retains >94% electrochemical activity at 150° bending angle and after 100 bending cycles.	[161]
Viologen-based 2D covalent organic framework	Mesoporous structure (avg. pore diameter ~12.5 nm,	N/A	N/A	Cycling Stability: over 20 desalination-regeneration cycles.	Low charge transfer resistance (R_{ct} ~5.816 Ω). High capacitance contribution (>70%	[162]

5 Fabrication and Integration Techniques

A variety of fabrication techniques such as MEMS microfabrication, laser engraving/ablation, and electrospinning have been explored for flexible devices and electronics as shown in **Table 3**. We focus on printing and roll-to-roll approaches because they offer several key advantages for large-area, low-cost, and high-throughput production. At the same time, we have systematically analyzed the interaction between material systems and fabrication techniques, as well as the advantages and constraints imposed by manufacturing processes on material design in **Table 4**.

Table 3. Comparison with advanced fabrication techniques from scalability, cost, and Substrate compatibility to industrial implementation

Techniques	Scalability	Cost	Substrate compatibility	Industrial implementation
Printing/ Roll to roll	High line speeds for mass production	Relatively simple, modular equipment	Flexible polymer substrates	Existing industrial sectors such as packaging, labels
Laser	Rely on serial patterning for limited production	High-cost laser setup and system	Special laser substrate	Laboratory or pilot-scale environments
MEMS	Rely on batch, wafer-scale patterning for limited production	Multi-step etching with fabrication complexity	Rigid silicon or glass substrates	Laboratory or pilot-scale environments

Table 4. Comparison with advanced fabrication techniques from advantages and disadvantages to materials systems for flexible electrochromic devices

Fabrication techniques	**Advantages**	**Disadvantages**	**Material systems**
Extrusion-based Printing	1.Programmable, monolithic fabrication with finely controlled layer integration [163]. 2. Optimizes micro-crossing density within printed structures. 3. Multi material integration and functional gradient design[164, 165]	1.Excessive ink concentration, nozzle clogging, and interlayer bubbles[163]. 2. Stacking mode and interlayer adhesion of materials may lead to discontinuous ion transport paths or increased interface contact resistance.[166]	Printable viologen/PVA hydrogel inks[163] . Electrochromic composite materials[167] MOFs[168] COFs[169]
Inkjet Printing	The realization of fabric-based flexible ECDs in	1.The nozzle can be blocked due to the high	Well-dispersed polyaniline nanosheets,

	a side-by-side configuration[170].	concentration of ink. 2.Interlayer bubbles reduce electrochemical performance. 3. Limited diversity of pigment	PVA-based semisolid electrolyte[170]. WO_3 [171]
Multimaterial 3D Printing	1.Multifunctional integration. 2.Creating complex 2D/3D architectures from viscoelastic inks[172]. 3.Fully printed three electrodes onto paper[173].	1.Material compatibility 2. Expensive equipment and lacks of uniform standards.[174]	Conductive elastomer electrode, dielectric elastomer insulator, and ZnS phosphor–loaded electroluminescent layer[172] .
Direct-Ink-Writing	1.Extensive material compatibility [175]. 2.Co-fabricates microstructured pressure sensors with patterned electrochromic displays[150]. 3. Printing without supported structure[176].	1. Limited printing resolution[177]. 2. A high level of rheological properties in multi-layered stacking[178]. 3. Relatively slow printing speed[176].	PEDOT:PSS[179] WO_3 , NiO, MXene based composites、polymer composite materials[180]. COFs[181] MOFs[182]
Roll-to-Roll Fabrication	1. Industrial production[183]. 2. Simplified process: one-step phase separation for all-solid-state devices 3. Eco-friendly aqueous/water-ethanol inks with excellent rheological properties. 4. Low power and fast response. 5. Uniform large-area film formation with controllable	1. Conjugated polymers can hardly achieve a fully colorless bleached state. 2. Difficulty in controlling large-area uniformity and consistency. 3.precision requirements for Multiple layer stacking. 4.Solvent compatibility between adjacent layers[184].	Electrochromic materials: side-chain-modified PEDOT (PEDOT-EthC6) [185], n-PBDF [186], $TiNb_2O_7$ [187] Inks/Electrolytes: water/ethanol-based eco-friendly inks[188]. Polymer-dispersed electrochromic

	thickness		systems[189].

5.1 Advanced Printing Technologies

Conventional organic/inorganic composites and microstructural engineering can significantly improve electrochromic device (ECD) performance, but typical core–shell designs often exhibit incomplete interfacial fusion, which elevates contact resistance and limits efficiency [190]. Three-dimensional printing offers a powerful route to mitigate these interfacial issues in flexible ECDs by enabling programmable, monolithic fabrication with finely controlled layer integration. For example, Du et al. [191] developed printable viologen/PVA hydrogel inks that simultaneously serve as electrochromic, electrolyte, and encapsulation layers, and used them to construct an integrated four-layer flexible ECD via continuous 3D printing. The seamless interfacial bonding between hydrogel layers yielded an interfacial strength of $88\ N\ m^{-1}$, along with excellent electrochromic performance and mechanical robustness, with less than 19% contrast loss after 5,000 bending cycles (**Fig. 15a**). For example, Xie et al. [192] employed inkjet printing to realize a fabric-based flexible ECD in a "side-by-side" configuration in **Fig. 15b**, where well-dispersed polyaniline nanosheets functioned both as the printable ink and the electrochromic material, and a PVA-based semisolid electrolyte acted as the gel medium. The resulting FECD exhibited a 22.9% reflectance change and maintained stable electrochromic behavior after 1,000 bending cycles. Jeong et al. [193] further demonstrated 3D-printed thin-film architectures for ultrafast ECD energy-storage devices using an automated micro–3D-printing platform. By optimizing the micro-crossing density within the printed structures, they improved both electron and Li-ion transport, shortened the diffusion paths between the FTO substrate and the electrolyte, and thereby enabled ultrafast charge-transfer kinetics (**Fig. 15c**).

Despite offering a route to scalable fabrication, 3D printing of soluble conductive polymers can suffer from excessive ink concentration, nozzle clogging, and interlayer bubbles, which suppress the electrode's electrochemical kinetics and pigment versatility. Multi-material 3D printing, a high-throughput, programmable manufacturing approach capable of creating complex 2D/3D architectures from diverse viscoelastic inks, provides a promising workaround. Zhang et al. [194] used this approach (**Fig. 15d**) to build a flexible electroluminescent device and soft robot comprising a conductive elastomer electrode, dielectric elastomer insulator, and ZnS phosphor–loaded electroluminescent layer. Liu et al. [195] fully printed three

electrodes onto paper—MnO_2 || PEDOT:PSS/PANI:PSS || Zn—to realize a compact, compliant, multimodal self-powered electrochromic platform (**Fig. 15e**) that blends complementary colors and latent gradients; the combined cathodic PEDOT:PSS/anodic PANI:PSS electrode outputs green, purple, or blue across redox states, enabling fast, reversible bidirectional switching. Zhu et al. [150] applied direct-ink-writing to co-fabricate microstructured pressure sensors (**Fig. 15f,** 20.25 kPa^{-1} sensitivity, 35 kPa linear range, 5,000-cycle durability) with patterned electrochromic displays (common-cathode design, <0.4 s coloration, >6,000 s stability). Despite progress in printing displays, wearables, solid-state lighting, and biomedical components, complex electroluminescent systems fabricated via multi-material 3D printing remain largely uncharted, leaving significant room for exploration.

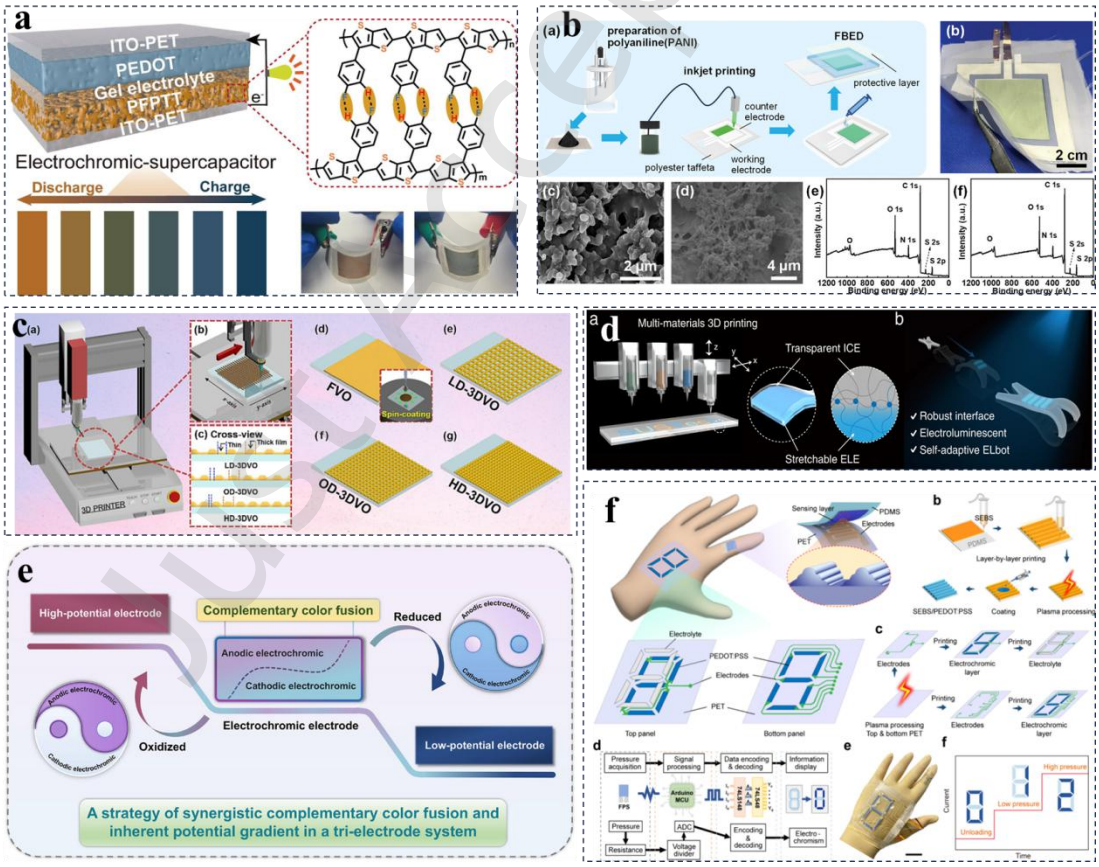

Fig.15 (a) Electrochromic supercapacitors based on PFPTT and different bending angles[191]. Reproduced with permission.[191] Copyright 2024, Elsevier. (b) The fabrication of fabric-based FECD[192]. Reproduced with permission.[192] Copyright 2025, Wiley-VCH GmbH. (c) Schematic illustrations of an automated 3D-printing system with precise x/y/z-axis control, vertically aligned VO line patterning,

cross-sectional architectures of 3DVO films with graded thickness intersections, and comparative electrode fabrication via spin-coating versus 3D printing[193]. Reproduced with permission.[193] Copyright 2023, Elsevier. (d) 3D‐printed electroluminescent devices and an all‐in‐one fabrication route for self‐adaptive soft robots [194].(e) Electrochromic mechanism based on synergistic complementary color fusion [195]. Reproduced with permission.[195] Copyright 2026, Wiley-VCH GmbH. (f) Overview of the flexible pressure sensing system[150]. Reproduced with permission.[150] Copyright 2025, American Chemical Society.

5.2 Roll-to-Roll and Large-Area Manufacturing

Most current electrochromic-device (ECD) studies remain confined to small footprints (e.g., 5 cm × 5 cm), leaving large-area ECDs (bECDs) underexplored despite their importance for real-world demands such as building energy management [125]. A principal bottleneck for commercial deployment lies in fabrication constraints. Molecular-structure design and additive engineering have yielded environmentally benign EC inks with superior rheology, which enable uniform thin-film deposition. Roll-to-roll (R2R) and other scalable assembly routes further bolster manufacturing throughput, positioning bECDs for industrial production. For instance, a novel all‐solid‐state, all‐in‐one flexible ECD (**Fig. 16a**) fabricated via a polymer‐dispersed electrochromic device (PDECD) strategy [189]. This all‐solid‐state flexible ECD can be efficiently prepared in a single phase‐separation step without any additional treatment, and it exhibits outstanding stability (92.1% of the initial ΔT retained after 10,000 cycles), high coloration efficiency, low power consumption, and a satisfactory response time of 12 s. Brändler et al.[196] examined side-chain-modified PEDOT (PEDOT-EthC6) films deposited onto PET-ITO via R2R slot-die coating; UV–Vis and IR analyses showed that residual iron salts (required for in situ polymerization) and storage-time variations between processing steps had no impact on photodegradation rates, while films exhibited 30% higher photostability under inert atmospheres than in ambient conditions (**Fig. 16b**). Flexible ECDs typically suffer from conjugated EC polymers that cannot reach a fully colorless bleached state; this shortcoming can be mitigated by implementing new side-chain-modified PEDOT derivatives, which can also be deposited as films through tailored, high-throughput, large-area R2R polymerization processes[185].

Researchers have substantially refined processing and ink-fill modifications in recent years. Lee et al. [186] employed a cosolvent precipitation route to formulate an customizable water/ethanol‐based inks for producing uniform, large‐area n‐PBDF films with accurate thickness control through ultrasonic spray coating

(**Fig. 16c**). The resulting n- PBDF EC electrodes exhibit deep- black coloration, fast switching, and excellent electrochemical stability; durability tests under continuous illumination and heating at 65 °C further confirm their robustness. In another work, Jia et al. [27] introduced an "electrode-free" electrochromic device (EECD) in which the EC layer is absent from the electrode during assembly and in the bleached state. This architecture simplifies fabrication while delivering excellent optical modulation, and a large-format 40 cm × 40 cm device demonstrated uniform coloration, underscoring its scalability (**Fig. 16d**). Wang et al. [197] designed a bistable reflective modulator based on reversible Zn electrodeposition (ZERD) for ultra-low-power thermal management. The device operates at voltages as low as –0.35 V, achieves coloration/bleaching in 4/8 s, maintains stability beyond 1,000 cycles, and was scaled to 625 cm² with uniform switching, highlighting a low-cost, scalable route toward net-zero-energy buildings (**Fig. 16e**). Ping et al. [187] leveraged slot-die coating and environmentally benign aqueous inks to rapidly produce films of a novel Wadsley-Roth shear-structured titanium-niobium oxide ($TiNb_2O_7$) at rates up to 600 cm² per minute (**Fig. 16f**).

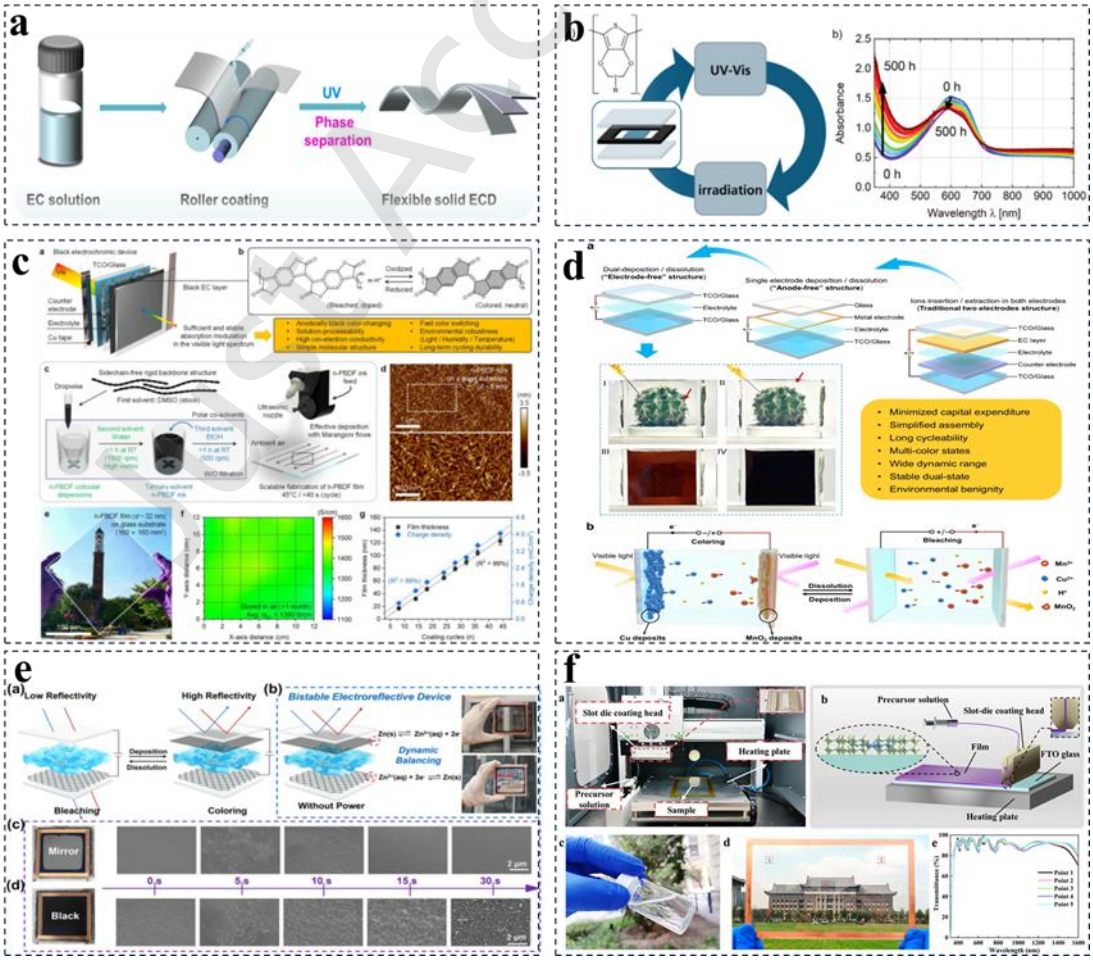

Fig.16 (a) Manufacturing route of the all‐ solid‐ state, all‐ in‐ one flexible ECD [189]. Reproduced with permission.[189] Copyright 2024, Elsevier. (b) PEDOT-EthC6 structure and general approach for the photodegradation and monitoring [196]. Reproduced with permission.[196] Copyright 2024, Wiley-VCH GmbH. (c) Scalable fabrication of n-PBDF films for black EC electrodes[186]. (d) Structure and working mechanism of "electrode-free" electrochromic device[27].(e) Schematic structure of the ZERD device, bistable operation schematics, SEM of time-resolved Zn electrodeposition, and comparative morphologies of ZERD versus black Zn-ECD[197]. Reproduced with permission.[197] Copyright 2025, Wiley-VCH GmbH. (f) Schematic illustration of the slot-die coating preparation process[187]. Reproduced with permission.[187] Copyright 2025, Wiley-VCH GmbH.

6. Advanced Applications

6.1 Electrochromic Bioinspired Skin

Flexible electrochromic (EC) wearable devices increasingly integrate multiple functions for real-time health monitoring and adaptive camouflage [125]. Unlike conventional physiological sensors that require complex electronics to interpret signals such as heart rate or oxygen saturation, EC modules can transduce pressure or strain directly into color shifts, yielding immediate, noninvasive visual feedback [120, 198]. Combining transparent, conformal strain sensors with EC layers enables chameleon-like artificial skin. Yu et al. [199] demonstrated a biomimetic multicolor EC skin built from colorless/blue $W_{18}O_{49}$ nanowires, green-to-pink AuNP@PANI, and a flexible conductor. Voltage sweeps between 0.4 V and -0.7 V drive electron/ion-transfer redox reactions that modulate the skin from green to blue to pink (**Fig. 17a**). Separately, a piezoelectric electrochromic tactile sensing display (PETSD) uses a pressure‐ sensing PVDF matrix integrated with a polyaniline electrochromic (EC) array for visual output, enabling handwriting capture with a 1.4 s response, 62.2% color contrast, and repeatable pattern recovery under varied pressures (**Fig. 17b**) [200].

For visual readouts of skin temperature and wrist motion (**Fig. 17c**), stretchable EC arrays integrate temperature and strain sensors by coating poly(3-hexylthiophene) and WO_3 as EC materials on flexible transparent ITO-coated PET electrodes [201]. Sun et al. [202] proposed a pressure-sensing/visual-display device in which both pressure and EC units are fabricated via photopolymerization, streamlining structure and integration. Ion gels and micro-pyramids in the sensing unit boost capacitive response, while the EC unit reuses electrodes and chromic layers to simplify

conventional multilayer stacks. The photopolymerized wearable hybrid shows 358.1 kPa^{-1} sensitivity, 16.8/28.0 ms response/recovery, and 4.2/4.8 s coloration/bleaching (**Fig. 17d**). Inspired by octopus-like stimulus perception/visualization, Guo et al. [203] demonstrated an ionic-sensing/EC-display hybrid for interactive pressure mapping; shared electrodes and ion gels enable quantitative sensing coupled to direct color changes (**Fig. 17e**). Lee et al. [204] showcased a transparent, flexible metal-oxide-based photovoltaic neuromorphic defense system. By monolithically integrating ultra-flexible optoelectronic circuits with EC elements, the entire signal chain—from history-dependent sensing and memory to risk recognition and UV blocking—is embedded in a flexible device. The system autonomously shields up to 97% of UV radiation (5–90 W m^{-2}) within 16.9 s, with self-adjusted sensitivity and response tied to UV conditions and applied bias (**Fig. 17f**). Overall, biomimetic EC skins largely rely on electrodes and ion gels to achieve quantitative sensing and immediate chromic feedback, and their tunable architecture permits remote monitoring and visual warning functionality.

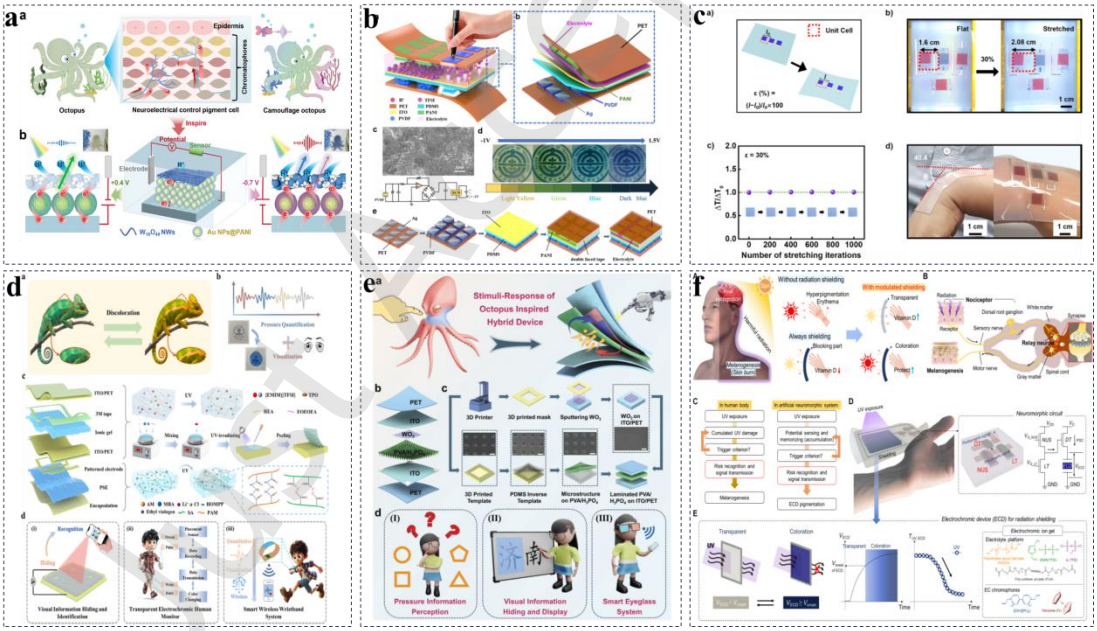

Fig.17 (a) The structure of the electrically controlled artificial chromatophore system[199].(b) A flexible, patterned PET-based tactile-sensing device integrates PVDF piezoelectric strain sensors and ITO-patterned PANI electrochromic arrays [200]. Reproduced with permission.[200] Copyright 2022, Elsevier. (c) ECD array with applied uniaxial strain (30%), cyclic stretchability, bending compliance [201]. Reproduced with permission.[201] Copyright 2022, Elsevier. (d) Design and application of the wearable hybrid device[202]. Reproduced with permission.[202] Copyright 2025, Wiley-VCH GmbH. (e) The octopus-inspired wearable hybrid device

[203]. Reproduced with permission.[203] Copyright 2022, Wiley-VCH GmbH. (f) Biomimetic radiation shielding system[205].

6.2 Electrochromic Textiles

Electrochromic devices (ECDs) also possess nonvolatile color-memory effects, meaning they can preserve damage records long after the stress is removed. This trait makes them ideal for monitoring subtle changes at opaque interfaces, such as long-term health conditions of human skin or sustained mechanical strain [206-208]. By transducing physiological signals (e.g., variations in electromagnetic field intensity) into color changes, flexible electrochromics open pathways for intelligent wearable textiles [209]. When integrated with textile architectures, flexible EC technology can endow fabrics with adaptive camouflage. For instance, weaving conductive weft yarns with luminescent warp fibers yields stable micron-scale electroluminescent units that maintain display functionality under bending, stretching, or compression. By employing solvent‐free polyurethane–urea ionic conductors, Wang et al. [210] constructed a stretchable, all‐solid‐state, multimodal electrochromic textile‐electronics system that features rapid switching (~3 s), high color contrast (~58.1%), and a long service life (>12,000 s), facilitating deep‐learning‐assisted adaptive camouflage on the human body in dynamic scenarios (**Fig. 18a**). Shi et al. [211] realized micron-scale electroluminescent nodes at warp-weft junctions that remain stable even under mechanical deformation (**Fig. 18b**). Fan et al. [212] employed diverse electrochromic active viologens and a parallel dual-counter-electrode layout to deliver sustained, uniform, fast color transitions (blue, magenta, green, dark red) over extended periods; woven into large patterned textiles, these EC fibers exemplified adaptive camouflage and wearable displays (**Fig. 18c**). Chen et al. [213] combined water-transfer printing by means of coaxial extrusion to produce meter‐long electronic fibers with a core-shell architecture, comprising a high-saturation structural-color cholesteric liquid-crystal sheath, a uniform liquid-crystal elastomer actuator layer, and a liquid-metal sensing core. Strategically designed sensing gloves woven from these fibers can visualize hand stress distributions in real time and enable unprecedented human–robot interaction for robotic hand control (**Fig. 18d**). Duan et al. [214] proposed an “adhesive-channel strategy” whereby silver nanoparticles and microfibrillar capillarity guide 3D flow of liquid metal on yarn surfaces. The resulting SBS/LM/Ag-SBS (SLMAS) yarns exhibit an initial resistance of $0.082\ \Omega\ cm^{-1}$, a relative resistance change of only 0.703 at 600% strain, and durability against twisting, bending, washing, and 5,000 stretch cycles; post-functionalization, they also enable smart thermal regulation and

electrochromism (**Fig. 18e**). Collectively, these all-textile, all-organic, multifunctional e-textiles integrate pressure, proximity, and temperature sensing while remaining washable and breathable, underscoring their promise for next-generation wearable displays and camouflage systems.

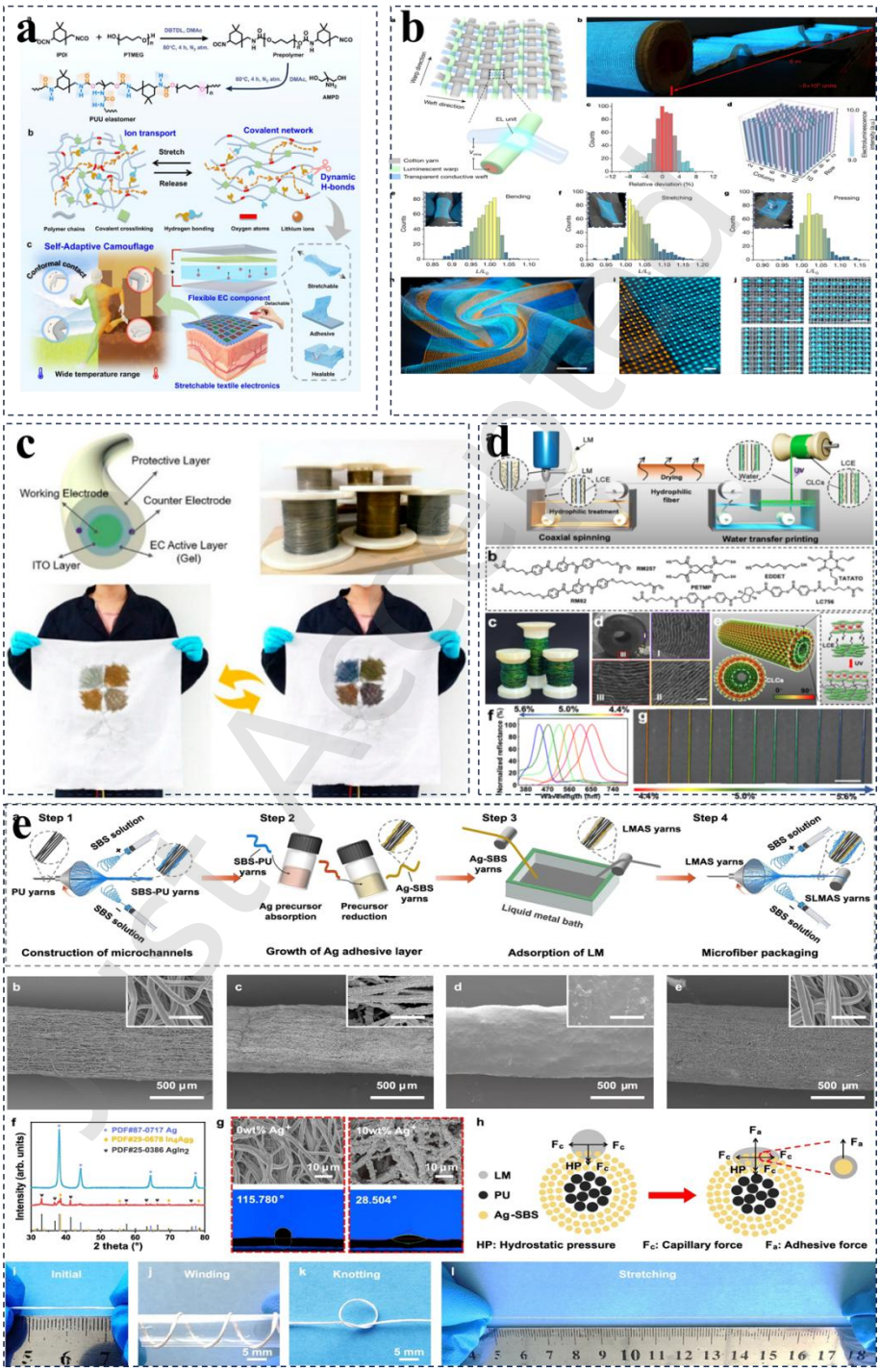

Fig.18 (a) Conceptual diagram of elastomeric ionic conductors enabling textile electronics [210]. Reproduced with permission.[210] Copyright 2025, Wiley-VCH GmbH. (b) Structure and electroluminescence performance of the display textile[211]. Reproduced with permission.[211] Copyright 2021, Springer Nature. (c)

Multifunctional applications of EC fibers[212]. Reproduced with permission.[212] Copyright 2020, American Chemical Society. (d) Continuous high‐throughput fabrication of meter‐long fibers [213]. Reproduced with permission.[213] Copyright 2025, Wiley-VCH GmbH. (e) SLMAS yarns with Ag–LM intermetallic bonding[214].

6.3 Self-powered systems based on electrochromic devices

6.3.1 Piezoelectric-Driven Self-Powered Systems

Integrating electrochromic devices (ECDs) with nanogenerators (NGs) is accelerating their transition from demonstrations to practical systems across smart windows, reflective displays, and mirrors. Piezoelectric-driven hybrids exemplify this trend: an NG harvests mechanical energy while the ECD visualizes the stored charge state via color shifts, yielding self-powered sensing or status-indication platforms. Stress-responsive piezoelectric materials—especially ZnO nanowires and (PVDF) composites—anchor these systems because they efficiently convert strain into electrical signals. ZnO is particularly attractive: its wide bandgap, strong piezoelectricity, and favorable optoelectronic properties support controllable growth of 1D nanostructures (nanowires, nanorods) by solution or vapor-phase routes, enabling large-area, patterned NG–ECD integrations with minimal added fabrication complexity.

For instance, Han et al. [215] integrated ZnO nanowire arrays with WO_3 electrochromic films to construct a self-powered, pressure-visualizing sensor, in which each pixel comprises ZnO nanowires whose piezoelectric output under external force directly drives an adjacent WO_3 unit to undergo a color change, enabling spatially resolved pressure mapping. Even light touches elicit a clear optical response, and the intrinsic color-memory effect of WO_3 preserves the encoded pressure information without continuous power input (**Fig. 19a**). Building on this concept, Bi et al. [200] replaced ZnO with a PVDF-based flexible piezoelectric layer and coupled it to a polyaniline electrochromic array, achieving precise handwriting visualization with a strong dynamic response. Owing to its high flexibility, easy processability, and stable β-phase formation, PVDF has become a mainstream piezoelectric polymer; the incorporation of $BaTiO_3$ nanoparticles or other polar fillers can markedly enhance the piezoelectric output of PVDF composite films (**Fig. 19b**). Zhang et al. [85] further designed a dual-mode display by integrating a triphenylamine–imidazolium

ionic-liquid electroactive unit with a PVDF/$BaTiO_3$ nanogenerator module. A rectifier bridge converts the alternating piezoelectric signal into DC, thereby powering electrochromic/electrofluorescent display elements suitable for smart-interface applications (**Fig. 19c**). Shao et al. [216] proposed an "ionic skin" that combines pressure sensing with in situ, nonpixelated pressure display; by patterning the deionized interface of the electrochromic device, pressure-induced interfacial charge transfer modulates the capacitance, yielding a continuous, spatially resolved readout of both the magnitude and distribution of applied loads (**Fig. 19d**).

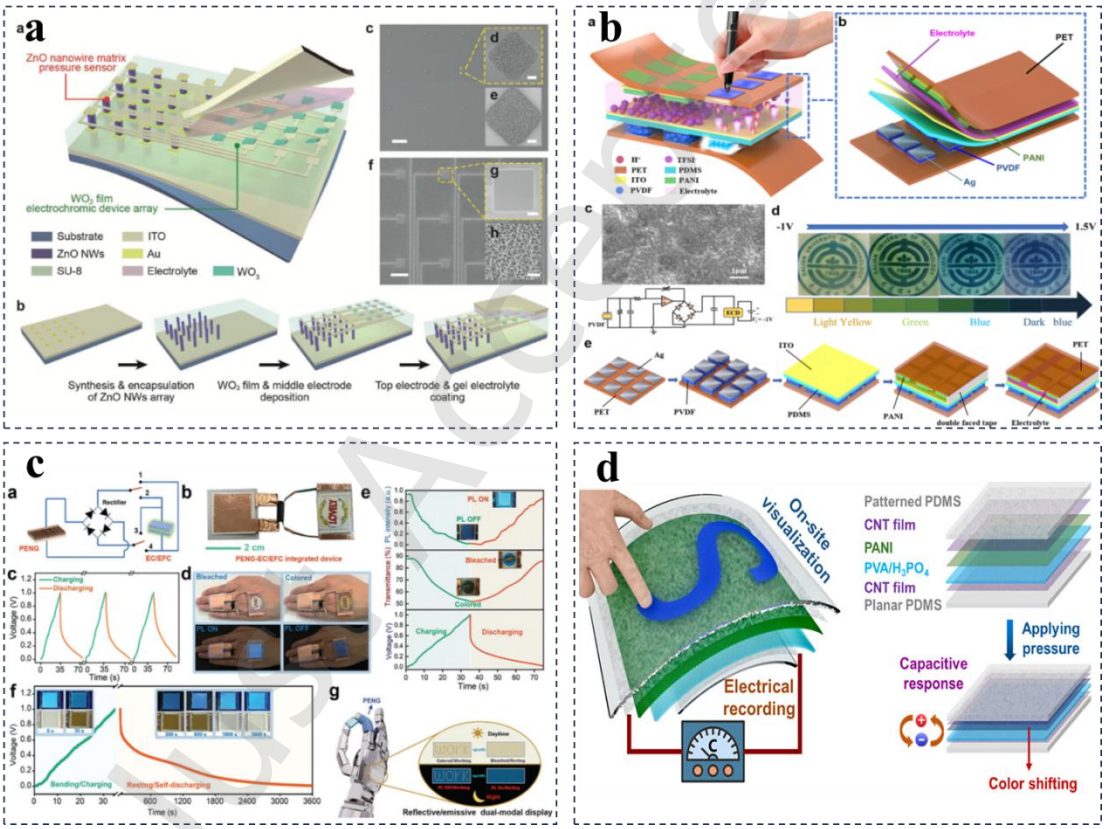

Fig.19 (a) Structure and fabrication process of the PVR system[215]. Reproduced with permission.[215] Copyright 2017, Wiley-VCH GmbH. (b) A flexible piezoelectric-electrochromic tactile sensor integrates patterned PVDF and PANI [200]. Reproduced with permission.[200] Copyright 2022, Elsevier. (c) A piezoelectric-driven, rectifier-integrated EC/EFC system [85]. Reproduced with permission.[85] Copyright 2023, Wiley-VCH GmbH. (d) The iontronic skin integrating bimodal sensing, pressure-triggered charge transfer for electrical signal generation and color shifting[216]. Reproduced with permission.[216] Copyright 2024, American Chemical Society.

Although piezoelectric self-powered electrochromic systems exhibit excellent sensitivity and fast response to dynamic pressure inputs, they are inherently unsuited for sensing static or quasi-static loads. Piezoelectric materials generate charge separation and potential differences only when time-varying mechanical stress deforms their crystal lattices and perturbs internal dipole moments[217, 218]. When the applied stress becomes constant (static load) or varies only very slowly (quasi-static load), the induced charges rapidly dissipate through intrinsic leakage within the material or through external circuits. As a result, the output voltage decays to zero and can no longer sustain a stable electrochromic state or provide a continuous driving signal. This intrinsic limitation greatly restricts their use in applications that demand long-term monitoring of structural deformation, stress relaxation, or gradual loading. For example, in structural health monitoring of critical components in unmanned systems, damage often accumulates progressively via small but persistent pressure increases—signals that conventional piezoelectric platforms are effectively blind [219].

6.3.2 Triboelectric Nanogenerator Integrated Systems

Triboelectric nanogenerators (TENGs), an emerging energy-harvesting technology, have recently found widespread use in self-powered sensing and display systems. Their operation relies on the synergy between contact electrification and electrostatic induction arising as two materials with unequal electron affinities experience relative motion, interfacial charge transfer occurs, and periodic contact–separation cycles yield alternating-current output[220, 221].

For example, Huang et al. [222] reported a nanoscale confined triboionic photonic device composed of an ion gel constrained by counterion electromigration, a poly(2,5-bis(3-alkylthiophen-2-yl)thieno[3,2-b]thiophene) (PBTTT) active layer, and an electrode wher triboelectric field modulation governs ion injection, enabling ultrahigh spatial resolution. The PBTTT conductivity and photoluminescence intensity can be finely tuned by the scanning force, rate, period, and applied AFM-tip bias. Accordingly, fine-structured patterns can be written and retained in the device, and the electrochromic effect allows instantaneous readout even under ambient illumination (**Fig. 20a**). Qin et al. [223] integrated a TENG with electrochromic micro-supercapacitors to form a self-charging system; Ag nanowire/NiO served as bifunctional electrodes that generated >3 V under mechanical stimuli such as palm strikes, thereby driving electrochromic reactions and lighting LEDs, demonstrating

portable-power potential (**Fig.20b**). Su et al. [224] co-developed a self-powered tactile–acoustic visualization sensor comprising a PVDF nanofiber tribolayer, a ZnS:Cu emissive layer, transparent mesh electrodes, and a flexible substrate. Leveraging triboelectric-induced electroluminescence, the device achieves a brightness of 0.5 mW cm^{-2} in lateral sliding mode with a detection limit of 0.5 kPa (**Fig.20c**). Similarly, Huang et al. [221] integrated TENGs with high-performance electrochromic devices to realize a self-powered smart window that modulates solar transmittance. Using a low-energy phenothiazine redox ionic liquid, they produced dual-band (visible-NIR) electrochromic cells featuring rapid response, broad tunability, and real-time visualization of transient pulse voltages, highlighting building-energy applications (**Fig. 20d**). Subsequently, an electroactive, fluorescent ionic liquid (EFIL‑ ThPA) was synthesized, incorporating triphenylamine as the electroactive unit, thiophene acrylonitrile as the fluorescent moiety, and an imidazolium segment for ion conduction. The resulting bifunctional electrochromic/electrofluorochromic device exhibited synchronized color and fluorescence switching with an optical response time of <2.4 s and high contrast. When integrated with a TENG, a self‑ powered reflective/self‑ emissive dual‑ mode display was realized, enabling simultaneous modulation of color and fluorescence within 15 s at ultralow driving voltages (<0.9 V) (**Fig. 20e**) [225].

When subjected to external force, putative piezoelectric nanogenerators (PENG) frequently manifest substantial triboelectric effects, stemming from interfacial shear friction, nanoparticle slip, residual static charges, and contact electrification, such that the triboelectric contribution can dominate the measured output (**Fig. 20f**) [226]. Earlier reports often overlooked these triboelectric signals, mistakenly attributing them solely to piezoelectric responses, which undermines accurate determination of dynamic pressure magnitude and direction. Distinguishing and quantifying the piezoelectric versus triboelectric components therefore demands purposefully designed experiments and high-precision measurements [227]. As a result, even though self-powered electrochromic platforms that exploit piezoelectric or triboelectric mechanisms have reached important milestones, their intrinsic signal overlap continues to impede precise discrimination of complex stress amplitudes and orientations. However, there are some decoupling methodologies, subtle yet powerful strategies that act as invisible bridges between complex systems, each designed to untangle interdependence with precision. For example，the popular frequency domain analysis technique, the fast Fourier transform is used for the first time to decouple the energy contributions of piezoelectric (PE) and triboelectric (TE) nanogenerators by comparing a PVDF PENG against a non-PE polyimide (PI) NG. The intensity and the bandwidth of PE and TE signals, relative to the excitation frequency, enabled rapid

identification of TE contributions in the PE measurements[228]. Akbarinejad et al. systematically investigated the signal output from organic piezoelectric materials (poled PVDF), moderately piezoelectric (heat-treated PVDF), and non-piezoelectric (non-poled PVDF), polytetrafluoroelthylene (Teflon) and nylon under tapping and compression (33 direction) and stretching (31 direction) in both encapsulated and non-encapsulated forms, and reveal that regardless of their piezoelectric properties, all tested materials exhibit substantial voltage outputs (4.2-4.6 V) during tapping, primarily attributed to the triboelectric effect at the contact interface. Moreover, elastomeric encapsulation is demonstrated to markedly increase triboelectric signals in tapping mode[229]. Li et al. propose the microscopic, coupled electrification model at the ferroelectric polymer/metal interface and clarify that the triboelectric and piezoelectric effects dominate at low and high pressures, respectively. Inspired by the above microscopic mechanism, we regulate the ferroelectric β phase of PVDF film to develop a tribo-piezoelectric coupled pressure sensor(T-PPS) with high sensitivity(0.95 V/kPa) and wide measurement range(>10 MPa)[230]. These results have important implications for the future design of piezoelectric-triboelectric devices and the accurate interpretation of the data obtained from such devices.

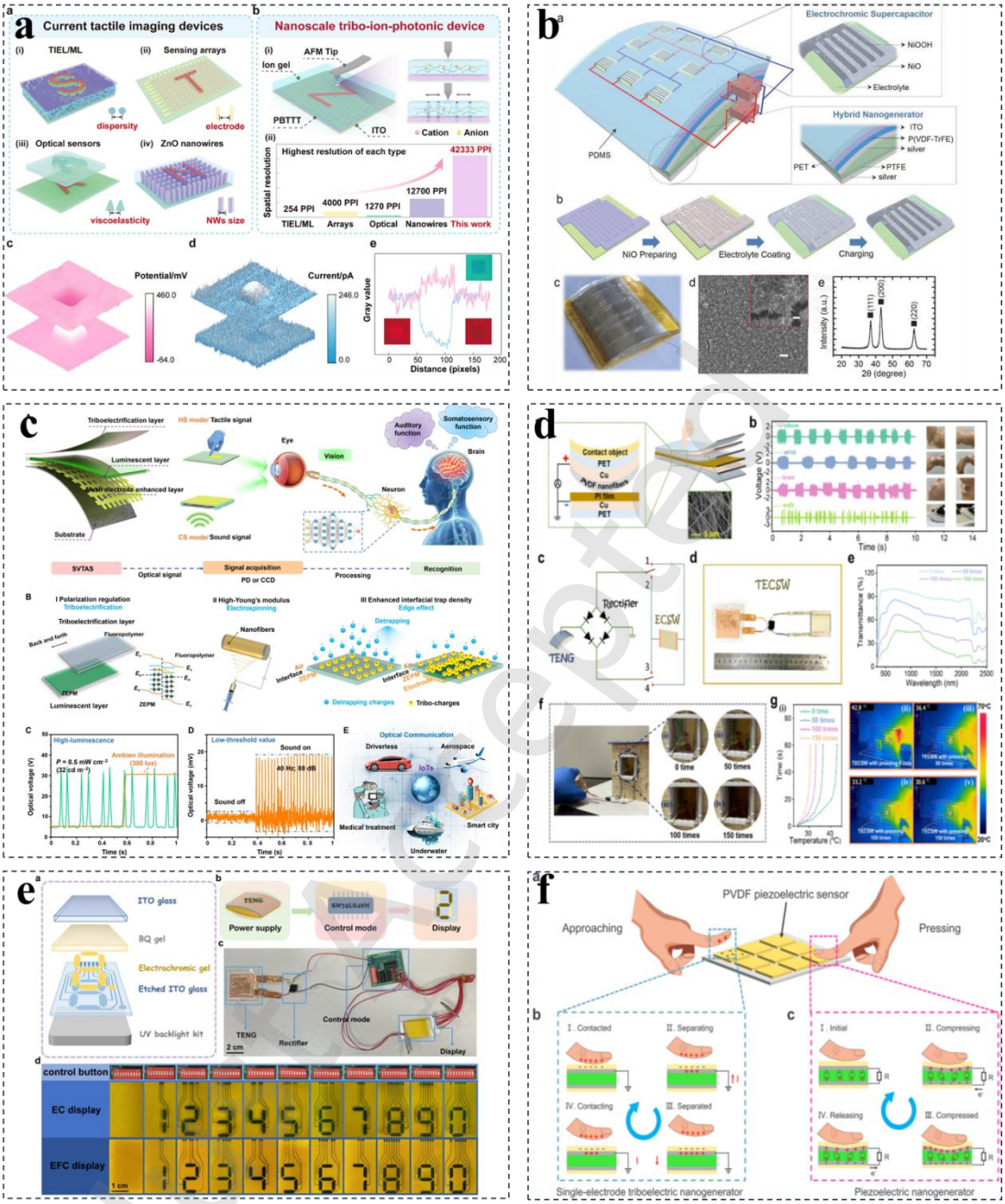

Fig.20 (a) Tribo- ion- photonics featuring adjustable conductivity, PL intensity, and electrochromic color [222]. Reproduced with permission.[222] Copyright 2025, Wiley-VCH GmbH. (b) Self-charging power package integrating electrochromic μ-SC and hybrid NG[223]. Reproduced with permission.[223] Copyright 2018, Wiley-VCH GmbH. (c) Structural design and application of SVTAS[231]. Reproduced with permission.[231] Copyright 2012, Springer Nature. (d) Basic construction and performance of TECSW integrated system[221]. Reproduced with permission.[221] Copyright 2024, Elsevier. (e) TENG- powered dual- mode display device featuring reflective and emissive modes [225]. Reproduced with permission.[225] Copyright 2025, Elsevier. (f) Representation of SE- TENG and PENG contributions during real- world operation of piezoelectric devices [226].

6.4 Electrochromic and Smart Energy Storage Devices

6.4.1 Electrochromic Supercapacitors

Electrochromic supercapacitors (ECSCs) combine energy storage with state-of-charge visualization, making them attractive for harsh environments where thermal runaway and temperature swings threaten device reliability. Electrolytes dictate temperature tolerance, yet conventional liquid electrolytes limit performance. Ion-gel solid electrolytes (IG-SEs) offer high-temperature durability and low-temperature flexibility, motivating broad interest. Cao et al. [232] engineered an organic hybrid ion/electron-conducting polymer that merges conjugated segments for electronic transport with polyelectrolyte moieties for ionic transport, enabling efficient charge redistribution within a single material. Their ECSC achieved transmittance modulation of 58.14% (TVIS) and 49.91% (TNIR), areal capacitance of 114.32 mF cm^{-2}, and 91.78% capacity retention after 10,000 cycles (**Fig. 21a**). Zheng et al. [233] built a 3D interconnected ionic network based on sulfonated poly(vinyl alcohol) and graphene oxide (c- SPVA- GO); incorporating GO and tuning its aggregation boosted IG-SE ionic conductivity from 0.49 to 0.91 mS cm^{-1}. Using polyaniline electrodes and c-SPVA-GO electrolyte yielded ion-gel ECSCs with outstanding electrochemical performance across -20 °C to 80 °C (**Fig. 21b**). Du et al. [191] introduced a fluorinated interpenetrating network within polythiophene-based flexible ECSCs, enabling reversible brown-to-blue switching under bending and real-time state-of-charge feedback (**Fig. 21c**). Guo et al. [142] fabricated MXene Ti_3C_2-based coplanar interdigitated electrochromic microsupercapacitors (EMSs) via assisted spray coating. Operating in a 1 M PVA/H_2SO_4 gel containing ethyl viologen dibromide, the EMS delivered 12.5 mF cm^{-2} areal capacitance, 2.6/2.5 s coloration/bleaching, 60% optical contrast, and strong mechanical robustness suitable for flexible wearables (**Fig. 21d**). Wang et al. [234] presented a co-optimization strategy, modulating micro/nano features of conductive substrates and pairing appropriate ion-storage layers, to develop a universal platform for high-performing electrochromic materials (**Fig. 21e**). With SnO_2 as a conductive substrate modifier to enhance electrochromic-layer stability and V_2O_5 as the ion-storage layer to balance charge and add storage capability, the device simultaneously achieved electrochromic and supercapacitive functionality.

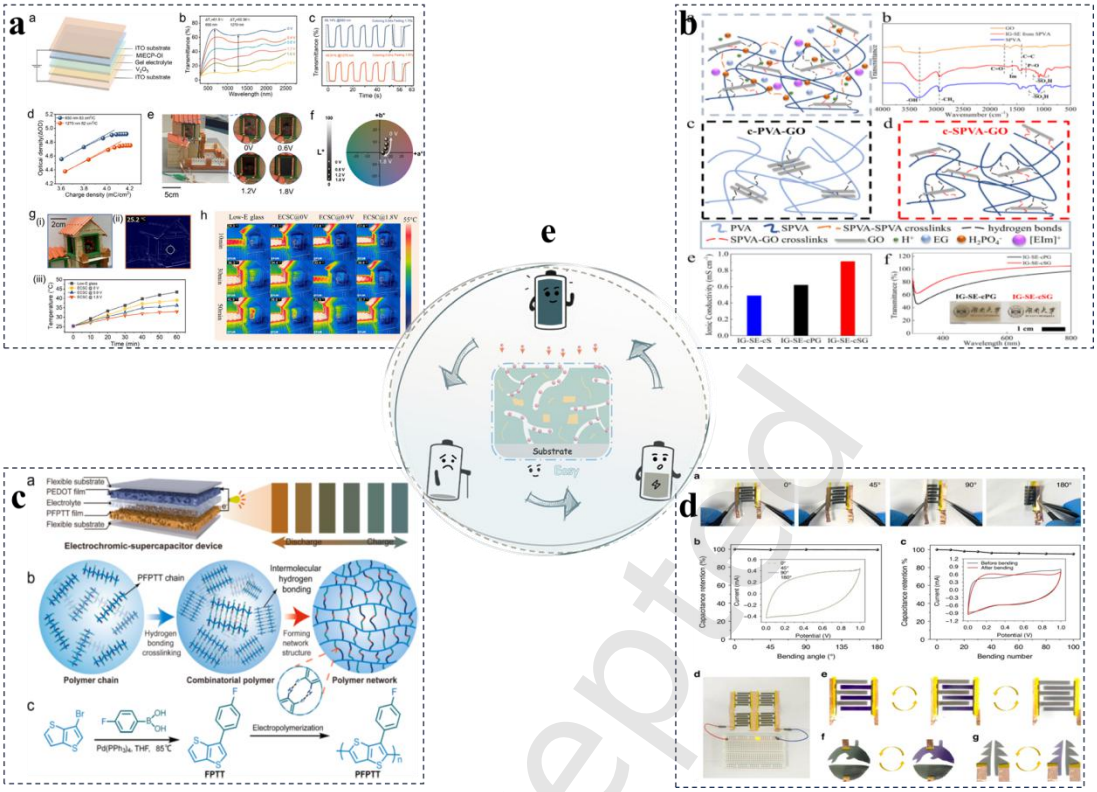

Fig.21 (a) The characterization of optical switching kinetics, voltage-dependent transmittance and dynamic thermal regulation performance [232]. Reproduced with permission.[232] Copyright 2025, Wiley-VCH GmbH. (b)The c-SPVA-GO–based IG-SE microstructure model, FT-IR spectra, comparative backbone architectures, ionic conductivities of IG-SE variants, and transmittance [233]. Reproduced with permission.[233] Copyright 2025, Wiley-VCH GmbH. (c) Electrochromic supercapacitors based on PFPTT[191]. Reproduced with permission.[191] Copyright 2024, Elsevier. (d) Application of the as-fabricated EMS[142].(e) Schematic diagram of the transparent-to-multicolored electrochromic supercapacitors[234].

6.4.2 Electrochromic Batteries

Electrochromic batteries couple reversible color changes with electrochemical energy storage, enabling direct visualization of state-of-charge and advancing prospects for transparent next-generation cells[235, 236]. Progress remains limited because few cathode materials unite high capacity with pronounced electrochromism—commonly studied candidates (PANI, Prussian blue, V_2O_5, WO_3, NiO_2) still exhibit modest specific capacities. To address this gap, Lv et al. [237] engineered flexible Fe||C-PANI EC batteries using cross-linked PANI cathodes and $Fe(TOF)_2$ electrolytes, achieving synchronized coloration and charge storage

(**Fig. 22a**). Wu et al. [238] realized rapid coloration, high optical contrast, and robust cycling by combining Nb–W oxides with Zn^{2+} /Al^{3+} hybrid electrolytes; subsequent work paired Wadsley–Roth $Nb_{1.8}W_{1.6}O_{9.3}$ with Prussian blue in Al^{3+} /K^{+} media to deliver fast response, high capacity, and strong efficiency through ion-selective intercalation (**Fig. 22b–c**) [236]. Liu et al. [239] reported flexible Zn-ion EC batteries with reversible orange-brown-green transitions, elevated specific capacity, and mechanical compliance (**Fig. 22d**). Song et al. [240] designed PANI-VO_x composites that provide 332 mAh g^{-1} at 0.1 A g^{-1} and retain 72% optical modulation after 500 cycles, as confirmed via in situ Raman analysis (**Fig. 22e**).

Because parasitic reactions at EC material–electrolyte interfaces degrade aqueous EC batteries, interface engineering is crucial. Wang et al. [60] deposited nanoscale C_{60} on Sn anodes to homogenize electric fields, suppress "dead Sn," and produce aqueous EC Sn cells with 61.1% modulation at 523 nm (**Fig. 22f**). Zhang et al. [241] realized multicolor EC batteries using inverted Fabry-Pérot cavities: porous PES supported the anode, WO_3 acted as the EC layer, and W served as both reflector and current collector, yielding 534.3 mAh m^{-2} at 0.5 mA cm^{-2} with 52.6% retention after 200 cycles (**Fig. 22g**). Chen et al. [242] fabricated WO_3 ||acid-treated graphite-foil cells employing Zn^{2+} /Al^{3+} hydrogel electrolytes; the AGF provided high ion storage and rapid kinetics, maintaining capacity even at elevated discharge potentials (**Fig. 22h**). Wang et al. [134] introduced carbon-dot electrolyte additives to build multicolor EC energy-storage displays (EESDs) with low self-discharge, vivid two-dimensional coloration, and reversible electrochromic/electrochemical performance from -25 °C to 65 °C (**Fig. 22i**). Collectively, these advances highlight tailored electrode/electrolyte engineering, interfacial stabilization, and multifunctional architectures as essential pathways toward practical electrochromic energy-storage devices.

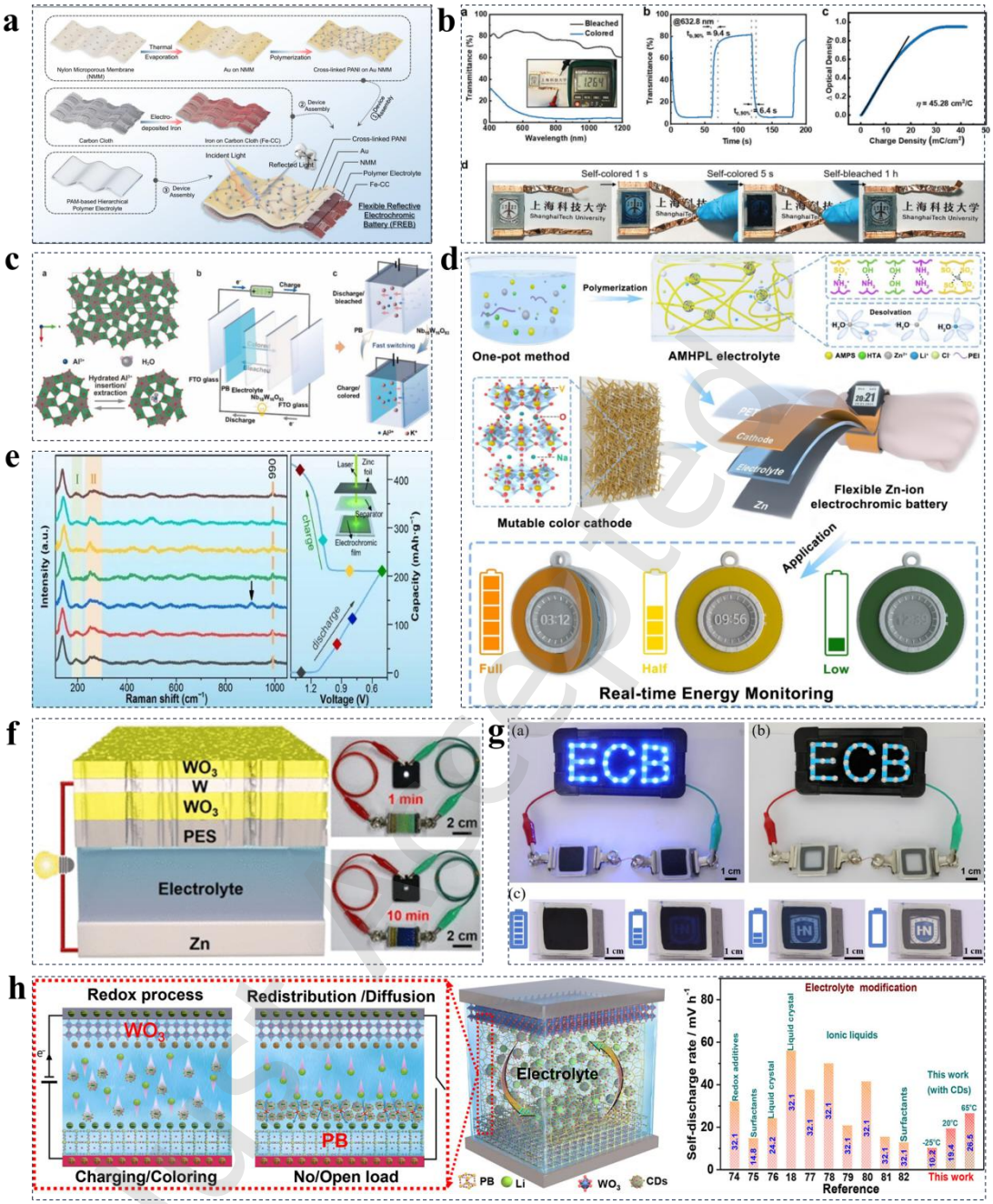

Fig.22 (a) Schematic of the preparation route for flexible reflective electrochromic batteries[237].(b) Electrochromic performance of a prototype device in the hybrid Zn^{2+}/Al^{3+} aqueous electrolyte[238]. Reproduced with permission.[238] Copyright 2023, Wiley-VCH GmbH. (c) The structure of $Nb_{18}W_{16}O_{93}$ and its applications in rechargeable Al^{3+} batteries[236]. Reproduced with permission.[236] Copyright 2025, Wiley-VCH GmbH. (d) Schematic of AMHPL electrolyte and VO_{Na^+} cathode preparation for flexible ZIEB assembly and application [239]. Reproduced with permission.[239] Copyright 2024, Wiley-VCH GmbH. (e) Schematic diagram of in-situ Raman-electrochemical testing system[240].(f) Schematic illustration of the inverted electrochromic device incorporating an inner WO_3 layer and device

demonstration[60]. (g) Two series-connected WO_3 ||AGF electrochromic batteries power a display [242].(h) Schematic illustration of the self-discharge mechanism[134]. Reproduced with permission.[134] Copyright 2024, Elsevier.

6.4.3 Smart Batteries and Self-Diagnostic Functional Integration

Battery and supercapacitor health monitoring is crucial for ensuring safety and longevity; however, conventional electrochemical metrics (voltage, current) provide limited insight into microscopic degradation processes and therefore require highly sensitive sensing combined with advanced signal analysis, particularly in noisy, complex environments where flexible sensors frequently exhibit signal instability (**Fig. 23a**) [243]. Intelligent batteries aim to overcome resource, safety, and environmental constraints by integrating real-time sensing with AI-driven lifetime prediction, thereby enabling unprecedented control over performance and safety profiles [244]. One recent approach couples high-capacitance storage with intrinsic self-diagnostics using carbon-quantum-dot-modified $W_{18}O_{49}$/carbon-cloth electrodes: during cycling, irreversible indigo-to-cyan/dark color changes emerge from cation-diffusion-induced W-lattice distortion and valence-state evolution, providing a direct visual warning of imminent failure while retaining flexibility and electrochromic responsiveness (**Fig. 23b**) [31]. Historically, electrochromic materials have been developed through empirical, trial-and-error strategies; now, AI and robotics are transforming this landscape. At Argonne National Laboratory, machine-learning-guided automated synthesis has yielded new conductive polymers and EC materials (**Fig. 23c**) [245], while the Chicago/Argonne “Polybot” platform autonomously designed and synthesized EC polymers with targeted colors, including previously unreported orange and green (**Fig. 23d–e**) [246]. These AI-enabled fabrication and monitoring frameworks are broadly applicable to EC batteries and smart cells, supporting predictive, full-lifecycle management via integrated sensing and data-driven control, and steering energy-storage technologies toward truly intelligent, adaptive operation.

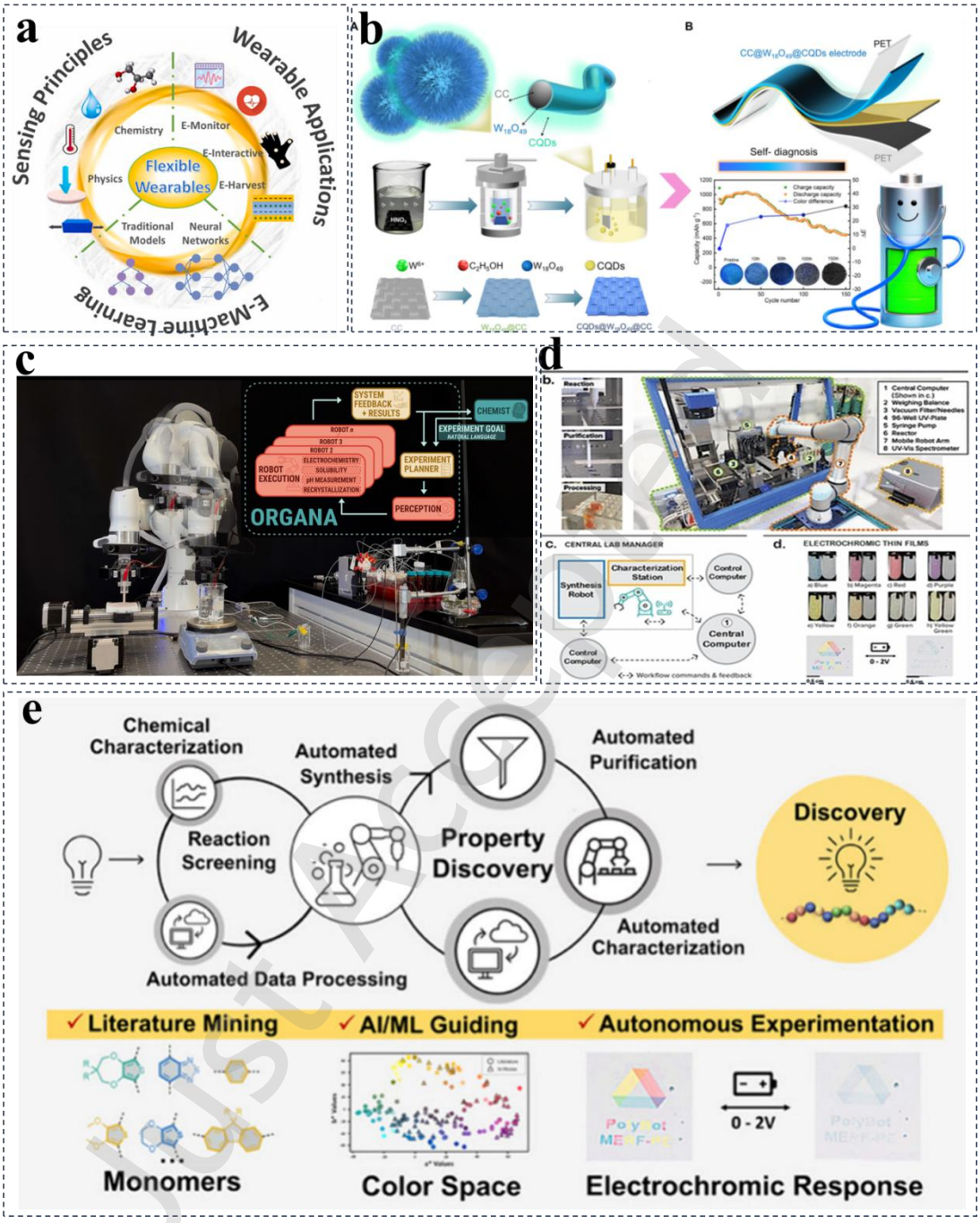

Fig.23 (a) The relation of the sensing mechanisms , wearable application and different machine learning models [243]. Reproduced with permission.[243] Copyright 2024, Elsevier. (b) Fabrication of smart battery with self-diagnosis[31]. (c) Robot setup with ORGANA's overall schema[245]. Reproduced with permission.[245] Copyright 2025, Elsevier. (d) key operations executed by the synthesis robot. Right: experimental modules enabling the autonomous discovery of ECPs, and (e) f the inverse design workflow for ECPs implemented in Polybot [246]. Reproduced with permission.[246] Copyright 2025, American Chemical Society.

7. Summary and Future Perspectives

EC technology, an intelligent means of modulating a material's optical properties via an applied electric field, is emerging as a transformative platform for building energy conservation, flexible displays, adaptive thermal management, and multifunctionally integrated systems. This review offers a systematic overview of the underlying EC mechanisms; the principal material classes (including inorganic transition-metal oxides, organic small molecules, conjugated polymers, metal-supramolecular polymers, and porous frameworks); flexible device architectures and performance-optimization strategies; self-powered integration schemes; and multifunctional applications spanning energy storage, sensing, and camouflage. Our analysis highlights that, despite rapid advances, the field still contends with sluggish ionic transport, limited cycling durability, difficulties in achieving coordinated broadband modulation, and significant complexity in system-level integration.

The EC material library has expanded well beyond early inorganic compounds such as WO_3 and NiO to encompass viologen-based organics, conjugated polymers (e.g., PEDOT), and porous frameworks (MOFs/COFs), each contributing improvements in coloration efficiency, color tunability, mechanical compliance, and scalable processing. Viologen derivatives, for example, enable finely controlled color tuning from bluish violet to black via molecular design, while their solution processability facilitates flexible-device manufacturing. PEDOT:PSS combines excellent film-forming properties with strong electrochemical activity, underpinning its widespread adoption in flexible electronics. MOF/COF-based architectures offer ordered ion-transport channels that support fast ion insertion and multistable EC states. On the device-engineering side, flexible EC devices (FECDs) are evolving from traditional five-layer stacks toward more compact, integrated configurations. Material hybrids (such as MXene/WO_3), micro/nanostructuring (e.g., wrinkled interfaces, nanodot arrays), and advanced fabrication routes (3D printing, roll-to-roll coating) have substantially enhanced mechanical robustness, response speed, and optical contrast. Fully printed, self-powered EC platforms already demonstrate multicolor switching in concert with energy harvesting, pointing toward near-zero-energy operation.

Multifunctional integration has become a focal point: EC technology now interfaces deeply with energy-storage platforms (such as EC supercapacitors and

batteries), health-monitoring systems, and adaptive camouflage[247-249]. ECSCs, for instance, unite charge storage with optical state-of-charge indication, while AI- and robotics-assisted materials discovery is propelling EC research toward intelligent, high-throughput development pipelines[250]. Importantly, EC systems are converging toward self-powered, multimodal functionality. Incorporation of piezoelectric or triboelectric nanogenerators (TENGs) enables direct conversion of mechanical energy into drive voltages, thereby realizing concurrent pressure sensing, visual feedback, and local power supply. Nonetheless, issues such as disentangling piezoelectric and triboelectric contributions and sensing static or quasi-static loads remain unresolved, calling for advances in materials design and signal-decoupling methodologies. Overall, EC technology still faces substantial barriers to large-scale commercialization, and future research should focus on the directions outlined in **Fig. 24**.

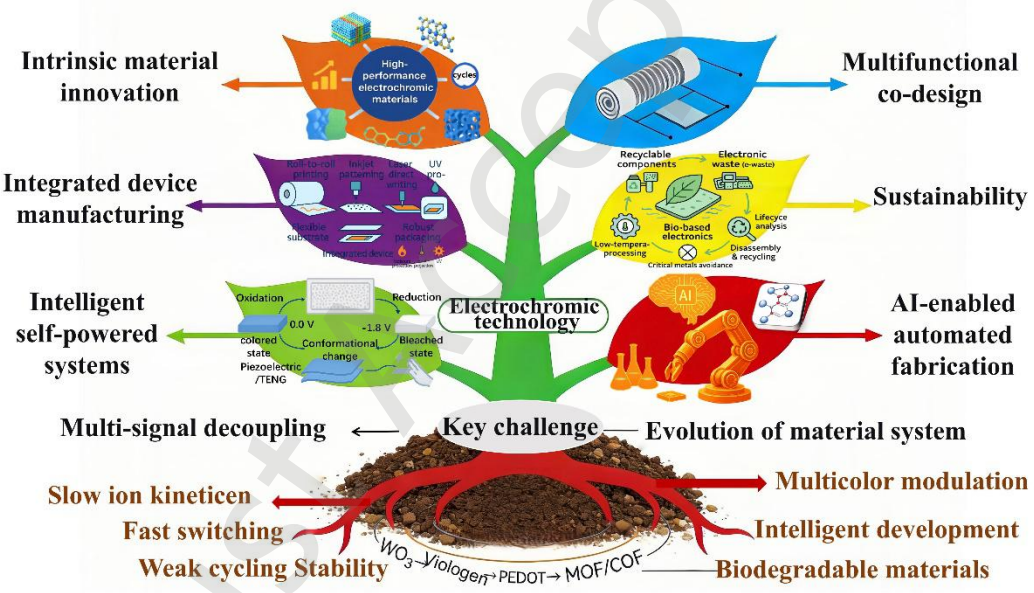

Fig.24. Schematic of future direction of EC technology from material innovation, integrated devices, self-powered systems, sustainability, AI, multifunctional co-design to signal decoupling.

(1) Intrinsic material innovation. State-of-the-art EC materials still struggle with limited ionic conductivity, restricted optical modulation, particularly in the near-infrared II region, cycling lifetimes rarely exceeding 10^5 cycles, and poor resistance to environmental stressors. The importance of controlling chain aggregation, crystallinity, and phase separation (e.g., via mixed solvent systems or additives) is attached to simultaneously optimizing optical contrast, switching speed, and

mechanical flexibility. Theory-driven design combined with machine-learning-assisted screening is essential to identify compositions that simultaneously deliver high ionic conductivity, broadband (visible plus NIR) modulation, elevated coloration efficiency, and long operational lifetimes. Promising avenues include crystalline-amorphous composites that host rapid ion-transport channels, next-generation conjugated polymers, and porous framework materials capable of surpassing current performance ceilings.

(2) Integrated device manufacturing. Multilayer heterostructures fabricated by photolithography or vacuum deposition suffer from interfacial mismatches, throughput limits, and escalating cost. One-step, solution-processable techniques—roll-to-roll printing, inkjet patterning, laser direct writing—should be advanced to enable large-area (>1 m^2), high-performance flexible EC devices at low cost. In parallel, packaging strategies must be strengthened to ensure long-term reliability under humidity, thermal cycling, and UV irradiation.

(3) Intelligent self-powered systems. Present piezoelectric or TENG-integrated EC modules offer low energy-conversion efficiency and unstable outputs, hindering sustained multifunctional operation. Future designs should merge high-efficiency power-management circuitry, low-power driving modes (e.g., pulsed operation), and embedded micro-energy storage (micro-supercapacitors) to build stable, adaptive energy ecosystems. Co-harvesting optical, thermal, and mechanical energy will further enhance autonomous capability in practical settings.

(4) Multifunctional co-design. Many “sensor + display” constructs merely stack discrete elements, resulting in weak coupling and asynchronous responses. Next-generation EC platforms must adopt holistic material-structure-circuit co-design so that sensing, processing, and feedback coexist within one framework. Examples include integrating EC pixels with neuromorphic computing units to realize adaptive optical systems endowed with learning and memory, or skin-like engineering, low-modulus (<100 kPa), biodegradable transient electronics for health monitoring and closed-loop therapeutic feedback.

(5) Sustainability. With electronic waste under growing scrutiny, EC devices should increasingly rely on bio-derived constituents, aqueous electrolytes, and recyclable components. Research priorities must include full life-cycle assessment, low-temperature/energy-efficient processing, avoidance of critical metals, and architectures intentionally engineered for disassembly and recycling. Highlight specific near-term opportunities for reducing environmental burden, such as replacing vacuum deposition with aqueous or low‑ temperature solution processing for suitable

oxide systems, developing electrolytes and counter‐ electrode chemistries based on earth‐ abundant, low‐ toxicity components, and designing device stacks that can be disassembled for material recovery at end of life.

(6) AI-enabled automated fabrication. AI-driven, high-throughput platforms such as “Polybot” already design and synthesize target EC polymers within tens of hours, dramatically accelerating discovery. Coupling digital twins with robotic automation can extend this paradigm from materials discovery through device optimization to system-level integration.

(7) Multi-signal decoupling. Although significant progress has been made in piezoelectric and triboelectric decoupling, challenges remain. For instance, the nonlinearity of mechanical-electrical coupling and the dynamic changes at the interface under real working conditions still limit the accuracy of signal decoupling. Future research may need to integrate more advanced data-driven methods, such as blind source separation (Independent Component Analysis, ICA) or deep learning models (Convolutional Neural Network-Long Short-Term Memory, CNN-LSTM), to model and perform independent component inversion of the mixed electrical signals. Additionally, developing universal decoupling methods and standards is also an important direction in this field.

Overall, commercial realization of high-performance EC smart devices demands simultaneous progress in rapid switching, multicolor modulation, and sustained redox/photochemical stability. These advances will hinge not only on materials breakthroughs but also on deep collaboration with flexible electronics, energy science, artificial intelligence, and green manufacturing. Addressing the priorities above will position electrochromic technology at the core of next-generation intelligent buildings, wearable electronics, adaptive camouflage, and human-machine interfaces, thereby supporting a greener, smarter, and more sustainable future.

Acknowledgements

We gratefully acknowledge financial support by the National Key Research and Development Program of China (No. 2023YFB4605504), China Postdoctoral Science Foundation (Grant No. 2025M771866), Natural Science Foundation of Chongqing (Grant No. CSTB2023NSCQ-MSX0929), Scientific and Technological Research Program of Chongqing Municipal Education Commission (Grant No. KJQN202500829 and KJQN202300815), the Chinese National Natural Science Fund (Grant No.: 12227801), National Key Research and Development Program of Ministry of Science and Technology of China (No. 2025YFE0115400), the Fund for

Innovative Research Groups of Natural Science Foundation of Hebei Province (No. A2024202045), Major Basic Research Project of Hebei Province Natural Science Foundation (No. A2023202049), Tianjin Science & Technology Program (24YFXTHZ00160), and the InnoHK initiative of the Innovation and Technology Commission of the Hong Kong Special Administrative Region Government.

Data availability

Not applicable.

Declaration of competing interest

All the contributing authors report no conflict of interests in this work.

Author contributions statement

Zhu W conceived the idea and led this project for this review. Zhang H, Tang S and Wang H collected the references, organized the images, and wrote the entire manuscript. Huang X and Xiang H modified the manuscript and participated in the discussion. Zhang H and Zhu W supervised the project. All the authors have approved the final manuscript.

Use of AI statement

None.

Reference.

[1] Mustafa, M. N.;Mohd Abdah, M. A. A.;Numan, A.;Moreno-Rangel, A.;Radwan, A.; Khalid, M. Smart window technology and its potential for net-zero buildings: A review. *Renewable and Sustainable Energy Reviews* **2023**, *181*.

[2] Qin, S.;Cao, S.;Liu, Y.;Chen, J.;Li, H.;Yang, T.;Liu, G.;Zhao, J.; Zou, B. A Wide Color Gamut and Noniridescent Zinc‐Anode Asymmetric Electrochromic Device for Self‐Sustaining Color‐Adaptive

Bio‐Camouflage System. *Small* **2024**, *20*.

[3] Fu, H.;Zhang, L.;Dong, Y.;Zhang, C.; Li, W. Recent advances in electrochromic materials and devices for camouflage applications. *Materials Chemistry Frontiers* **2023**, *7*, 2337-2358.

[4] Zhu, W.;Chow, L.;Ye, D.;Qiu, Y.;Li, J.;Zhang, B.;Guo, Y.;Jia, S.; Yu, X. Advances in smart textiles for personal thermal management. *Med-X* **2025**, *3*, 6.

[5] Zhang, H.;Chen, Z.;Wu, B.;Ji, X.;Tang, S.; Zhu, W. Multifunctional wearable sensor based on DNA-inspired helically structured conductive cotton threads with applications in electronic skin, joule heater and supercapacitor. *Surfaces and Interfaces* **2025**, *60*.

[6] Fan, H.;Wei, W.;Hou, C.;Zhang, Q.;Li, Y.;Li, K.; Wang, H. Wearable electrochromic materials and devices: from visible to infrared modulation. *Journal of Materials Chemistry C* **2023**, *11*, 7183-7210.

[7] Luo, Z.;Wang, Q.;Feng, R.;Wang, S.;Zhou, Z.;Hu, Y.;Li, Q.;Yan, Q.;Feng, Z.;Hou, Y.;Ying, T.;Weng, Y.;Fang, L.; You, L. Reversible electrochromism in α-In2Se3 through ferroelectric switching induced phase transition. *Science China Materials* **2025**, *68*, 906-911.

[8] Hassan, M.;Ghaffar, A.;Lou, G.;Miao, Z.;Peng, Z.; Celebi, K. Enhanced Transport Kinetics of Electrochromic Devices by W18O49 NW/Ti3C2Tx Composite Films. *Advanced Functional Materials* **2024**, *34*.

[9] Park, J.;Bark, H.;Gupta, A.;Tan, A. W. M.;Wu, W.; Lee, P. S. Electrode Potential‐Resolved Mechanistic Insights into Flexible Electrochromic Devices with Photocurable Redox‐Active Electrolyte. *Advanced Optical Materials* **2025**, *13*.

[10] Zhang, L.;Wang, J.;Zhang, W.;Li, J.;Xie, W.;Ouyang, M.;Dong, Y.;Li, W.; Zhang, C. Super‐High Stable Dual Polymer Electrochromic Device Over 35 000 Cycles with Red‐to‐Green Switching for Realistic Adaptive Camouflage. *Small* **2025**, *21*.

[11] Wang, B.;Zhang, W.;Zhao, F.;Yu, W. W.;Elezzabi, A. Y.;Liu, L.; Li, H. An overview of recent progress in the development of flexible electrochromic devices. *Nano Materials Science* **2023**, *5*, 369-391.

[12] Fan, X.;Zhang, C.;Wang, S.;Ma, S.;Gu, Q.;Li, Y.;Tong, Z.;Xu, H.; Zhang, Q. Porous Electrochromic Structures: A Review. *SmartMat* **2025**, *6*.

[13] Yao, L.;Zhao, L.;Gaishunr, V.;Sun, S.;Wu, J.;Yang, C.;Zhang, Y.; Liu, Z. Effects of hydrothermal temperature and coloring/bleaching voltage on the electrochromic performance of WO3. *Journal of Alloys and Compounds* **2025**, *1029*.

[14] Zhou, C.;Wang, C.;Xiang, S.;Li, K.;Bao, B.;Xu, G.;Zhang, C.;Wang, Q.;Cao, H.; Zhang, H. Hexagonal WO_3 nanogranular thin films with oxygen-vacancy engineering for ultra-stable electrochromic energy storage devices. *Applied Materials Today* **2026**, *48*.

[15] Zhang, X.;Han, Z.;Cao, T.;Zhu, Y.;Wang, Z.;Zhang, Z.;Zhou, Z.;Zhang, D.;Yan, N.;Zhang, Y.; He, G. Multi-responsive thiazolothiazole viologen-based electrochromic materials for smart windows and electronic displays. *Chemical Engineering Journal* **2025**, *503*.

[16] Wu, W.;Guo, S.;Bian, J.;He, X.;Li, H.; Li, J. Viologen-based flexible electrochromic devices. *Journal of Energy Chemistry* **2024**, *93*, 453-470.

[17] Chen, X.;Liu, Q.;Cheng, L.;Zhou, S.;Chen, L.;Liang, G.;Wei, J.; Mo, F. Advanced Electrochromic Energy Storage Devices Based on Conductive Polymers. *Advanced Materials Technologies* **2024**, *9*.

[18] Mei, Z.;Zhang, Y.;Sun, S.;He, Y.; Meng, H. Triarylamine-based electrochromic materials: From design to multifunctional devices. *Chemical Engineering Journal* **2025**, *526*.

[19] Zhou, Q.;Shao, P.;Zhang, R.;Huang, S.;Zhang, Y.;Zhu, Y.;Yin, M.;Niklasson, G. A.; Wen, R.-T. Photo-electrochemical synergistically induced ion detrapping for electrochromic device rejuvenation. *Matter* **2025**, *8*.

[20] Zhang, H.;Lin, L.;Kong, W.;Yin, H.;Hu, W.;Bi, X.;Yang, Z.;Chen, W.; Hu, N.

Hierarchically bread-derived carbon foam decorated with defect engineering in reduced graphene oxide/carbon particle nanocomposites as electrode materials for solid-state supercapacitors. *Journal of Energy Storage* **2023**, *68*.

[21] Long, J.; Zhu, W. Advancing carbon fiber reinforced epoxy composites with enhanced mechanical properties and liquid oxygen compatibility. *Composites Part B: Engineering* **2026**, *314*.

[22] Zhang, H.;Lin, L.;Hu, N.;Yin, D.;Zhu, W.;Chen, S.;Zhu, S.;Yu, W.; Tian, Y. Pillared carbon@tungsten decorated reduced graphene oxide film for pressure sensors with ultra-wide operation range in motion monitoring. *Carbon* **2022**, *189*, 430-442.

[23] Xue, S.;Cui, J.;Zhou, C.;Shen, M.;Liang, X.;Wang, M.;Zhao, Q.;Ye, Y.;Xu, K.;Zhao, Y.;Jiao, R.;Wen, R. T.;Yang, C.;Yu, Z.;Yu, R.; Xing, W. Decoding the gradient-distributed colour centers in electrochromic WO(3). *Nat Commun* **2026**, *17*, 1286.

[24] Nguyen, T. P.;Easley, A. D.;Kang, N.;Khan, S.;Lim, S. M.;Rezenom, Y. H.;Wang, S.;Tran, D. K.;Fan, J.;Letteri, R. A.;He, X.;Su, L.;Yu, C. H.;Lutkenhaus, J. L.; Wooley, K. L. Polypeptide organic radical batteries. *Nature* **2021**, *593*, 61-66.

[25] Matsuhisa, N.;Niu, S.;O'Neill, S. J. K.;Kang, J.;Ochiai, Y.;Katsumata, T.;Wu, H. C.;Ashizawa, M.;Wang, G. N.;Zhong, D.;Wang, X.;Gong, X.;Ning, R.;Gong, H.;You, I.;Zheng, Y.;Zhang, Z.;Tok, J. B.;Chen, X.; Bao, Z. High-frequency and intrinsically stretchable polymer diodes. *Nature* **2021**, *600*, 246-252.

[26] Guo, X.;Chen, L.;Liu, R.;Fan, B.;Cong, S.;Wang, Z.; Zhao, Z. Ionic Liquid MPII(3) Elevates Electrochromic Battery Capacity to Practical Applications. *Adv Mater* **2025**, *37*, e2504575.

[27] Jia, Z.;Sui, Y.;Qian, L.;Ren, X.;Zhao, Y.;Yao, R.;Wang, L.;Chao, D.; Yang, C. Electrochromic windows with fast response and wide dynamic range for visible-light modulation without traditional electrodes. *Nature*

Communications **2024**, *15*.

[28] Park, J.;Kim, J.;Kim, K.;Kim, S. Y.;Cheong, W. H.;Park, K.;Song, J. H.;Namgoong, G.;Kim, J. J.;Heo, J.;Bien, F.; Park, J. U. Wearable, wireless gas sensors using highly stretchable and transparent structures of nanowires and graphene. *Nanoscale* **2016**, *8*, 10591-10597.

[29] Ma, B.;Li, C.;Li, Z.;Han, Z.;Huang, A.;Luo, H.;Bell, J.;Jin, P.; Cao, X. A Redox-Mediated Stepwise Reversible Electrodeposition Smart Window. *Adv Mater* **2026**, 10.1002/adma.202520939, e20939.

[30] Xu, L.;Zhang, L.;Liu, D.;Ren, Z.;Liu, W.;Zhang, Y.;Wang, Y.;Sun, J.;Yang, R.;Lv, Z.;Zhao, J.; Li, Y. A Comprehensive Review of the Functionalized Integrated Application of Gel Polymer Electrolytes in Electrochromic Devices. *Nanomicro Lett* **2026**, *18*, 106.

[31] Li, J.-K.;Wang, K.-Z.;Shi, J.;Wang, Y.-F.;Sun, Z.-W.;Liu, F.;Wang, K.-J.;Wu, J.-L.;Zhu, C.;Park, H.;Hwang, J.-Y.;Hu, J.; Xiong, S.-Z. Carbon quantum dot modified W18O49 electrode enables smart energy storage device with a self-diagnosis character. *Rare Metals* **2025**, 10.1007/s12598-025-03601-7.

[32] Bao, B.;Hao, Y.;Wu, X.;Xiao, R.;Hou, C.;Li, Y.;Zhang, Q.;Li, K.; Wang, H. Redox-bipolar mesoporous two-dimensional covalent organic framework for multi-color electrochromism. *Science Advances*, *11*, eaea1304.

[33] Chen, J.;Xiong, P.;Li, K.; Yang, S. Optimization Study of Fire Prevention Structure of Electric Vehicle Based on Bottom Crash Protection. *Fire* **2024**, *7*.

[34] Tong, X.;Wang, J.;Zhang, P.;Lei, P.;Gao, Y.;Ren, R.;Zhang, S.;Zhu, R.; Cai, G. Insight into the structure–activity relationship in electrochromism of WO3 with rational internal cavities for broadband tunable smart windows. *Chemical Engineering Journal* **2023**, *470*.

[35] Chen, M.;Deng, J.;Zhang, H.;Zhang, X.;Yan, D.;Yao, G.;Hu, L.;Sun, S.;Zhao, J.; Li, Y. Advanced Dual‐Band Smart Windows: Inorganic All‐Solid‐State Electrochromic Devices for Selective Visible and Near‐Infrared Modulation. *Advanced Functional Materials* **2024**, *35*.

[36] Tong, X.;Wang, J.;Zhang, P.;Lei, P.;Gao, Y.;Ren, R.;Zhang, S.;Zhu, R.; Cai, G. Insight into the structure–activity relationship in electrochromism of WO3 with rational internal cavities for broadband tunable smart windows. *Chemical Engineering Journal* **2023**, *470*, 144130.

[37] Manjakkal, L.;Pereira, L.;Kumi Barimah, E.;Grey, P.;Franco, F. F.;Lin, Z.;Jose, G.; Hogg, R. A. Multifunctional flexible and stretchable electrochromic energy storage devices. *Progress in Materials Science* **2024**, *142*.

[38] Li, R.;Ma, X.;Li, J.;Cao, J.;Gao, H.;Li, T.;Zhang, X.;Wang, L.;Zhang, Q.;Wang, G.;Hou, C.;Li, Y.;Palacios, T.;Lin, Y.;Wang, H.; Ling, X. Flexible and high-performance electrochromic devices enabled by self-assembled 2D TiO(2)/MXene heterostructures. *Nat Commun* **2021**, *12*, 1587.

[39] Li, G.;Tseng, M.-C.;Chen, Y.;Yeung, F. S.-Y.;He, H.;Cheng, Y.;Cai, J.;Chen, E.; Kwok, H.-S. Color-conversion displays: current status and future outlook. *Light: Science & Applications* **2024**, *13*.

[40] Bai, Z.;Zhang, H.;Xue, R.;Lu, X.;Li, X.;MacSwain, W.;Zheng, W.;Xu, J.;Yu, Y.; Bai, Y. L. Viologen‐based host–guest supramolecule with tunable intramolecular/intermolecular electron transfer chromism and dynamic fluorescence. *Aggregate* **2024**, *5*.

[41] Li, G.;Tseng, M. C.;Chen, Y.;Yeung, F. S.;He, H.;Cheng, Y.;Cai, J.;Chen, E.; Kwok, H. S. Color-conversion displays: current status and future outlook. *Light Sci Appl* **2024**, *13*, 301.

[42] Du, C.;Cheng, X.;Lu, B.;Zhou, W.;Zhang, J.;Xu, J.;Zhang, G.; Nie, G. Engineering a 3D conductive polythiophene network with conformational locking for camouflaged wearable electrochromic-supercapacitor devices. *Energy Storage Materials* **2025**, *80*.

[43] Jeon, S.;Lee, S. E.;Kim, W.;Lee, S. H.;Min, S.;Seon, S. W.;Han, S. H.;Kim, B. H.;Lee, H.; Shin, J. Visual and thermal camouflage on different terrestrial environments based on electrochromism. *Nanophotonics* **2023**, *12*, 3199-3209.

[44] Fan, Y.;Chen, H.;Liu, X.;Zhao, Y.;Huang, Y.;Liu, J.; Wang, C. Radiative

Cooling in Outer Space: Fundamentals, Advances in Materials and Applications, and Perspectives. *Advanced Materials* **2025**, *37*.

[45] Du, C.;Cheng, X.;Lu, B.;Zhou, W.;Zhang, J.;Xu, J.;Zhang, G.; Nie, G. Engineering a 3D conductive polythiophene network with conformational locking for camouflaged wearable electrochromic-supercapacitor devices. *Energy Storage Materials* **2025**, *80*, 104394.

[46] Liu, S.;Wei, C.;Wang, H.;Yang, W.;Zhang, J.;Wang, Z.;Zhao, W.;Lee, P. S.; Cai, G. Processable nanoarchitectonics of two-dimensional metallo-supramolecular polymer for electrochromic energy storage devices with high coloration efficiency and stability. *Nano Energy* **2023**, *110*, 108337.

[47] Zhang, X.;Hao, L.;Xie, J.;Tan, Z.;Li, S.;Gan, C.;Xiong, W.;Duan, X.;Li, S.;Xu, Z.;Zhang, K.;Wang, Y.;Tang, H.; Huang, F. Multifunctional integrated electrochromic device by p-n conductive polymers for self-powered smart windows and miniaturized spectrometers. *Nat Commun* **2025**, *16*, 11574.

[48] Guo, J.;Jia, H.;Shao, Z.;Jin, P.; Cao, X. Fast-Switching WO3-Based Electrochromic Devices: Design, Fabrication, and Applications. *Accounts of Materials Research* **2023**, *4*, 438-447.

[49] Li, M.;Yang, Q.;Liu, H.;Qiu, M.;Lu, T. J.; Xu, F. Capillary Origami Inspired Fabrication of Complex 3D Hydrogel Constructs. *Small* **2016**, *12*, 4492-4500.

[50] Zhong, J.;Huang, B.;Song, J.;Zhang, X.;Du, L.;Gao, Y.;Liu, W.; Kang, L. Stable WO3 electrochromic system based on NH4+ hydrogen bond chemistry. *Chemical Engineering Journal* **2024**, *480*.

[51] Santosa, A. S. S.;Chang, Y.-W.;Dahlin, A. B.;Österlund, L.;Volpe, G.; Xiong, K. Video‐rate tunable colour electronic paper with human resolution. *Nature* **2025**, *646*, 1089-1095.

[52] Santosa, A. S. S.;Chang, Y. W.;Dahlin, A. B.;Osterlund, L.;Volpe, G.; Xiong, K. Video-rate tunable colour electronic paper with human resolution. *Nature* **2025**, *646*, 1089-1095.

[53] Deng, J.;Chen, M.;Zhang, X.;Zhang, H.;Hu, L.;Sun, S.;Zhao, J.; Li, Y.

Water-in-eutectogel electrolytes for scalable solid-state electrochromic devices. *Chemical Engineering Journal* **2025**, *516*, 163746.

[54] Li, W.;Li, A.;Wang, Y.;Ding, M.;Liu, J.;Wang, H.;Zheng, Z.; Zhang, Q. Anion-Selective Ion Conductor Boosting Highly Flexible All-In-One Electrochromic Fabrics. *Advanced Functional Materials* **2025**, *35*, 2420459.

[55] Lan, F.;Li, R.;Zhang, Y.;Ding, Y.;Wu, X.;Li, Y.;Zhao, Y.;Ma, Z.;Xi, A.;Zhao, S.;Huang, Y.;Xu, J.;Zhao, Z.;Wang, C.;Xu, C.; Zhang, R. A Quasi‐Solid Electrolytes Based on Crystalline Phase Modulation of PVDF‐HFP for High‐Performance Electrochromic Devices. *Advanced Optical Materials* **2025**, *13*.

[56] Chen, Y.;Jiang, W.;Zhang, C.;Shen, Q.;Li, D.; Wang, Z. Enhanced Electrochromic Performance and Cycling Stability via Built‐In Electric Field in WO3/Nb2O5 Heterostructure. *Advanced Functional Materials* **2025**, 10.1002/adfm.202519286.

[57] Zhao, F.;Chen, Y.;Shi, G.;Liu, Q.;Liu, Y.; Han, G. Revealing the Mechanism of Ni Vacancies on Ion Storage, Diffusion Kinetics, and Electrochromic Performance of Nickel Oxide Electrodes. *Small* **2025**, *21*, e2411995.

[58] Li, P.;Lv, Y.;You, X.;Ma, H.;Wang, T.;Shen, Y.;Li, X.;Guo, X.;Cai, G.; Liu, X. Bio‐Inspired Ordered WO3 Nano‐Helixes Enable Multi‐Band Electrochromic Smart Windows with Ultrafast Switching and Robust Cyclability. *Energy & Environmental Materials* **2025**, 10.1002/eem2.70185.

[59] Huang, B.;Wang, B.;Zhao, F.;Li, H.; Yu, W. W. A Dual‐Mode Anode‐Free Zinc‐Prussian Blue Electrochromic Device. *Advanced Functional Materials* **2025**, *35*.

[60] Wang, Y.;Wang, N. Z.;Wu, Z. A.;Liu, J.;Guan, K. L.;Zhang, Z. L.;Wan, H. Z.;Wang, H.;Sun, D. Y.; Xie, A. Nanofullerene regulated electric field to achieve stable Sn metal anode for aqueous Sn batteries. *Rare Metals* **2025**, *44*, 3869-3880.

[61] Song, C.;Zheng, R.;Li, Y.;Tian, M.;Wu, W.;Tang, Y.;Zhou, G.; Shao, J.

Flexible electrochromic zinc ion battery based on Prussian blue prepared by MXene‐assisted in situ growth. *Rare Metals* **2025**, *44*, 6102-6114.

[62] Li, P.;Huang, H.;Yang, Z.;Zheng, R.; Jia, C. Facile fabrication of Prussian blue films via in-situ growth for multicolor electrochromic applications. *Chemical Engineering Journal* **2025**, *519*, 165524.

[63] Zhang, Q.;Liu, X.;He, Y.;Yan, M.;Murtaza, I.;Zou, D.;Xu, T.;Cui, Y.;Zeng, L.; Meng, H. High optical contrast and stable black electrochromic devices enabled by viologen and fluoran materials. *Chemical Engineering Journal* **2025**, *516*, 164117.

[64] Gu, C.;Wang, S.;He, J.;Zhang, Y.-M.; Zhang, S. X.-A. High-durability organic electrochromic devices based on in-situ-photocurable electrochromic materials. *Chem* **2023**, *9*, 2841-2854.

[65] Zhang, H.;Sun, M.;Sun, F.;Sun, Q.;Cao, G.;Wu, X.;Ling, H.;Su, F.;Tian, Y.;Liu, Y. J.;Xu, L.; Tian, Y. High-Efficiency and High-Capacity Aqueous Electrochromic Energy Storage Devices Enabled by Decoupled Titanium Oxide/Viologen Derivative Hybrid Materials. *Research (Wash D C)* **2025**, *8*, 0909.

[66] Li, H.;Wen, M.;Dong, W.;Duan, Y.;Hu, F.;Yang, J.;Jiang, Z.;Fan, H.;Hu, B.;Mahalingam, R.; Song, J. Viologen Derivatives in Aqueous Organic Redox Flow Batteries: Progress and Perspectives. *Adv Mater* **2025**, 10.1002/adma.202514004, e14004.

[67] Hwang, S.;Oh, M.;Lee, K. J.;Jin, C. S.;Park, S. K.;Seo, C.;Yeon, S. H.;Kim, D. H.;Gueon, D.;Han, Y. K.; Shin, K. H. Integration of Functional Groups to Enhance the Solubility and Stability of Viologen in Aqueous Organic Redox Flow Batteries. *ACS Appl Mater Interfaces* **2024**, *16*, 28645-28654.

[68] Nandi, R. P.;Zuo, J.;Shibu, A.; Jakle, F. B-N Fused Anthracene as Functional Linker for pi-Extended Viologens: Near-IR Emission and Electrochromism. *Angew Chem Int Ed Engl* **2025**, 10.1002/anie.202521634, e21634.

[69] Zong, H.;Zhou, F.;Zhang, Z.-D.;Cai, J.-W.;Zhong, Y.-N.;Xu, J.-L.;Gao,

X.;Wang, S.-D.; Zhou, G. Flexible multimode electrochromic artificial synapses for visualized health monitoring. *Nano Energy* **2025**, *142*, 111260.

[70] Bian, W.;Chen, H.;Liu, J.;Zeb, S.;Li, Y.;Li, C.; Liu, Y. The electrochromic devices based on viologen derivatives and deep eutectic solvents for excellent light modulation efficiency and thermal insulation. *Journal of Alloys and Compounds* **2025**, *1032*, 181227.

[71] Jiang, Z.;Di, Y.;Dong, Z.;Ravivarma, M.;Duan, Y.;Hu, F.;Liu, K.;Fan, H.; Song, J. Uncovering the Electrochemical Origin of Alkalization in Viologen-Based Aqueous Flow Batteries. *Angew Chem Int Ed Engl* **2025**, *64*, e202514131.

[72] Gao, Y.;Liu, C.;Li, Y.;Li, G.;Sun, Q.;Shi, S.; He, G. 2,2′‐Thienoviologens with Low Reduction Potential for Electrochromism and Visible‐Light‐Driven Hydrogen Evolution Using g‐C3N4‐Based Composites via Hydrogen Bonds. *Advanced Energy Materials* **2024**, *14*.

[73] Yu, X.;Wei, Z.;Qin, Y.;Zhang, X.;Hao, D.;Jing, L.;Liu, Y.;Dai, H.;Deng, J.; Zhu, Y. Functional Groups-Regulated Organic Semiconductors for Efficient Artificial Photosynthesis of Hydrogen Peroxide. *Adv Mater* **2025**, *37*, e2501494.

[74] Ouyang, B.;Ma, M.;Gao, B.;Liu, G.; Xu, A. Synergistic modification of self-healing silicone coatings with fluorocarbon and zwitterionic side chains for enhanced antifouling properties. *Chemical Engineering Journal* **2025**, *521*, 167167.

[75] Wu, Y.;Xu, J.;Qin, X.;Xu, J.; Liu, X. Dynamic upconversion multicolour editing enabled by molecule-assisted opto-electrochemical modulation. *Nat Commun* **2021**, *12*, 2022.

[76] Wu, X.;Bao, B.;Bai, Z.;Fan, Q.;Hou, C.;Zhang, Q.;Li, Y.;Jiang, W.;Li, K.; Wang, H. Heteroaromatic π-stacking engineered near-infrared absorption for highly stable near-zero transmittance electrochromic window. *Nature Communications* **2025**, *16*.

[77] Chen, D.;Zhang, X.;Xu, H.;Wang, M.;Zhu, M.;Yang, M.;Zhu, Q.;He, Y.;Liu, Z.;Xu, J.; Meng, H. Synthetic Design of Dual Polar Side Chain Polymers for Enhancing Electrochromic Performance. *Macromolecules* **2024**, *57*, 6419-6428.

[78] Chiu, S.-H.;Widjajana, M. S.;Nor-Azman, N.-A.;Allioux, F.-M.;Yu, R.;Liu, L.;Flores, N.;Wang, Y.;Asgharnejad-Laskoukalayeh, M.;O'Mullane, A. P.; Kalantar-Zadeh, K. Electrochromic PEDOT:PSS with Embedded Liquid Gallium Nanoparticles. *ACS Applied Materials & Interfaces* **2025**, *17*, 43968-43978.

[79] Wu, Y.;Liu, J.;Wang, M.;Wu, X.;Cai, W.;Niu, H.; Lang, K. Reversible formation and control of linear conjugation in polymers. *Nature Chemistry* **2025**, *17*, 1265-1274.

[80] Sun, F.;Pal, R.;Eom, S. Y.;Choi, J. W.;Zhang, W.;Jeong, B.; Park, J. S. Fast-switching dual-cathode electrochromic smart windows for year-round building energy savings. *Nat Commun* **2025**, *16*, 9569.

[81] Wu, L.;Fang, H.;Jing, K.;Zhang, L.;Yu, H.; Chai, Y. Electrochromic Artificial Synapses for Spatiotemporal Dual‐Encryption Display. *Advanced Functional Materials* **2025**, 10.1002/adfm.202522755.

[82] Chen, G.;Wang, J.;Chen, W. C.;Gong, Y.;Zhuang, N.;Liang, H.;Xing, L.;Liu, Y.;Ji, S.;Zhang, H. L.;Zhao, Z.;Huo, Y.; Tang, B. Z. Triphenylamine‐Functionalized Multiple‐Resonance TADF Emitters with Accelerated Reverse Intersystem Crossing and Aggregation‐Induced Emission Enhancement for Narrowband OLEDs. *Advanced Functional Materials* **2023**, *33*.

[83] Cheng, X.;Du, C.;Li, J.;Zhang, Y.;Xu, W.;Zhang, J.;Shi, H.;Zhang, G.; Zhang, L. Dual redox-centered p(thiophene-TPA) conjugated polymers for high-performance flexible electrochromic supercapacitors. *Chemical Engineering Journal* **2025**, *510*, 161744.

[84] Li, M. D.;Zhang, L. Y.;Wang, J. Y.;Han, J. Y.;Qian, X. Y.;Ye, X. L.;Dai, F. R.;

Chen, Z. N. Metallopolymer Films of a Manganese(II) Chelate with Hexadentate Ligand for High-Performance Electrochromism. *Angew Chem Int Ed Engl* **2025**, 10.1002/anie.202525500, e25500.

[85] Zhang, Y.;Jia, X.;Sun, B.;Huang, R.;Wang, C.; Chao, D. A Piezoelectric-Driven Electrochromic/Electrofluorochromic Dual-Modal Display Device. *Small* **2023**, *19*, e2301886.

[86] Shao, Y. J.;Lin, C. H.;Chang, C. W.;Kao, Y. T.;Ho, H. L.;Mizuno, R.;Shimizu, M.; Liou, G. S. Molecule‐Engineered Triarylamine Polymers: Tailoring Multifunctional Optoelectrochemical and Energy‐Saving Applications. *Small Structures* **2025**, *6*.

[87] Liu, X.-S.;Liu, R.-A.;Yang, B.;Qu, Y.;Zhang, W.;Zhang, S. X.-A.; Zhang, Y.-M. An electrochemically switchable "Cu−S" coordination of copper(II)-doped conjugated polymer for electrochromic energy-saving smart windows. *Chemical Engineering Journal* **2025**, *523*, 168253.

[88] Wang, Y.;Zhao, P. C.;Sun, J.;Liang, J.;Shen, T.;Li, C. H.; Jin, Z. Titanium-Polyoxometalate Crosslinked Metallo-Supramolecular Polymer as Artificial Interfacial Layer for Highly Persistent and Low-Temperature Tolerant Lithium Metal Batteries. *Angew Chem Int Ed Engl* **2025**, *64*, e202508224.

[89] Wang, Y.;Lei, C.;Guan, W.;Wu, K.;Zhang, B.; Yu, G. Bistable Electrochromic Ionogels via Supramolecular Interactions for Energy-Efficient Displays. *Adv Mater* **2024**, *36*, e2403499.

[90] Yang, W.;Liu, S.;Jia, S.;Huang, J.;Bian, C.;Yan, Y.;Ma, M.;Ma, J.;Feng, J.;Wei, C.; Cai, G. Introducing Conjugation Spacer in Electrochromic Metallo‐Supramolecular Polymer for Enhanced Optical Memory Effect. *Advanced Optical Materials* **2025**, *13*.

[91] Liu, X. S.;Yang, B.;Qu, Y.;Liu, R. A.;Yan, Y.;Zhang, W.;Zhang, S. X.; Zhang, Y. M. Multicolor and multistable transparent electrochromic materials and displays. *Nat Commun* **2025**, 10.1038/s41467-025-67462-5.

[92] Zhang, Z.;Jiang, Y.;Du, Y.;Jiao, J.;Liu, B.;Cai, D.; Shan, H. Synergistic improvement in performance: recent advances and applications in hybrid MOF/COF materials. *Coordination Chemistry Reviews* **2025**, *544*, 216970.

[93] Shao, G.;Huang, X.;Shen, X.;Li, C.; Thomas, A. Metal-Organic Framework and Covalent-Organic Framework-Based Aerogels: Synthesis, Functionality, and Applications. *Adv Sci (Weinh)* **2024**, *11*, e2409290.

[94] Zhang, Y.;Bao, R.;Qiu, J.;Liu, Y.;Yang, Z.; Pan, C. Electrochromic-based visualised flexible biosensing platforms: from single device to multifunctional device integration. *Chem Soc Rev* **2025**, *54*, 11827-11855.

[95] Meng, Z.;Qiu, Z.;Shi, Y.;Wang, S.;Zhang, G.;Pi, Y.; Pang, H. Micro/nano metal–organic frameworks meet energy chemistry: A review of materials synthesis and applications. *eScience* **2023**, *3*, 100092.

[96] Wade, C. R.;Li, M.; Dinca, M. Facile deposition of multicolored electrochromic metal-organic framework thin films. *Angew Chem Int Ed Engl* **2013**, *52*, 13377-13381.

[97] Check, B.;Choi, J. Y.;Santarelli, J.;Lu, C.;Pham, H. T. B.;Lopez, G.;Davis, C. M.; Park, J. Harnessing Truxone-Based Electrically Conductive Metal-Organic Framework for Electrochromism. *J Am Chem Soc* **2025**, *147*, 46806-46811.

[98] Hao, Q.;Li, Z. J.;Lu, C.;Sun, B.;Zhong, Y. W.;Wan, L. J.; Wang, D. Oriented Two-Dimensional Covalent Organic Framework Films for Near-Infrared Electrochromic Application. *J Am Chem Soc* **2019**, *141*, 19831-19838.

[99] Kumar Silori, G.;Chien, S. C.;Lin, L. C.; Ho, K. C. Four-State Electrochromism in Tris(4-aminophenyl)amine- terephthalaldehyde-based Covalent Organic Framework. *Angew Chem Int Ed Engl* **2025**, *64*, e202416046.

[100] Mushtaq, N.;Ahmad, A.;Wang, X.;Khan, U.; Gao, J. MOFs/COFs hybrids as next-generation materials for electrocatalytic CO2 reduction reaction. *Chemical Engineering Journal* **2024**, *486*, 150098.

[101] Li, C.;Zhang, H.;Lang, F.;Liu, Y.;Xu, L.;Xi, X. J.;Li, Y.;Pang, J.;Zhou, H. C.;

Bu, X. H. Efficiently regulating the electrochromic behavior of naphthalene-diimide-based zirconium-organic frameworks through linker installation. *Nat Commun* **2025**, *16*, 1405.

[102] Shupletsov, L.;Topal, S.;Schieck, A.;Helten, S.;Grunker, R.;Deka, A.;De, A.;Werheid, M.;Bon, V.;Weidinger, I.;Poppl, A.;Senkovska, I.; Kaskel, S. Linker Conformation Controls Oxidation Potentials and Electrochromism in Highly Stable Zr-Based Metal-Organic Frameworks. *J Am Chem Soc* **2024**, *146*, 25477-25489.

[103] Thomas, B.;Basak, S.;Smith, Q.;Yan, M.; Morris, A. J. Rapid Redox Hopping Charge Transfer and Electrochromism in a Multivariate Metal-Organic Framework. *J Am Chem Soc* **2025**, *147*, 33655-33665.

[104] Hao, Y.;Bao, B.;Li, R.;Hou, C.;Li, Y.;Zhang, Q.;Li, K.; Wang, H. Facilitating Charge Transfer via Ti-Knot Pathway in Electrochromic Three-Dimensional Metalated Covalent Organic Frameworks. *ACS Appl Mater Interfaces* **2024**, *16*, 57571-57579.

[105] Zhao, Q.;Yang, J.;Wang, Q.;Zhang, Y.-W.; Wang, J. 2D Conjugated Metal-Organic Frameworks for New Generation Flexible Multicolor Electrochromic Devices. *Advanced Materials* **2025**, *37*, 2413452.

[106] Patel, S.;Park, H.;Bonato, P.;Chan, L.; Rodgers, M. A review of wearable sensors and systems with application in rehabilitation. *J Neuroeng Rehabil* **2012**, *9*, 21.

[107] Liu, X.;Zhao, D.; Wang, J. Challenges and Opportunities in Preserving Key Structural Features of 3D-Printed Metal/Covalent Organic Framework. *Nanomicro Lett* **2024**, *16*, 157.

[108] Wang, J.;Guo, X.;Bian, C.;Zhong, Y.;Tu, J.;Lee, P. S.; Cai, G. Roadmap for electrochromic smart devices: From materials engineering and architectures design to multifunctional application. *Progress in Materials Science* **2025**, *153*, 101461.

[109] Ding, B.;Fan, Q.;Wu, X.;Hao, Y.;Bao, B.;Zhang, Q.;Li, Y.;Hou, C.;Li, K.;

Wang, H. Lithium‐Rich Solid Polymer Electrolytes Enabled by Thermal‐Assisted Dual‐Phase Dissociation for Highly Stable Flexible Electrochromic Devices. *Advanced Functional Materials* **2025**, *35*.

[110] Huang, Z.;Peng, Y.;Zhao, J.;Zhang, S.;Qi, P.;Qu, X.;Yan, F.;Ding, B.;Xuan, Y.; Zhang, X. An Efficient and Flexible Bifunctional Dual-Band Electrochromic Device Integrating with Energy Storage. *Nanomicro Lett* **2024**, *17*, 98.

[111] Li, R.;Lan, F.;Tang, L.;Huang, Y.;Zhao, S.;Wang, B.;Han, Y.;Gao, D.;Jiang, Q.;Zhao, Y.;Zhao, Z.;Wang, F.; Zhang, R. A Local‐Dissociation Solid‐State Polymer Electrolyte with Enhanced Li+ Transport for High‐Performance Dual‐Band Electrochromic Smart Windows. *Advanced Functional Materials* **2024**, *35*.

[112] Song, I.;Lee, W.-J.;Ke, Z.;You, L.;Chen, K.;Naskar, S.;Mehra, P.; Mei, J. An n-doped capacitive transparent conductor for all-polymer electrochromic displays. *Nature Electronics* **2024**, *7*, 1158-1169.

[113] Guo, J.;Diao, X.;Wang, M.;Zhang, Z.-B.; Xie, Y. Self-Driven Electrochromic Window System Cu/WOx-Al3+/GR with Dynamic Optical Modulation and Static Graph Display Functions. *ACS Applied Materials & Interfaces* **2022**, *14*, 10517-10525.

[114] Zhong, J.;Huang, B.;Yang, K.;Ma, Z.;Du, L.;Luo, N.;Tang, F.;Hou, C.;Jiang, F.; Kang, L. Neutral color and self-healable electrochromic system based on CuI/Cu and $${{\rm{I}}_3}^ - /{{\rm{I}}^ - }$$conversions. *Nano Research* **2024**, *17*, 4437-4443.

[115] Yamazaki, S.;Okimura, K.;Mochinushi, M.; Kimura, R. Electrochromic properties of TiO2 doped with molybdenum ions. *New Journal of Chemistry* **2025**, *49*, 20631-20640.

[116] Jia, S.;Guo, X.;Lv, Y.;Zhou, H.;Wang, J.;Yang, G.; Cai, G. Ultrathin WO3·H2O nanosheets derived from the Aurivillius phase for high-performance dual-band electrochromic smart windows. *Materials Horizons* **2025**, *12*, 10147-10156.

[117] Zhao, H.;Yu, X.;Yu, S.;Yang, H.;Guo, W.;Li, S.; Zheng, J. Y. Review on amorphous WO3 for electrochromic devices: Structure, optimization strategies and applications. *Materials Today Chemistry* **2025**, *43*, 102513.

[118] Chen, D.;Tong, Z.;Rao, Q.;Liu, X.;Meng, H.; Huang, W. High-Performance Black Copolymers Enabling Full Spectrum Control in Electrochromic Devices. *Nature Communications* **2024**, *15*, 8457.

[119] Zhang, L.;Wang, J.;Zhou, X.;Li, J.;Xie, W.;Qin, Q.;Ouyang, M.;Dong, Y.;Li, W.; Zhang, C. Infinite dimming black-to-transmissive copolymers featuring low chromatic color based on cyclopentadithiophene. *Chemical Engineering Journal* **2025**, *524*, 169120.

[120] Wang, Z.; Liu, R. PEDOT:PSS-based electrochromic materials for flexible and stretchable devices. *Materials Today Electronics* **2023**, *4*, 100036.

[121] Cao, L.;Zhang, W.;Lu, B.;Du, C.;Zhang, J.;Zhou, W.;Zhao, L.;Cheng, X.;Zhang, Y.;Zhang, G.;Xu, J.; Zhang, L. A dual-functional PEDOT-based electrochromic supercapacitor with excellent electrochemical stability. *Journal of Power Sources* **2025**, *657*, 238186.

[122] Manjakkal, L.;Pereira, L.;Kumi Barimah, E.;Grey, P.;Franco, F. F.;Lin, Z.;Jose, G.; Hogg, R. A. Multifunctional flexible and stretchable electrochromic energy storage devices. *Progress in Materials Science* **2024**, *142*, 101244.

[123] Wu, W.; Lee, P. S. Flexible and stretchable electrochromic displays: strategies, recent advances, and prospects. *Soft Science* **2024**, *4*.

[124] Wang, X.;Qiu, Y.;Cao, W.; Hu, P. Highly Stretchable and Conductive Core–Sheath Chemical Vapor Deposition Graphene Fibers and Their Applications in Safe Strain Sensors. *Chemistry of Materials* **2015**, *27*, 6969-6975.

[125] Huang, B.;Zhao, F.;Liu, P.;Xu, Y.;Wang, B.;Yang, J.;Chen, J.;Li, H.; Yu, W. W. Zn Anode‐Based Electrochromic Devices: Progress & Challenges. *Energy & Environmental Materials* **2025**, *9*.

[126] Xue, W.;Zhang, Y.;Liu, F.;Dou, Y.;Yan, M.; Wang, W. Self-Powered Flexible

Multicolor Electrochromic Devices for Information Displays. *Research (Wash D C)* **2023**, *6*, 0227.

[127] Wang, K.;Zhang, F.;Jiang, X.;Zhang, W.;Dai, L.;Zhang, J.;Li, Z.; Jia, H. Bionic Nanogel Interfaces Unlock Long-Term Stability in Zn Metal Electrodeposition-Based Electrochromic Windows. *Adv Mater* **2025**, *37*, e09980.

[128] Kim, D. C.;Seung, H.;Yoo, J.;Kim, J.;Song, H. H.;Kim, J. S.;Kim, Y.;Lee, K.;Choi, C.;Jung, D.;Park, C.;Heo, H.;Yang, J.;Hyeon, T.;Choi, M. K.; Kim, D.-H. Intrinsically stretchable quantum dot light-emitting diodes. *Nature Electronics* **2024**, *7*, 365-374.

[129] Eom, S. Y.;Sun, F.;Pal, R.;Lee, J.;Jeong, B.; Park, J. S. Leakage-free flexible and stretchable electrochromic devices enabled by acrylate viologens and perfluorinated CNT-modified transparent electrodes. *Solar Energy Materials and Solar Cells* **2025**, *288*, 113651.

[130] Zhao, X.;Chen, Q.;Fan, F.;Wang, Q.;Su, Y.;Liu, M.;Zhu, F.; Zhao, D. Dual-Band Electrochromic Smart Window for Dynamic Switching Between Radiative Cooling and Solar Heating. *Adv Sci (Weinh)* **2025**, *12*, e04483.

[131] Zhao, F.;Li, C.;Li, S.;Wang, B.;Huang, B.;Hu, K.;Liu, L.;Yu, W. W.; Li, H. Continuous Solar Energy Conversion Windows Integrating Zinc Anode-Based Electrochromic Device and IoT System. *Adv Mater* **2024**, *36*, e2405035.

[132] Zhang, H.;Sun, F.;Cao, G.;Zhou, D.;Zhang, G.;Feng, J.;Wang, S.;Su, F.;Tian, Y.;Liu, Y. J.; Tian, Y. Bifunctional flexible electrochromic energy storage devices based on silver nanowire flexible transparent electrodes. *International Journal of Extreme Manufacturing* **2022**, *5*, 015503.

[133] Gong, H.;Li, A.;Fu, G.;Zhang, M.;Zheng, Z.;Zhang, Q.;Zhou, K.;Liu, J.; Wang, H. Ultrathin flexible electrochromic devices enabled by highly transparent ion-conducting films. *Journal of Materials Chemistry A* **2023**, *11*, 8939-8949.

[134] Wang, M.;Li, X.;Liu, L.;Li, B.;Xun, J.;Wang, L.;Wang, H.;Hu, S.; Li, C. Carbon dots as multifunctional electrolyte additives toward multicolor and low

self-discharge electrochromic energy storage devices. *Energy Storage Materials* **2024**, *65*, 103110.

[135] Wu, W.;Fang, H.;Ma, H.;Wu, L.;Zhang, W.; Wang, H. Boosting Transport Kinetics of Ions and Electrons Simultaneously by Ti(3)C(2)T(x) (MXene) Addition for Enhanced Electrochromic Performance. *Nanomicro Lett* **2020**, *13*, 20.

[136] Lei, K.;Jiang, Q.;Gong, D.;Wang, W.;Wu, J.;Chang, Q.;Wang, G.; Pang, X. Hydrogel Smart Windows: Working Mechanisms, Recent Developments, and Perspectives. *Small* **2025**, *21*, e10382.

[137] Guo, X.;Zhang, C.;Mi, S.;Li, M.;Han, Z.;Tang, X.;Zhang, T.;Chen, Y.;Wang, X.;Wang, C.;Wang, Z.;Cong, S.; Zhao, Z. Realizing Flexible Multicolored Electrochromism on Carbon Nanotubes through Thin-Film Interference. *ACS Photonics* **2024**, *11*, 2335-2341.

[138] Zhao, Y.;Lan, F.;Li, Y.;Huang, Y.;Wang, F.;Wang, K.; Zhang, R. Coaxial Electroluminochromic Fibers with Dynamic RGB Switching for Pixelated Smart Textiles. *Adv Mater* **2025**, *37*, e2505012.

[139] Jiao, K.;Zhang, Z.;Liu, Y.;Li, J.;Xue, C.;Zhang, J.;Chen, Y.;Chen, Z.;Hou, X.;Zhang, L.;Anguita, J. V.;Zhang, W.;Gao, Y.; Silva, S. R. P. Carbon nanotube-based solid-state mid-infrared electrochromic devices for smart outdoor thermal management. *Chemical Engineering Journal* **2025**, *507*, 160802.

[140] Fang, R.;Liu, Y.;Shi, C.;Jin, H.;Chen, Z.;Sun, H.;Lv, B.;He, D.;Zheng, X.; Xiong, Y. Reduced graphene oxide-induced

in-situ uniform growth of hydrated WO

3 film for enhanced electrochromic performance. *Nano Research* **2025**, *18*, 94907269.

[141] Li, Y.;Yu, T.;Pui, T.;Chen, P.;Zheng, L.; Liao, K. Fabrication of transparent and conductive carbon nanotube/polyvinyl butyral films by a facile solution surface dip coating method. *Nanoscale* **2011**, *3*, 2469-2471.

[142] Guo, S.;Zhu, R.;Chen, J.;Liu, W.;Zhang, Y.;Li, J.; Li, H. MXene-based all-solid flexible electrochromic microsupercapacitor. *Microsyst Nanoeng* **2024**, *10*, 89.

[143] Ding, Y.;Qiu, Q.;Li, Y.;Shi, J.;Du, L.;Zhang, T.;Liu, X.;Li, C.; Li, Z. Reversible Metal Electrodeposition Enabled by Composites of PEDOT:PSS/MXene for Durable Smart Windows with Broadband Electromagnetic Wave Modulation. *Small* **2025**, *21*, e06630.

[144] Lu, F.;Shi, D.;Tan, P.; Han, Y. A novel infrared electrochromic device based on Ti3C2T MXene. *Chemical Engineering Journal* **2022**, *450*, 138324.

[145] Wang, J.;Guo, X.;Li, C.;Zhou, H.;Yan, Y.;Zhu, F.;Wang, J.;Cai, G.; Schmidt, O. G. Tunable MXene/WO3 Fabry−Pérot Microcavity Architecture for Bioinspired Soft Electrochromic Actuators with Vivid Colors. *Advanced Functional Materials* **2024**, *35*.

[146] Yang, Y.;Xiu, Z.;Pan, F.;Liang, H.;Jiang, H.;Guo, H.;Wang, X.;Li, L.;Yuan, B.; Lu, W. Tuning the Multilevel Hierarchical Microarchitecture of MXene/rGO‐Based Aerogels Through a Magnetic Field‐Guided Strategy Toward Stepwise Enhanced Electromagnetic Wave Dissipation. *Advanced Functional Materials* **2024**, *35*.

[147] Zhang, X.;Yang, Y.;Xue, P.;Valenzuela, C.;Chen, Y.;Yang, X.;Wang, L.; Feng, W. Three-Dimensional Electrochromic Soft Photonic Crystals Based on MXene-Integrated Blue Phase Liquid Crystals for Bioinspired Visible and Infrared Camouflage. *Angew Chem Int Ed Engl* **2022**, *61*, e202211030.

[148] Hu, Z.;Tang, X.;Yi, Y. Q.;Nie, S.;Chen, X.;Xu, W.;Huang, C.;Mu, X.;Ma, Z.;Tang, P.;Wu, X.;Su, W.; Luscombe, C. K. A general strategy to achieve see-through devices through the micro-structuring of colored functional materials. *Nat Commun* **2024**, *15*, 10836.

[149] Chen, C.;Wang, M. H.;Zhu, M. H.;Zhao, F. X.;Yu, B.;Pan, Q. H.;Guo, X.;Sheng, S. Z.;He, Z.;Wang, J. L.; Yu, S. H. Electrochromic Pressure-Sensitive Device for In Situ and Instantaneous Pressure Visualization.

Nano Lett **2025**, *25*, 4154-4162.

[150] Zhu, M.;Chen, C.;Yu, A.;Feng, Y.;Cui, H.;Zhou, R.;Zhuang, Y.;Hu, X.;Liu, S.; Zhao, Q. Multilayer Step-like Microstructured Flexible Pressure Sensing System Integrated with Patterned Electrochromic Display for Visual Detection. *ACS Nano* **2025**, *19*, 19488-19496.

[151] Zhang, Y.;Liu, D.;Ren, Z.;Liu, W.;Wang, B.;Song, S.;Hao, T.;Xu, L.;Ji, H.;Sun, J.;Zhang, L.; Li, Y. Rapid-response electrochromic devices with self-wrinkling polyaniline for enhanced infrared emissivity modulation. *Chemical Engineering Journal* **2024**, *499*, 155960.

[152] Zhao, Q.;Wang, J.;Ai, X.;Duan, Y.;Pan, Z.;Xie, S.;Wang, J.; Gao, Y. Three‐dimensional knotting of W17O47@PEDOT:PSS nanowires enables high‐performance flexible cathode for dual‐functional electrochromic and electrochemical device. *InfoMat* **2022**, *4*.

[153] Chen, Y.;Li, A.;Chen, H.;Zhang, L.; Ma, H. Research on a method for recovering the performance of flexible WO3 electrochromic thin films. *Ceramics International* **2025**, *51*, 59364-59374.

[154] Wang, Y.;Zhang, Z.;Wang, Z.;Zuo, Y.;Zhou, H.;Sun, D.;Li, Y.;Yan, Y.;Feng, T.; Xie, A. Self-seeded growth of hexagonal-phase WO3 film by a one-step hydrothermal method for high-performance electrochromic energy storage devices. *Journal of Power Sources* **2025**, *633*, 236350.

[155] Xu, Z.;Ji, D.;Wang, J.;Zhang, Y.;Chen, C.;Li, J.;Shen, Y.;Ma, P.;Zhou, Y.;Wolff, J.;Lv, Y.; Ruhlmann, L. Effects of annealing time on ITO and PEDOT-ITO electrodes for electrochromic supercapacitors. *Electrochimica Acta* **2025**, *535*, 146638.

[156] Kim, J. W.;Kim, S.;Jeong, Y. R.;Kim, J.;Kim, D. S.;Keum, K.;Lee, H.; Ha, J. S. Self-healing strain-responsive electrochromic display based on a multiple crosslinked network hydrogel. *Chemical Engineering Journal* **2022**, *430*, 132685.

[157] Liu, J.-n.;He, Q.;Pan, M.-y.;Du, K.;Gong, C.-B.; Tang, Q. An energy-saving,

bending sensitive, and self-healing PVA-borax-IL ternary hydrogel electrolyte for visual flexible electrochromic strain sensors. *Journal of Materials Chemistry A* **2022**, *10*, 25118-25128.

[158] Dutta, P.;Goswami, S.;Roy, R.; Singh, A. K. Spray-Coated W(18)O(49)/Ti(3)C(2)T(x) MXene Electrodes for High-Performance Electrochromic Energy Storage Devices. *Small* **2025**, *21*, e2503529.

[159] Si, T.;Ye, Y.;Zhang, Z.;Gong, Z.;Li, Y.;Huang, S.;Zhang, K.;Wang, D.; Li, H.-J. Hydrogen bond-mediated lattice engineering of amorphous WO3 via CDs-carbomer synergy for dual electro-/photochromic flexible devices. *Chemical Engineering Journal* **2026**, *528*, 172027.

[160] Wu, P.;Zhang, S.;Wu, Y.;Zhang, W.; Song, W. Carbazole-Based Dual-Band Electrochromic Polymers: The Effect of Linkage Sites on Electrochromic Performance. *ACS Appl Mater Interfaces* **2024**, *16*, 58952-58960.

[161] Zhang, X.-C.;Scarpa, F.;McHale, R.;Limmack, A. P.; Peng, H.-X. Carbon nano-ink coated open cell polyurethane foam with micro-architectured multilayer skeleton for damping applications. *RSC Adv.* **2016**, *6*, 80334-80341.

[162] Zhang, J.;Chen, Z.;Zhang, H.;Cui, Y.;Zheng, F.;Duan, Y.;Guo, L.;Jiang, D.;Feng, J.;Lin, Y.;Yang, Y.;Feng, D.;Tang, P.; Liang, Z. Viologen‐Based Cationic Covalent Organic Frameworks for Efficient Dechlorination via Capacitive Deionization. *Advanced Functional Materials* **2026**, 10.1002/adfm.202530236.

[163] Luo, X.;Wan, R.;Zhang, Z.;Song, M.;Yan, L.;Xu, J.;Yang, H.; Lu, B. 3D-Printed Hydrogel-Based Flexible Electrochromic Device for Wearable Displays. *Advanced Science* **2024**, *11*, 2404679.

[164] Asghar, A.;Khan, K.;Rashid, M. S.;Hamza, M.;Liu, Z.;Liu, C.; Chen, Z. Extrusion-Based Additive Manufacturing of Carbonaceous and Non-Carbonaceous Electrode Materials for Electrochemical Energy Storage Devices. *Advanced Materials Technologies* **2025**, *10*, 2400136.

[165] Massetti, M.;Zhang, S.;Harikesh, P. C.;Burtscher, B.;Diacci, C.;Simon, D.

T.;Liu, X.;Fahlman, M.;Tu, D.;Berggren, M.; Fabiano, S. Fully 3D-printed organic electrochemical transistors. *npj Flexible Electronics* **2023**, *7*, 11.

[166] Sanumi, O. J.;Ndungu, P. G.; Oboirien, B. O. Challenges of 3D printing in LIB electrodes: Emphasis on material-design properties, and performance of 3D printed Si-based LIB electrodes. *Journal of Power Sources* **2022**, *543*, 231840.

[167] Ye, H.;He, Y.;You, T.; Xu, F. Advanced MXene/Graphene Oxide/Lignosulfonate Inks for 3D Printing Thick Electrodes with Vertically Aligned Pores to Dually Boost Mass Loading and Areal Capacitance. *Advanced Functional Materials* **2025**, *35*, 2413343.

[168] Wu, T.;Karimi-Maleh, H.;Li, Y.;Zhang, D.;Zhang, Z.;Zhong, N.;Wen, Y.; Aminabhavi, T. M. 3D printed porous chitosan/metal–organic framework composites as effective adsorbents to remove heavy metals from wastewater. *Chemical Engineering Journal* **2024**, *493*, 152780.

[169] Abdelhamid, H. N.;Sultan, S.; Mathew, A. P. Three-Dimensional Printing of Cellulose/Covalent Organic Frameworks (CelloCOFs) for CO2 Adsorption and Water Treatment. *ACS Applied Materials & Interfaces* **2023**, *15*, 59795-59805.

[170] Xie, H.;Peng, S.;Huang, X.;Fan, S.; Zhang, Y. Electrochromic Fabric Device Based on Lamellar Polyaniline through Inkjet Printing. *Macromolecular Rapid Communications* **2025**, *46*, 2400945.

[171] Kwon, H.;Kim, S.;Ham, M.;Park, Y.;Kim, H.;Lee, W.; Lee, H. Enhanced Coloration Time of Electrochromic Device Using Integrated WO3@PEO Electrodes for Wearable Devices. **2023**, *13*, 194.

[172] Zhang, P.;Lei, I. M.;Chen, G.;Lin, J.;Chen, X.;Zhang, J.;Cai, C.;Liang, X.; Liu, J. Integrated 3D printing of flexible electroluminescent devices and soft robots. *Nature Communications* **2022**, *13*, 4775.

[173] Liu, G.;Han, T.;Cao, H. H.;Jiang, X.;Zhang, W.;Liu, H.; Li, Z. J. A. F. M. Bidirectional Color Switching and Multimodal Energy Outputs Enabled by

Synergistic Complementary Color Fusion and Inherent Potential Gradient in a Fully‐Printed Tri‐Electrode Electrochromic System. **2026**.

[174] Li, Z.;Xu, Z.;Propst, S.;Page, Z. A.;Chen, Y.;Majidi, C.; Mueller, J. Ultrawide Property Range Thiol-Ene Photopolymers for 3D Printing. *Advanced Materials Technologies* **2025**, *10*, e00422.

[175] Mubarak, S.;Dhamodharan, D.; Byun, H.-S. Recent advances in 3D printed electrode materials for electrochemical energy storage devices. *Journal of Energy Chemistry* **2023**, *81*, 272-312.

[176] Wu, Q.;Song, K.;Zhang, D.;Ren, B.;Sole-Gras, M.;Huang, Y.; Yin, J. Embedded extrusion printing in yield-stress-fluid baths. *Matter* **2022**, *5*, 3775-3806.

[177] Kwon, Y.;Kim, J.;Kim, H.;Kang, T. W.;Lee, J.;Jang, S. S.;Lee, Y.; Yeo, W.-H. Printed Nanomaterials for All-in-One Integrated Flexible Wearables and Bioelectronics. *ACS Applied Materials & Interfaces* **2024**, *16*, 68016-68026.

[178] Ng, A.;Telles, R.;Riley, K. S.;Lewis, J. A.;Cook, C. C.;Lee, E.; Yang, S. Coaxial Direct Ink Writing of Cholesteric Liquid Crystal Elastomers in 3D Architectures. *Advanced Materials* **2025**, *37*, 2416621.

[179] Zhang, W.;Liu, G.;Zhang, Z.;Jiang, X.;Zhang, W.;Liu, H.; Li, Z. J. A. A. P. M. Flexographically Printed PEDOT:PSS Electrodes Enabling Stable Paper-Based Self-Powered Electrochromic Devices. **2026**.

[180] Chen, Z.;Jin, Y.;Li, Z.;Wang, B.;Liu, B.;Xu, B.;Gong, F.;Jiang, L.-t.; Li, H. J. A. F. M. An AI‐Powered, All‐Printed, Scalable, Stretchable Triboelectric E‐Skin for Multifunctional Perception in Dexterous Hand. **2026**.

[181] Liu, X.;Zhao, D.; Wang, J. Challenges and Opportunities in Preserving Key Structural Features of 3D-Printed Metal/Covalent Organic Framework. *Nano-Micro Letters* **2024**, *16*, 157.

[182] Liu, D.;Wang, Y.;Bai, C.;Hu, D.;Yang, X.;Lu, Y.;Wu, T.;Zhai, F.;Jiang, P.;Wang, X.; Liu, W. Biomimetic Gradient Lubrication Hydrogel Contrived by Self-Reinforced MOFs Nanoparticle Network. *Nano-Micro Letters* **2026**, *18*,

150.

[183] Abbel, R.;Galagan, Y.; Groen, P. Roll-to-Roll Fabrication of Solution Processed Electronics. *Advanced Engineering Materials* **2018**, *20*, 1701190.

[184] Zhong, H.;Wang, Y.;Hou, L.;Song, X.; Zhang, F. Advancing Roll-to-Roll Manufacturing of Flexible Perovskite Solar Cells From Lab to Fab. *ACS Applied Materials & Interfaces* **2025**, *17*, 50168-50190.

[185] Macher, S.;Schott, M.;Sassi, M.;Facchinetti, I.;Ruffo, R.;Patriarca, G.;Beverina, L.;Posset, U.;Giffin, G. A.; Löbmann, P. New Roll‐to‐Roll Processable PEDOT‐Based Polymer with Colorless Bleached State for Flexible Electrochromic Devices. *Advanced Functional Materials* **2019**, *30*.

[186] Lee, W. J.;Mehra, P.;Thurston, J. R.;Tian, Y.;Liu, X.;Samal, S.;You, L.;Song, I.;Ruan, X.;Toney, M. F.; Mei, J. Robust fast-switching black electrochromic windows based on solution-processed n-doped transparent organic conductor. *Nat Commun* **2025**, *17*, 575.

[187] Ping, F.;Zhong, Y.;Guo, X.;Jia, S.;Ma, J.;Liu, H.;Liu, L.; Cai, G. Unlocking Scalable Manufacturing of Electrochromic Windows: Wadsley‐Roth TiNb2O7 Films with Open Shear Channels for Intelligent Photo‐Thermal Management. *Advanced Functional Materials* **2025**, 10.1002/adfm.202527930.

[188] Zi, W.;Jin, Z.;Liu, S.; Xu, B. Flexible perovskite solar cells based on green, continuous roll-to-roll printing technology. *Journal of Energy Chemistry* **2018**, *27*, 971-989.

[189] Ling, H.;Zhang, J.;Wang, Y.; Zeng, X. One-step achieving high performance all-solid-state and all-in-one flexible electrochromic supercapacitor by polymer dispersed electrochromic device strategy. *Journal of Colloid and Interface Science* **2024**, *665*, 969-976.

[190] Zhang, H.;Chen, Z.;Wu, B.;Ji, X.;Tang, S.; Zhu, W. Multifunctional wearable sensor based on DNA-inspired helically structured conductive cotton threads with applications in electronic skin, joule heater and supercapacitor. *Surfaces*

and Interfaces **2025**, *60*, 106020.

[191] Du, C.;Li, H.;Zhang, G.;Wan, R.;Zhang, W.;Xu, X.;Zheng, L.;Deng, X.;Xu, J.;Lu, B.; Nie, G. Design of robust fluorinated interpenetrating poly(thieno[3,2-b]thiophene) network for highly stable flexible electrochromic-supercapacitor devices. *Chemical Engineering Journal* **2024**, *495*, 153692.

[192] Xie, H.;Peng, S.;Huang, X.;Fan, S.; Zhang, Y. Electrochromic Fabric Device Based on Lamellar Polyaniline through Inkjet Printing. *Macromolecular Rapid Communications* **2025**, *46*.

[193] Jeong, S.-J.;Jo, M.-H.; Ahn, H.-J. 3D-printed film architecture via automatic micro 3D-printing system: Micro-intersection engineering of V2O5 thin/thick films for ultrafast electrochromic energy storage devices. *Chemical Engineering Journal* **2023**, *475*, 146503.

[194] Zhang, P.;Lei, I. M.;Chen, G.;Lin, J.;Chen, X.;Zhang, J.;Cai, C.;Liang, X.; Liu, J. Integrated 3D printing of flexible electroluminescent devices and soft robots. *Nat Commun* **2022**, *13*, 4775.

[195] Liu, G.;Han, T.;Cao, H.;Jiang, X.;Zhang, W.;Liu, H.; Li, Z. Bidirectional Color Switching and Multimodal Energy Outputs Enabled by Synergistic Complementary Color Fusion and Inherent Potential Gradient in a Fully‐Printed Tri‐Electrode Electrochromic System. *Advanced Functional Materials* **2026**, 10.1002/adfm.202528745.

[196] Brändler, L.;Niklaus, L.;Schott, M.;Giffin, G. A.; Löbmann, P. Factors Impacting the Photostability of a Roll‐to‐Roll Processed PEDOT Derivative for Flexible Electrochromic Devices. *Advanced Materials Technologies* **2024**, *9*.

[197] Wang, J.;Zhang, Z.;Wang, G.;Hu, X.;Dong, C.;Kobayashi, N.;Li, C.;Zhang, J.; Duan, Y. Low-Energy Consumed Switchable Windows with Ultralong Optical Memory via Semiconductor-Enabled Reversible Zinc Electrodeposition. *Adv Mater* **2025**, 10.1002/adma.202521622, e21622.

[198] Lee, C. H.;Ma, Y.;Jang, K.-I.;Banks, A.;Pan, T.;Feng, X.;Kim, J. S.;Kang, D.;Raj, M. S.;McGrane, B. L.;Morey, B.;Wang, X.;Ghaffari, R.;Huang, Y.; Rogers, J. A. Soft Core/Shell Packages for Stretchable Electronics. *Advanced Functional Materials* **2015**, *25*, 3698-3704.

[199] Yu, Y.;Zhu, X.;Jiang, S.;Wu, S.;Zhao, Y.;Zhang, L.;Song, L.; Huang, Y. Cephalopods' Skin-Inspired Design of Nanoscale Electronic Transport Layers for Adaptive Electrochromic Tuning. *Adv Sci (Weinh)* **2024**, *11*, e2405444.

[200] Bi, S.;Jin, W.;Han, X.;Cao, X.;He, Z.;Asare-Yeboah, K.; Jiang, C. Ultra-fast-responsivity with sharp contrast integrated flexible piezo electrochromic based tactile sensing display. *Nano Energy* **2022**, *102*, 107629.

[201] Kim, D. S.;Lee, Y. H.;Kim, J. W.;Lee, H.;Jung, G.; Ha, J. S. A stretchable array of high-performance electrochromic devices for displaying skin-attached multi-sensor signals. *Chemical Engineering Journal* **2022**, *429*, 132289.

[202] Sun, T.;Yue, W.;Sun, T.;Niu, H.; Li, Y. A "One‐Stone‐Two‐Birds" Strategy Constructed Hybrid Wearable Device Based on Chameleon‐Inspired Integrated Pressure Sensing and Visualization. *Advanced Functional Materials* **2025**, *35*.

[203] Guo, Y.;Li, H.;Li, Y.;Wei, X.;Gao, S.;Yue, W.;Zhang, C.;Yin, F.;Zhao, S.;Kim, N. Y.; Shen, G. Wearable Hybrid Device Capable of Interactive Perception with Pressure Sensing and Visualization. *Advanced Functional Materials* **2022**, *32*.

[204] Fu, X.;Dong, H.;Zhen, Y.; Hu, W. Solution-Processed Large-Area Nanocrystal Arrays of Metal-Organic Frameworks as Wearable, Ultrasensitive, Electronic Skin for Health Monitoring. *Small* **2015**, *11*, 3351-3356.

[205] Lee, J. M.;Cho, S. W.;Jo, C.;Yang, S. H.;Kim, J.;Kim, D. Y.;Jo, J.-W.;Park, J. S.;Kim, Y.-H.; Park, S. K. Monolithically integrated neuromorphic electronic skin for biomimetic radiation shielding. *Science Advances*, *10*, eadp9885.

[206] <157-0 前 -Monolithically integrated neuromorphic electronic skin for biomimetic radiation shielding.pdf>.

[207] Koo, J.;Amoli, V.;Kim, S. Y.;Lee, C.;Kim, J.;Park, S.-M.;Kim, J.;Ahn, J. M.;Jung, K. J.; Kim, D. H. Low-power, deformable, dynamic multicolor electrochromic skin. *Nano Energy* **2020**, *78*, 105199.

[208] Banihashemi Jozdani, S. M.;Hashemian, Z.;Ebrahim Damavandi, S.;Elyasigorji, Z.; Vosough, M. Emerging Trends in the Biomedical Application of Carbon-based Nanomaterials. *Nano Biomedicine and Engineering* **2024**, *16*, 357-369.

[209] Wang, J.;Guo, X.;Lan, D.;Wang, Y.;Huang, H.;Zhang, C.;Wu, G.;Zhang, S.; Jia, Z. Multifunctional electromagnetic wave absorbing materials: research progress from component structural design to intelligent integration. *Carbon* **2025**, *245*, 120818.

[210] Wang, X.;Guo, X.;Wang, Y.;Hu, K.;Cai, J.;Wang, M.;Jiang, J.;Ma, Y.; Yu, J. Stretchable Polymorphic Electrochromic Textile Electronics for Deep Learning-Assisted Self-Adaptive Camouflage. *Small* **2025**, *21*, e10137.

[211] Shi, X.;Zuo, Y.;Zhai, P.;Shen, J.;Yang, Y.;Gao, Z.;Liao, M.;Wu, J.;Wang, J.;Xu, X.;Tong, Q.;Zhang, B.;Wang, B.;Sun, X.;Zhang, L.;Pei, Q.;Jin, D.;Chen, P.; Peng, H. Large-area display textiles integrated with functional systems. *Nature* **2021**, *591*, 240-245.

[212] Fan, H.;Li, K.;Liu, X.;Xu, K.;Su, Y.;Hou, C.;Zhang, Q.;Li, Y.; Wang, H. Continuously Processed, Long Electrochromic Fibers with Multi-Environmental Stability. *ACS Appl Mater Interfaces* **2020**, *12*, 28451-28460.

[213] Chen, Y.;Liu, Y.;Valenzuela, C.;Feng, Y.;Yang, Y.;Bi, R.;Feng, W.; Wang, L. Universal Water Transfer Printing Enables Scalable Structural Coloration of Responsive Textile Fibers for Wearable Electronics. *Adv Mater* **2025**, 10.1002/adma.202516769, e16769.

[214] Duan, Y.;Sun, Z.;Zhang, Q.;Dong, Y.;Lin, Y.;Ji, D.; Qin, X. Constructing electrospun 3D liquid metal adhesion channel on stretchable yarns for broad-range strain-insensitivity smart textiles. *Nat Commun* **2025**, *16*, 6362.

[215] Han, X.;Du, W.;Chen, M.;Wang, X.;Zhang, X.;Li, X.;Li, J.;Peng, Z.;Pan, C.; Wang, Z. L. Visualization Recording and Storage of Pressure Distribution through a Smart Matrix Based on the Piezotronic Effect. *Adv Mater* **2017**, *29*.

[216] Shao, B.;Zhang, S.;Hu, Y.;Zheng, Z.;Zhu, H.;Wang, L.;Zhao, L.;Xu, F.;Wang, L.;Li, M.; Shi, J. Color-Shifting Iontronic Skin for On-Site, Nonpixelated Pressure Mapping Visualization. *Nano Letters* **2024**, 10.1021/acs.nanolett.3c04755.

[217] Gong, Z.;Qin, J.;Liu, D.;Lv, S.;Du, Y.;Zhang, T.; Ke, Q. Flexible PVDF/SiC/FeCl3 nanofiber membrane generators with synergistically enhanced piezoelectricity. *Nano Energy* **2024**, *122*, 109290.

[218] Singh, P. K.;Kaur, G. A.;Shandilya, M.;Rana, P.;Rai, R.;Mishra, Y. K.;Syväjärvi, M.; Tiwari, A. Trends in piezoelectric nanomaterials towards green energy scavenging nanodevices. *Materials Today Sustainability* **2023**, *24*, 100583.

[219] Zhang, H.;Ji, X.;Wang, Z.;Tang, S.;Wang, Z.; Zhu, W. Advances in Intelligent Polyvinylidene Fluoride-Based Piezoelectric Composites for Self-Powered Wearable Electronics. *Small* **2026**, *22*, e09387.

[220] Xiahou, X.;Wu, S.;Guo, X.;Li, H.;Chen, C.; Xu, M. Strategies for enhancing low-frequency performances of triboelectric, electrochemical, piezoelectric, and dielectric elastomer energy harvesting: recent progress and challenges. *Sci Bull (Beijing)* **2023**, *68*, 1687-1714.

[221] Huang, R.;Xie, Y.;Cao, N.;Jia, X.; Chao, D. Self-powered electrochromic smart window helps net-zero energy buildings. *Nano Energy* **2024**, *129*, 109989.

[222] Wang, Z.;Bu, T.;Cao, J.;Luan, R.;Dong, S.;Feng, Y.;Fan, B.;Jiang, Z.;Wang, Z. L.; Zhang, C. Nanoscale Confined Tribo-Ion-Photonics for Ultrahigh-Resolution Imaging. *Adv Mater* **2025**, 10.1002/adma.202515545, e15545.

[223] Qin, S.;Zhang, Q.;Yang, X.;Liu, M.;Sun, Q.; Wang, Z. L. Hybrid

Piezo/Triboelectric‐Driven Self‐Charging Electrochromic Supercapacitor Power Package. *Advanced Energy Materials* **2018**, *8*.

[224] Wu, Z. S.;Liu, Z.;Parvez, K.;Feng, X.; Mullen, K. Ultrathin Printable Graphene Supercapacitors with AC Line-Filtering Performance. *Adv Mater* **2015**, *27*, 3669-3675.

[225] Huang, R.;Zhou, M.;Liu, X.; Chao, D. TENG-driven reflective/emissive dual-mode display. *Chemical Engineering Journal* **2025**, *521*, 166525.

[226] Chen, C.;Zhao, S.;Pan, C.;Zi, Y.;Wang, F.;Yang, C.; Wang, Z. L. A method for quantitatively separating the piezoelectric component from the as-received "Piezoelectric" signal. *Nat Commun* **2022**, *13*, 1391.

[227] He, Q.;Zeng, Y.;Jiang, L.;Wang, Z.;Lu, G.;Kang, H.;Li, P.;Bethers, B.;Feng, S.;Sun, L.;Sun, P.;Gong, C.;Jin, J.;Hou, Y.;Jiang, R.;Xu, W.;Olevsky, E.; Yang, Y. Growing recyclable and healable piezoelectric composites in 3D printed bioinspired structure for protective wearable sensor. *Nat Commun* **2023**, *14*, 6477.

[228] Leon, R. T.;Sherrell, P. C.;Šutka, A.; Ellis, A. V. Decoupling piezoelectric and triboelectric signals from PENGs using the fast fourier transform. *Nano Energy* **2023**, *110*, 108445.

[229] Akbarinejad, A.;Fiedler, H.;Nguyen, J.;Li, Z.;Gito, D. A.;Sherrell, P. C.;Ellis, A. V.;Aw, K.; Malmstrom, J. Stretching, Tapping, or Compressing–What Role Does Triboelectricity Play in the Signal Output from Piezoelectric Nanogenerators? *Advanced Electronic Materials* **2024**, *10*, 2400019.

[230] Li, L.;Wang, X.;Hu, Y.;Li, Z.;Zhao, Z.; Zheng, G. The tribo-piezoelectric microscopic coupling mechanism of ferroelectric polymers and the synchronous online monitoring of load distribution/roller speed for intelligent bearings. *Nano Energy* **2023**, *115*, 108724.

[231] Pang, C.;Lee, G. Y.;Kim, T. I.;Kim, S. M.;Kim, H. N.;Ahn, S. H.; Suh, K. Y. A flexible and highly sensitive strain-gauge sensor using reversible interlocking of nanofibres. *Nat Mater* **2012**, *11*, 795-801.

[232] Cao, N.;Lang, Y.;Gu, G.;Jia, X.; Chao, D. Mixed Ionic‐Electronic Conducting Polymer Enables Efficient Electrochromic Supercapacitor. *Advanced Functional Materials* **2025**, 10.1002/adfm.202517668.

[233] Zheng, Q.;Chen, S.;Ma, H.;Wan, J.;Gao, X.;Wang, B.;Guo, K.;Liu, S.; Chen, X. Proton Conductive Solid Electrolyte with High Transmittance and Temperature Adaptability for Electrochromic Supercapacitor. *Advanced Sustainable Systems* **2025**, 10.1002/adsu.202501210.

[234] Wang, Q.;Bian, C.;Zheng, Z.;Shen, H.;Feng, K.;Cai, G.;Chen, Z.; Jiang, Z. Micro-Nano Composite Structures: General Resolution for Transparent-to-Multicolored Electrochromic Supercapacitors Assembly. *Polymer Science & Technology* **2025**, *1*, 787-798.

[235] Liu, L.;Liu, C.;Wang, M. Y.;Li, B.;Wang, K.;Fan, X. Q.;Wang, L. Y.;Wang, H. Q.;Hu, S. L.; Diao, X. G. Anti‐self‐discharge ultrathin all‐inorganic electrochromic asymmetric supercapacitors enabling intelligent and effective energy storage. *Rare Metals* **2023**, *42*, 2957-2971.

[236] Wu, C.;Zhang, Y.;Shi, H.;Yu, J.;Yang, Y.;Zhang, C.;Yu, Y.; Liu, W. High-Performance Complementary Electrochromic Batteries using Nb(18)W(16)O(93) by the Synergistic Effects of Aqueous Al(3+)/K(+) Dual-Ion. *Angew Chem Int Ed Engl* **2025**, *64*, e202415050.

[237] Lv, H.;Wei, Z.;Han, C.;Yang, X.;Tang, Z.;Zhang, Y.;Zhi, C.; Li, H. Cross-linked polyaniline for production of long lifespan aqueous iron||organic batteries with electrochromic properties. *Nat Commun* **2023**, *14*, 3117.

[238] Wu, C.;Shi, H.;Zhao, L.;Chen, X.;Zhang, X.;Zhang, C.;Yu, J.;Lv, Y.;Wei, R.;Gao, T.;Xie, J.;Yu, Y.; Liu, W. High‐Performance Aqueous Zn2+/Al3+ Electrochromic Batteries based on Niobium Tungsten Oxides. *Advanced Functional Materials* **2023**, *33*.

[239] Liu, Q.;Ou, X.;Niu, Y.;Li, L.;Xing, D.;Zhou, Y.; Yan, F. Flexible Zn-ion Electrochromic Batteries with Multiple-color Variations. *Angew Chem Int Ed Engl* **2024**, *63*, e202317944.

[240] Song, Y. X.;Li, S. L.;Liu, X. H.; Zhang, J. Polyaniline‐vanadium oxide composite for Zn‐ion electrochromic devices and mechanistic investigation by in‐situ Raman spectroscopy. *Rare Metals* **2025**, *44*, 7700-7709.

[241] Zhang, C.;Chen, Y.;Wang, X.;Wang, J.;Chen, J.;Xie, H.;Yan, D.;Liu, Y.;Wang, Z.; Ye, W. High-Capacity Electrochromic Battery Enabled by Inverted Fabry–Pérot Nanocavity. *ACS Photonics* **2025**, *12*, 6671-6679.

[242] Chen, Y.;Wan, J.;Zhang, C.;Tang, X.;Chen, L.;Tang, Z.;Li, D.;Chen, Y.;Wang, C.;Cong, S.;Zhao, Z.; Wang, Z. Enhanced high-energy-density WO

3-based electrochromic batteries via acid-modified graphite foil cathode. *Nano Research* **2025**, *18*, 94907799.

[243] Vu, C. C. Embedded-machine learning and soft, flexible sensors for wearable devices - viewing from an AI engineer. *Materials Today Physics* **2024**, *42*, 101376.

[244] Zhang, N.;Hou, T.;Han, G.;Yu, Y.;Xu, H.; Huang, Y. Smart batteries: materials, monitoring, and artificial intelligence. *Chem Soc Rev* **2025**, *54*, 10006-10139.

[245] Darvish, K.;Skreta, M.;Zhao, Y.;Yoshikawa, N.;Som, S.;Bogdanovic, M.;Cao, Y.;Hao, H.;Xu, H.;Aspuru-Guzik, A.;Garg, A.; Shkurti, F. ORGANA: A robotic assistant for automated chemistry experimentation and characterization. *Matter* **2025**, *8*, 101897.

[246] Wu, Y.;Vriza, A.;Ozgulbas, D.;Vescovi, R.;Zhou, J.;Wang, Z.;Hu, S.;Zhang, Y.;Yang, Q.;Osterholm, A. M.;Reynolds, J. R.;Sankaranarayanan, S.;Chan, M. K. Y.;Foster, I. T.;Mei, J.;Chan, H.; Xu, J. Autonomous Synthesis and Inverse Design of Electrochromic Polymers with High Efficiency and Accuracy. *J Am Chem Soc* **2025**, *147*, 44101-44113.

[247] Zhu, W.;Mo, X.;Wang, Z.;Liu, H.;Chen, J.;Wang, L.; Shou, D. Machine learning-enhanced low-hysteresis conductive auxetic strain sensors with curved re-entrant honeycomb structures based on MXene/graphene for human rehabilitation training. *Chemical Engineering Journal* **2025**, *505*.

[248] Zhu, W. B.;Wang, Y. Y.;Fan, T.;Zhu, Y.;Tang, Z. H.;Huang, P.;Li, Y. Q.; Fu, S.

Y. Comprehensive Investigation of the Temperature-Dependent Electromechanical Behaviors of Carbon Nanotube/Polymer Composites. *Langmuir* **2024**, *40*, 8170-8179.

[249] Xue, S.-S.;Tang, Z.-H.;Zhu, W.-B.;Li, Y.-Q.;Huang, P.; Fu, S.-Y. Stretchable and ultrasensitive strain sensor from carbon nanotube-based composite with significantly enhanced electrical and sensing properties by tailoring segregated conductive networks. *Composites Communications* **2022**, *29*.

[250] Huang, K.;Ma, Z.; Khoo, B. L. Advancements in Bio‐Integrated Flexible Electronics for Hemodynamic Monitoring in Cardiovascular Healthcare. *Advanced Science* **2025**, *12*.